This is to certify that the

dissertation entitled

UNDERSTANDING INTRAMOLECULAR AND

INTERMOLECULAR CONTRIBUTIONS

TO ENERGY RELAXATION

presented by

Scott Nelson Goldie

has been accepted towards fulfillment
of the requirements for

Ph. D. degree in Analytical Chemistry

Major professor

Date 24 January 2001

UNDERSTANDING INTRAMOLECULAR AND INTERMOLECULAR CONTRIBUTIONS TO ENERGY RELAXATION

By

Scott Nelson Goldie

A DISSERTATION

Submitted to
Michigan State University
in partial fulfillment of the requirements
for the degree of

DOCTOR OF PHILOSOPHY

Department of Chemistry

2001

ABSTRACT

UNDERSTANDING INTRAMOLECULAR AND INTERMOLECULAR CONTRIBUTIONS TO ENERGY RELAXATION

By

Scott Nelson Goldie

A fundamental understanding of intermolecular interactions is required to achieve predictability in liquid-phase systems. Using a pump-probe laser spectrometer to detect stimulated emission, we have studied solution phase local organization by measuring induced orientational anisotropy and vibrational population relaxation dynamics. We have studied perylene and 1-methylperylene in a series of normal alkanols (methanol to decanol), and selected aliphatic aldehydes and ketones, to probe local organization in low viscosity liquids. The reorientation behavior of the chromophores in the alkanol solvents is different than that seen in *n*-alkanes. The T_1 data for the ring breathing vibrational modes of these same chromophores points to efficient and solvent-dependent relaxation. We can infer from these data the type of local organization characteristic of the alkanols.

In both the aliphatic aldehydes and the ketones, there is a change in the nature of the solvent-solute interactions with both probe molecules as the hydrodynamic volume of the solvent molecules approaches that of the probes. The solvent-dependent change in behavior occurs for different solvent aliphatic chain lengths in the two systems. Vibrational population relaxation measurements for two probe molecule vibrational modes reveal efficient intermolecular coupling in all cases. The data point to the role of the solvent aldehyde proton in mediating solvent-solvent and solvent-solute interactions,

leading to chromophore dynamics reminiscent of those seen in the *n*-alcohols. Reorientation of the two probes in the ketones yields results that are more consistent with those seen in the alkanes, suggesting the relative weakness of dipole-induced dipole interactions relative to H-bonding interactions in the solvation of perylene and 1-methylperylene.

We have also applied transient spectroscopies to the characterization of polymer curing for a deep-UV, chemically amplified polymer photoresist used in the fabrication of semiconductors. We characterized changes in polymer free volume as a function of cure using ground state recovery measurements of crystal violet, a probe molecule doped in the polymer matrix. These data, in conjunction with linear spectroscopy, will ultimately be used to provide insight into the diffusional behavior of protons in the polymer matrix as a function of cure.

To everyone who believed in me before I knew enough to believe in myself...

ACKNOWLEDGMENTS

My sincere thanks and genuine appreciation goes to...

My entire family, especially my parents, Don and Virginia, my brother Shawn and his wife Andrea, for their love and support.

Michelle for her love, support and understanding; I wish her own success in her goals, dreams and aspiration.

To Micheal, Kathy, Allison Marie, and the entire May family for their love and support.

Professor Julie L. P. Jessop and Chair Alec B. Scranton, for the opportunities provided by the photoresist project.

The Blanchard research group members, both past, Punit, Wendy, Jennifer, Patty, Jeff and Selezion and present, Stephen, John, Lee, Shawn, Jay and Joe for their direct and indirect contributions to this dissertation.

My committee, consisting of Professors Dantus, Berglund and Cukier, for their constructive comments and guidance.

Joseph S. Ward, III for providing guidance and invaluable information to the first chapter of this dissertation, and for showing me a thing or two computing and chemistry.

Geoff Hoekstra, Dr. Tom Cullen, Dr. Tom Carter, Dr. Emily Brown, and Dr. Eric Saari for assistance in the design of the LabView® virtual instrument presented in the Appendix.

The past and present members of the Machine Shop, Glass Shop, and Electronics Shop, including Sam, Glenn, Tom, Dick, Richard, Scott, Manfred, Ron, Scott and David;

all were helpful with technical information, a quick wit, or a quick turnaround for projects when needed.

My students, all of them, have made an indelible impression on me, as I hope I have on them. Thanks should especially go to Ilene Cohen, Troy M. Ferguson, Allison Fouch, Lori Hallman, and Edmund Tillet, who gave me an encouraging word, accolade or accomplishment that motivated me to continue working toward my goal. Dr. Paul Hunter, Mr. Steve Poulios, and Ms. Wendy N. Whitford have supported the teaching endeavors that I have undertaken during the end of this work. Their encouragement and assistance has allowed me to improve as an instructor as I completed this dissertation.

Professor David S. Karpovich, for his genuine friendship and opinions that helped to bring things back into perspective. I am blessed and honored to be his friend and him to me. May we continue to "fish" for more than just salmon.

Professor Gary J. Blanchard for the science, for the encouragement, and for the guidance, but more importantly for the boat rides in the Cadillac, for the coffee, for the jokes, for the politics and for knowing when to kick me in the teeth and knowing when it was enough. The sunrise over the marsh in St. Charles or in Ovid helped to bring me back to center, clear my head, and allow me to "hunt" for a higher level of understanding and knowledge. It is those memories that I will have for the rest of my life, and for this reason I am deeply indebted to him and his family. Thank you Gary, for being so much more than a research advisor.

TABLE OF CONTENTS

LIST OF TABLES

LIST OF FIGURES

INTRODUCTION

Understanding solvation has been a subject of considerable interest because of the effect that solvent identity has on chemical processes and reactions. To have any hope of controlling these processes and reactions, a fundamental understanding of the molecular interactions, including dynamics and the energetics, that proceed between a solute molecule and adjacent solvent molecules is necessary. Energy relaxation can occur within a molecule initially, or between two molecules by electronic, vibrational, rotational, or translational (collisional) channels.

The liquid phase is a widely used medium for chemical manipulation and reaction. A further understanding of intermolecular interactions in this state would be of value to the chemical community. Working in liquid media holds inherent challenges to examining energy transfer processes. Interactions between solutes and their surrounding solvent molecules are difficult to resolve because, unlike solids, the spatial relationships between the molecules are not fixed on time scales that can be accessed using structural measurements such as X-ray diffraction or multidimensional NMR spectrometry. The existence of the liquid phase is a consequence of strong intermolecular interactions that are difficult to examine directly because of their combined long-range distance and short-time duration within the medium. Collisional processes necessarily occur over short distances, where there is actual "contact" between molecules. Long-range interactions include electronic-electronic and vibrational-vibrational non-collisional energy transfer, and these processes can proceed over tens of Angstrom distances. It is possible to probe these interactions by measuring molecular motion and energy relaxation through the use of time domain spectroscopies. With the advent of picosecond lasers, the study of liquids

expanded greatly because many of the dynamics relevant to solvation processes proceed on the picosecond or longer timescale, especially in polar, strongly associative systems. For motional processes, information about how a molecule physically interacts within its' surroundings can be extracted by interpretation of the data within the framework of a well-developed model. With an understanding of how an excited state population relaxes, a complementary picture of local organization can be inferred, albeit at a lower level at this point owing to the less mature nature of the theory available to treat this problem. Local organization information is obtained from the efficiency of energy transfer in a donor-acceptor pair, which depends on average donor-acceptor separation, relative orientation and the nature of the coupling between the two species.

There are essentially three time-resolved spectroscopic approaches to the measurement of solvent-solute interactions. These are measurement of the time-delayed fluorescence Stokes shift (TDFSS) of selected solutes,[1-10] rotational diffusion[11-31] and vibrational population relaxation.[32-44] Of these, TDFSS measurements have provided the most insight into the early-time separation of inertial and diffusive contributions to solvent reorganization about excited solute molecules, and at the same time these reports have proven to be the most controversial in terms of their interpretation.[45-49] Perhaps the most significant issue that needs to be addressed regarding TDFSS measurements is the lack of generality of the effect. Despite the broad conclusions drawn from these experimental results, only a handful of chromophores with complicated spectroscopic responses are known to exhibit resolvable transient Stokes shifts.[2,50] The two other approaches to the measurement of solvent-solute interactions do not offer the same time-resolution as the TDFSS measurements, but the phenomena of rotational diffusion and

vibrational relaxation are not limited to a few chromophores - these are general effects, and the characteristic time scales over which they proceed are consonant with chemical reaction processes.

Molecular probes that exhibit a change in an optical property in response to a change in the local environment can provide valuable *in situ* information about chemical and physical processes.[51] For example, there are a number of molecules whose optical response is sensitive to the pH of the local environment.[52] Typically, these compounds possess two or more different protolytic forms, each with a unique absorption and/or fluorescence spectrum. Examples of such probe molecules include xanthene dyes, aromatic azines and coumarin dyes. These probes have been used in various biological and medical applications to detect or quantify acid concentration in a system.[53] Recently, acid-sensitive dyes have been used to investigate photoacid generation in microlithographic systems. For example, Pohlers *et al.* have reported the use of such dyes to characterize the efficiency of photoacid generators.[54] These authors observed a shift in the absorbance spectrum of these dyes upon protonation from the neutral state to the singly-charged state. In prior work, Pohler *et al.* observed shifts in the absorbance spectra and large changes in fluorescence intensity upon protonation of aromatic monoazines.[55] Dentinger *et al.* evaluated several xanthene dyes for monitoring and imaging photoacid production.[56] Finally, Okoroanyanwu *et al.* reported the use of an aromatic monoazine to monitor photoacid generation in films and solutions.[57]

In addition to measuring the concentration of acid, fluorescence can be used to probe the local viscosity or free volume of the system. There are a number of probe molecules that exhibit an increase in the fluorescence signal and excited-state lifetime as

the local viscosity is increased. As the intramolecular isomerization or rotation becomes hindered, non-radiative pathways for energy transfer are less efficient; therefore, a greater fraction of the excited-state energy must be dissipated through radiative (fluorescent) pathways. Crystal violet and malachite green are two such "propeller" probe molecules that have been used to investigate free volume in solid matrices. Other free volume sensitive-probes are based upon photoisomerization and intramolecular excimer formation. With a small amount of a viscosity-sensitive molecule, the microviscosity or free volume of the system can be measured. For example, Francis Wang *et al.* have used 1,3-bis-(1-pyrene) (BPP) to monitor the polymerization of methyl methacrylate *in situ*.[58] Moorjani and coworkers further demonstrated the utility of fluorescence monitoring when dealing with diffusion-controlled reactions in media of different viscosity.[59] Victor and Torkelson have also used molecular probes to measure the free volume available in polymer structures.[60]

We have undertaken a series of studies in an attempt to better understand solute-solvent interactions for a variety of media, ranging from neat liquids to reactive polymer matrices. We have used molecular reorientation, fluorescence lifetime, vibrational population relaxation and steady-state fluorescence measurements, and report our findings in this dissertation.

The picosecond pump-probe laser spectrometer used for most of the laser-based experiments has been described in detail previously,[61] and we present only a brief outline of its performance characteristics here. A graphical representation of the instrument is presented in Figure 1. A mode-locked CW Nd:YAG laser (Coherent Antares 76-S)

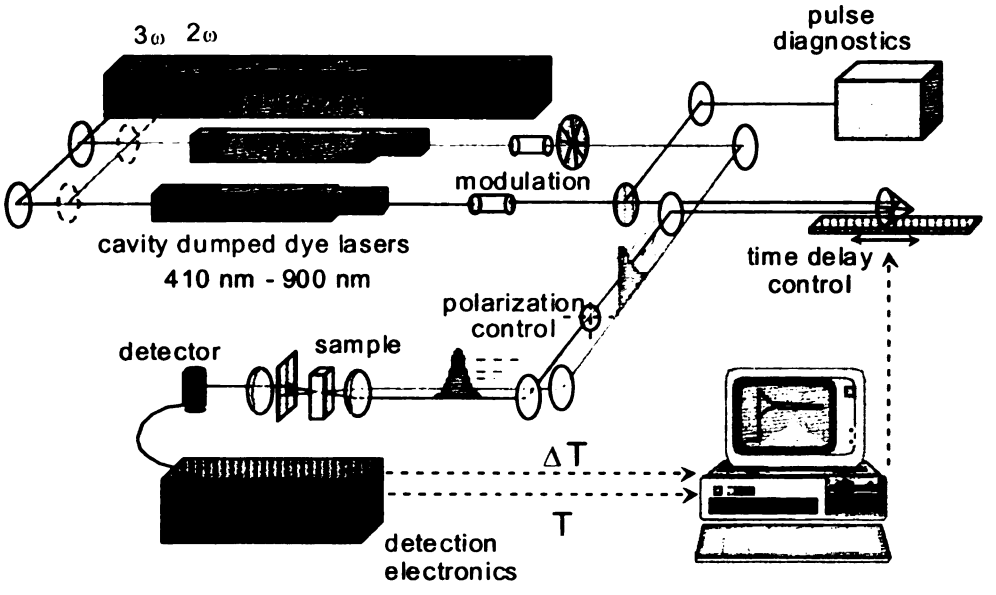

Figure 1 – Schematic of picosecond pump-probe laser spectrometer used in this work.

produces 30 W of average power (1064 nm, 100 ps pulses, 76 MHz repetition rate). The output of this laser is either frequency-tripled to produce ~1.3 W of average power at 354.7 nm for experiments involving perylene and 1-methylperylene as probe molecules, or frequency-doubled to produce ~2.1 W of average power at 532 nm, for the fluorescence lifetime experiments where crystal violet is used as a probe molecule. In both situations, this output is used to excite two cavity-dumped dye lasers synchronously (Coherent 702-3). The laser dye used in both lasers is dependent upon the wavelengths of interest. For experiments involving perylene and 1-methylperylene as probe molecules, both lasers operate with Stilbene 420 laser dye (Exciton). Rhodamine 6G laser dye (Kodak) was used in both laser systems for the free volume characterization experiments. The output of each laser, regardless of the dye used is ~10-100 mW average power at 8 MHz repetition rate with a pulse that produces a 7 ps FWHM autocorrelation trace using a three plate birefringent filter.

The pump wavelength for experiments with perylene and 1-methylperylene was chosen to access the 0-0 transition of the chromophore and the probe wavelength to stimulate emission from the $S_1^{v=0}$ state to the $S_0^{v=1}$ state, where the vibrational resonance of interest is the 1375 cm^{-1} v=1 ring breathing mode, or the 1730 cm^{-1} v=1 combination mode. These wavelengths were used for the vibrational relaxation and the reorientation measurements. It has been demonstrated previously, that the ground state and excited state reorientation behavior of perylene are identical[30] and we assume that this is also the case for 1-methylperylene. The probe beam was polarized at 0°, 90°, or 54.7° with respect to the pump beam depending upon the experiment being performed. For rotational diffusion measurements, the 0° and 90° polarizations are of interest, while the

vibrational population relaxation measurements use a probe beam polarization of 54.7° to eliminate molecular reorientation contributions to the signal.

For the free volume characterization experiments, the pump laser wavelength was set to 589.5 nm, coincident with the absorption maximum of the first singlet transition of crystal violet. The probe wavelength was chosen to lie within the absorption band of crystal violet. The absorption spectrum of crystal violet is presented in Chapter 4. The probe beam was polarized at 54.7° with respect to the pump beam to eliminate molecular reorientation contributions to the signal.

Detection of the transient signals, regardless of the experiment, was accomplished using a radio and audio frequency triple-modulation scheme, with synchronous demodulation detection.[62-64] Each reported time constant is the average of at least five individual determinations that are themselves the average of seven to ten time-scans.

The arrival time of the probe pulse relative to the pump is controlled through the use of a computer interfaced translation stage and stepper motor controller. The distance that the probe pulse travels is changed through the positioning of the translation stage, resulting in a change of the arrival time of the probe laser pulse train. The time resolution of this system, ~10 ps, is determined by the cross-correlation between the pump and probe laser pulse trains.

In rotational diffusion measurements, the probe molecule sweeps out a specific volume. The solvent cage formed around the solute can influence the ability of the solute to rotate about specific axes and can determine the shape of the volume swept out. This information provides for some insight into how inter-molecular interactions influence the motion of the probe, and by inference the average organization of the solvent molecules

around the solute. The solute/solvent system can also be studied to determine its energy relaxation behavior. The key to this approach is to identify systems where inter-molecular energy transfer dominates as the initial relaxation step, and the other properties of the system (inter-molecular orientation and distance) can be examined.

To examine the inter-molecular interactions in solution we use two complementary methods that share a single experimental apparatus. Induced orientational anisotropy measurements provide information about the forces that serve to inhibit molecular motion by the examining the time required for an ensemble of molecules to randomize. Vibrational population relaxation measurements provide information about the local environment by revealing how energy is transferred to the surrounding solvent bath over distances longer than those characteristic for inelastic collisions. Information about the density of donor-acceptor sites, orientation, and coupling can help to construct a preliminary model of how the solute and solvent molecules interact in solution.

The examination of rotational diffusion dynamics is a widely used method to probe the nature of solvent-solute interactions.[25,26,65-69] The theoretical framework needed to understand these interactions is well documented.[70-75] From the application of the theory to the experimental data, the solute rotational diffusion constant, the angle between the excited and probed transition moments and, in some cases, a sense of the dielectric properties of the local environment can be obtained. This information can then be used to extend the understanding of the average local organization of the solvent around the solute.

Using linearly polarized light, an ensemble of molecules with transition dipole moments oriented parallel to the polarization of the incident electric field can be excited,

inducing a transient anisotropy in the system. This induced anisotropy will decay in time due to the rotational dynamics of the system. The induced orientational anisotropy function is extracted from the raw data through Equation (1).

$$R(t) = \frac{I_{\parallel}(t) - I_{\perp}(t)}{I_{\parallel}(t) + 2I_{\perp}(t)} \qquad (1)$$

$I_{\parallel}(t)$ and $I_{\perp}(t)$ are the intensities of the response when the polarizations of the two beams are oriented parallel and orthogonal relative to each other. We present a representative sample data set in Figure 2. When these data are related according to Equation (1), an exponential decay curve results (Figure 3).

Chuang and Eisenthal have formulated the relationship between R(t) and solute properties such as the angle between the excited and probed one photon transition moments and the actual anisotropy in the diffusion constant.[64] They found that R(t) can decay with as many as five exponential components, although the most common case is that of a single exponential. In cases where more than one decay component is resolved, it is possible to interpret the details of the reorientation dynamics in substantial detail.

For the purposes of the following discussion, we consider that the chromophores have their π-system in the approximate *xy* plane with *x* being the long, in-plane axis, and *z* is perpendicular to the π-system plane (Figure 8.) For each chromophore our intention was to assign the coordinate system such that the *x*-axis coincides with the absorption transition moment. For perylene this assignment is coincident with specific bond axes because of its high symmetry while for 1-methylperylene it is not since the π-system for this chromophore is non-planar. Using these approximations and Chuang and Eisenthal's equations,[64] we can relate the experimental reorientation times to the shape of the volume

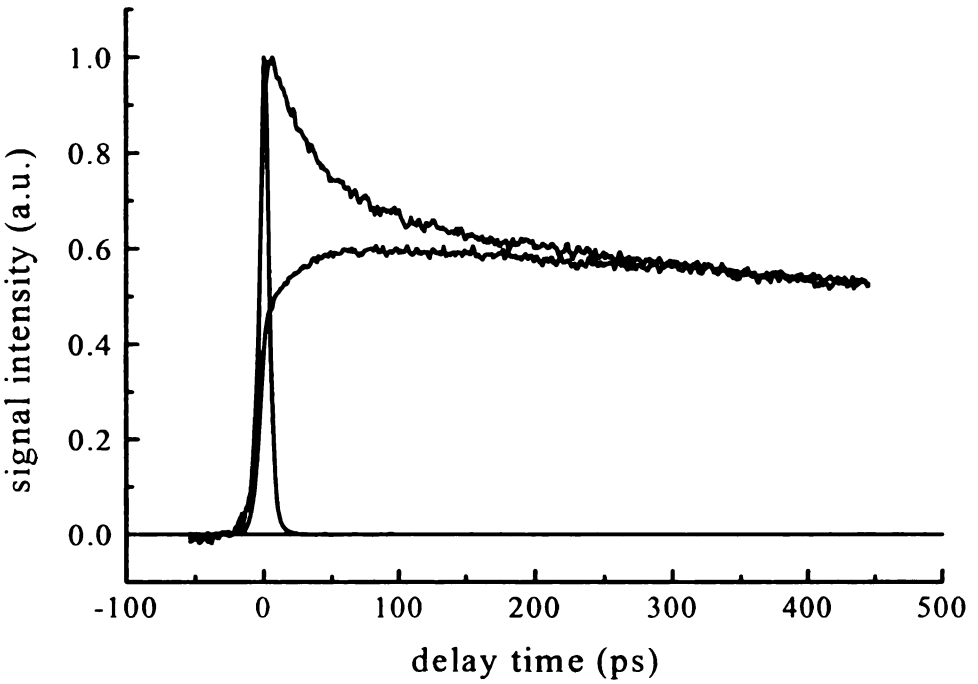

Figure 2 – Experimental $I_{\parallel}(t)$ and $I_{\perp}(t)$ scans for 1-methylperylene in *n*-pentanol, along with the instrumental response function. These data are typical of those recorded for reorientation measurements.

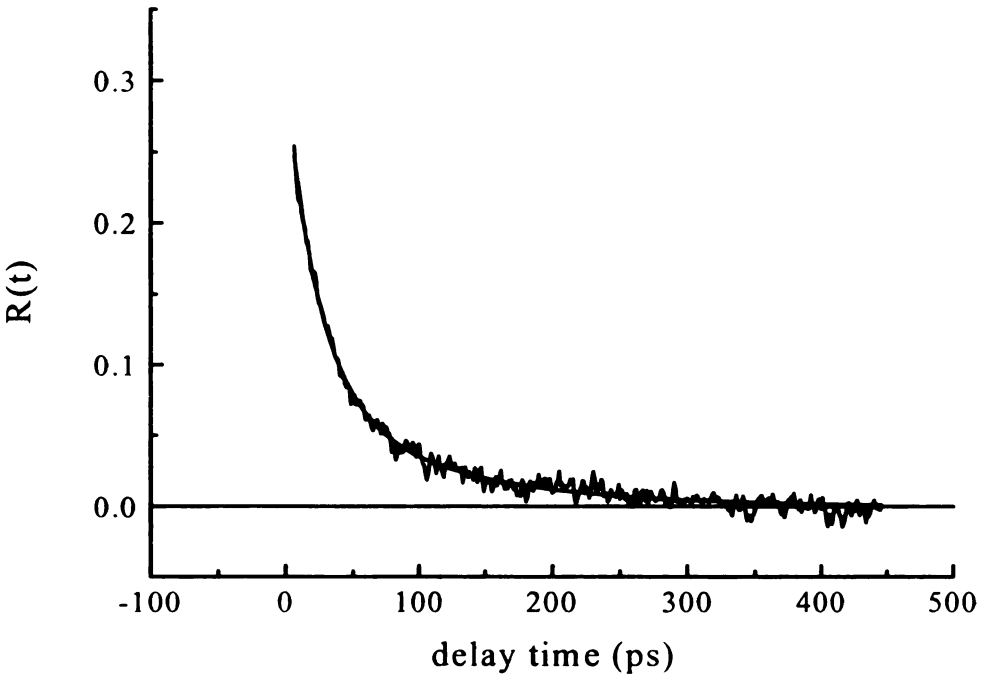

Figure 3 – Anisotropy function, R(t), for the data shown in Figure 2. The decay is fit to the function $R(t) = R_1(0)\exp(-t/\tau_1) + R_2(0)\exp(-t/\tau_2)$

swept out by the rotating molecule. We describe this volume in terms of ellipsoids, where a prolate ellipsoid, Equation (2) and Figure 4, is characterized by rotation primarily about its long in-plane axis, $D_x > D_y \sim D_z$ and an oblate ellipsoid, Equation (3) and Figure 5, by is characterized by rotation about the axis perpendicular to the chromophore π-system, $D_z > D_x \sim D_y$.

Prolate: $R(t) = 0.4\exp(-6D_z t)$ (2)

Oblate: $R(t) = 0.3\exp(-(2D_x + 4D_z)t) + 0.1\exp(-6D_x t)$ (3)

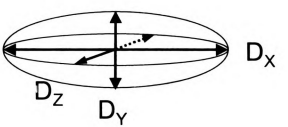

Figure 4 – Prolate ellipsoid with Cartesian coordinate system superimposed. See text for discussion.

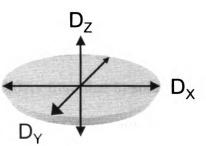

Figure 5 – Oblate ellipsoid with Cartesian coordinate system superimposed. See text for a discussion.

A single exponential decay fit of the reorientation anisotropy function R(t) is the most common observation, but this observation can be attributed to either a spherical rotor shape or a prolate rotor shape being swept out of solution by the probe molecule. We model this behavior as a prolate rotor, since both perylene and 1-methylperylene are

not spherical molecules in shape. A double exponential decay fit is described to be an oblate rotor shape being swept out of solution by the probe chromophore. The rotor shape of the chromophore and changes in the rotational behavior result from intermolecular and intramolecular interactions between the solute and the solvent in solution, and determination of the rotor shape can elucidate information regarding these solvation processes.

Vibration population relaxation dynamics can also be used as a probe of solvation processes. Vibrational population relaxation provides information about the specific relaxation pathways that are used to dissipate energy in a molecule. Rotational diffusion measurements sense the entire molecule and its' average response to a perturbation. When a molecule is excited, it is generally true that there are multiple ways for it to dissipate that energy, with many solvent cage configurations that lie within a narrow energetic window, capable of interconversion on a fast time scale. A determination of how molecules at room temperature dissipate energy to surroundings can give information on how molecules interact. In gases, the spacing between molecules can be determined statistically and differs from that in solution. Analogous arguments can be made for solids. In these systems, the dissipation of energy is not random – but occurs through specific pathways and over relatively defined distances. In solutions, both collisional and non-collisional energy transfer processes have to be taken into account.[76] Non-collisional energy transfer can occur over relatively long distances. These types of energy transfer are significant in solution.[77]

Energy transfer can be described in terms of coupling of transition moments that scale as r^{-n} where the specific type of interaction determines the value of n. Dipole-

dipole, dipole-induced dipole and induced dipole-induced dipole interactions all scale over r^{-6}, and it is this sort of coupling that Förster discussed most thoroughly. Coupling between higher order multipole moments (quadrupole, octupole) scale with r^{-n} where $n \geq 8$. The interaction energy falls off more rapidly the higher the order of the multipole,[78] and this consideration is important for our work.

Förster described this for dipole-dipole coupling.[77,79] Experimentally, an excited donor molecule (D^*) transfers energy to a ground state acceptor molecule (A) with a characteristic rate constant k_{DA}:

$$D^* + A \xrightarrow{k_{DA}} D + A^*$$

$$k_{DA} = \frac{3}{2}\kappa^2\left(1/\tau_D\right)\left(R_0/R\right)^6 \qquad (4)$$

where τ_D is the radiative lifetime of D^*, R_0 is the critical transfer distance which incorporates the spectral overlap term and the magnitudes of the transition dipole moments, R is the D-A intermolecular distance and κ^2 describes the orientation of the donor with respect to the acceptor:

$$\kappa^2 = \left(\sin\theta_D \sin\theta_A \cos\phi - 2\cos\theta_D \cos\theta_A\right) \qquad (5)$$

The strength of the coupling is dependent upon the spectral overlap considerations (detuning) between the donor and acceptor and the average distance between the two species and their relative orientations. The information about the efficiency of the coupling then provides additional complementary information to the rotational diffusion measurements, since both address the separation distance and orientation of the donor-acceptor pair. For electronic-electronic transitions, R_0 is approximately 25-50Å and ~10Å for vibrational-vibrational transfer. The angles θ_D and θ_A indicate the orientation

of the donor and acceptor transition moments with respect to the plane containing the two species, and ϕ is the relative angle between the transition moments along the connecting vector.

Under our two-pulse measurement scheme for vibrational population relaxation molecules possessing a center of inversion, such as perylene, vibrational modes that are infrared active will be Raman inactive and *vice versa*. In 1-methylperylene, the center of inversion is removed by the addition of the methyl group to the ring, and this result is that all modes are both infrared and Raman active.[80] Infrared active vibrations modulate the dipole moment of the molecule and Raman active vibrations modulate the polarizability. These two types of transitions may involve different types of coupling with characteristically different interaction lengths. If a donor mode is infrared active ($\Delta\mu$), and the acceptor mode is also IR active, the coupling will scale as r^{-6}. If Raman active donor resonances are not also IR active, coupling to the acceptor through a higher moment is operative, and such coupling operates over a shorter distance than dipolar coupling. This change in the range probed makes it difficult to relate such data to other types of information increasing the number of possible explanations. Rotational dynamics and vibrational population relaxation measurements that probe approximately the same distance surrounding the donor molecule simplify the explanations involved.

This method[40,41] examines the depopulation of a vibrational mode of the chromophore on the picosecond time scale. The time constraints for relaxation are highly dependent upon the mode in question and the solute/solvent system. If this system-dependency can be understood, significant information can be gained on local organization in solution.

In this method the chromophore under examination is treated as a strongly coupled three level system. We present a schematic in Figure 6. Spontaneous and stimulated emission from the S_1 state to the S_0 state, stimulated absorption from an excited vibrational level in the S_0 electronic manifold to the S_1 state, and depopulation of the excited vibrational level to the ground vibrational level in the S_0 state all influence the experimental signal. The difference between the pump laser frequency and the probe laser frequency is set to a Raman resonance in the solute. The solvent system is chosen such that it possesses vibrational resonances in close energetic proximity of the solute ($\Delta\nu_{DA}$~0) providing a specific, hopefully efficient pathway for energy transfer via long range polar vibrational-vibrational coupling. These choices bias the measurement to make intra-molecular relaxation a non-dominant pathway. Here, perylene and 1-methylperylene have ring breathing modes at ~1375 cm^{-1}. The terminal methyl groups of the alkanols, aldehydes and ketones used in this work exhibit rocking motions at ~1378 cm^{-1}, essentially degenerate with the solvent mode. In addition to this donor/acceptor system, the donor solute molecules also possess a vibrational mode near ~1730 cm^{-1}. This mode is degenerate with the carbonyl-stretching mode in the aldehydes and ketones (~1727 and 1716 cm^{-1}, respectively). These donor/acceptor modes will be examined throughout this work to understand the role of molecular structure and functionality in mediating solution phase vibrational excitation transport.

As a function of time, the population of state A will exhibit an exponential fluorescence decay, while the population of state B will build up and reach a steady-state, if the decay rate constant from the intermediate vibrational level is much larger than the decay rate constant from state A. We have chosen our solute/solvent system such that

this is the case. If the population changes of states A and B are measured as a function of time, a buildup, related to the populating of state B, followed by long time decay related to the fluorescence depopulation of state A will result. We present a typical dataset that demonstrates this in Figure 7.

The time constant for population relaxation gives information about the conditions necessary to transfer energy from the donor to the acceptor. This information is then used to infer the presence or absence of local organization in these systems. By itself, this information does not provide a complete picture. When taken with complementary rotational diffusion data, however, some insight into local organization can be obtained.

These principles of interactions between solutes and solvents can be used to elucidate information about applied chemical systems. Probe molecules can be used to determine changes in the local environment of solutions. Crystal violet is a useful probe of microviscosity in solution. Crystal violet (Scheme 4, Chapter 4 – this work), a member of the triphenylmethane dye family, is predominantly a D_3 "propeller" shaped molecule in solution with three identical N,N-dimethylaniline rings bound to a central carbon atom tilted slightly out of the molecular plane. Ring rotation around the bonds between the phenyl rings to the central carbon atom in what is believed to be a barrierless process along the excited state potential energy surface. Studies have indicated a strong dependence of the excited state lifetime on solvent viscosity, which is indicative of essentially no intra-molecular rotational barrier to ring rotation.[81,82] The characteristically low fluorescence quantum yield of this family of molecules prevents us from using a fluorescence lifetime measurement to explore these changes. Instead, we examine the

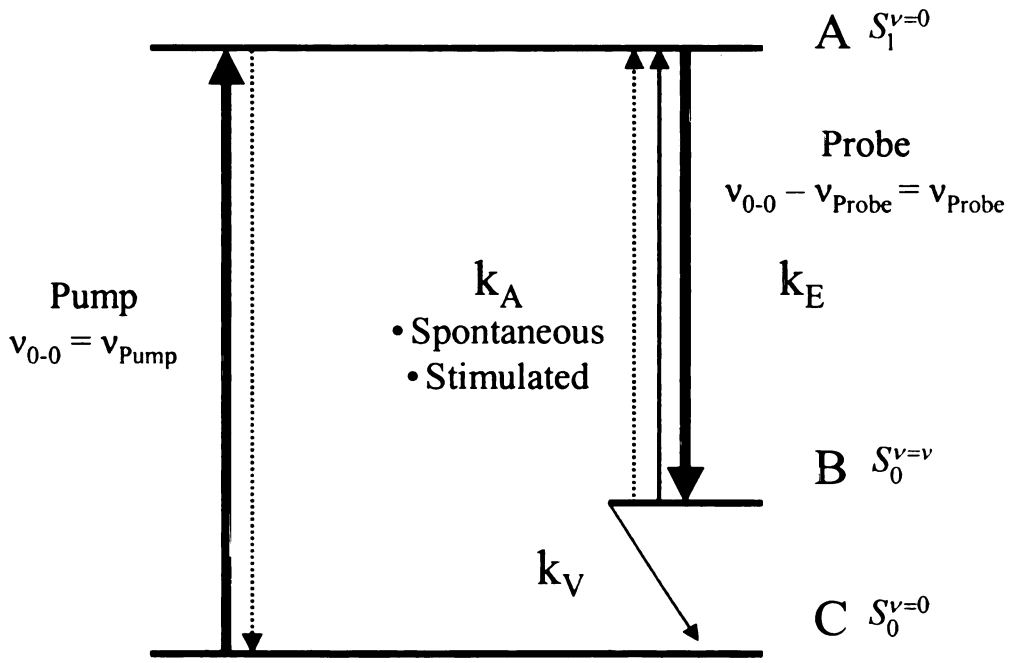

Figure 6 – Three level system model for vibrational population relaxation measurements.

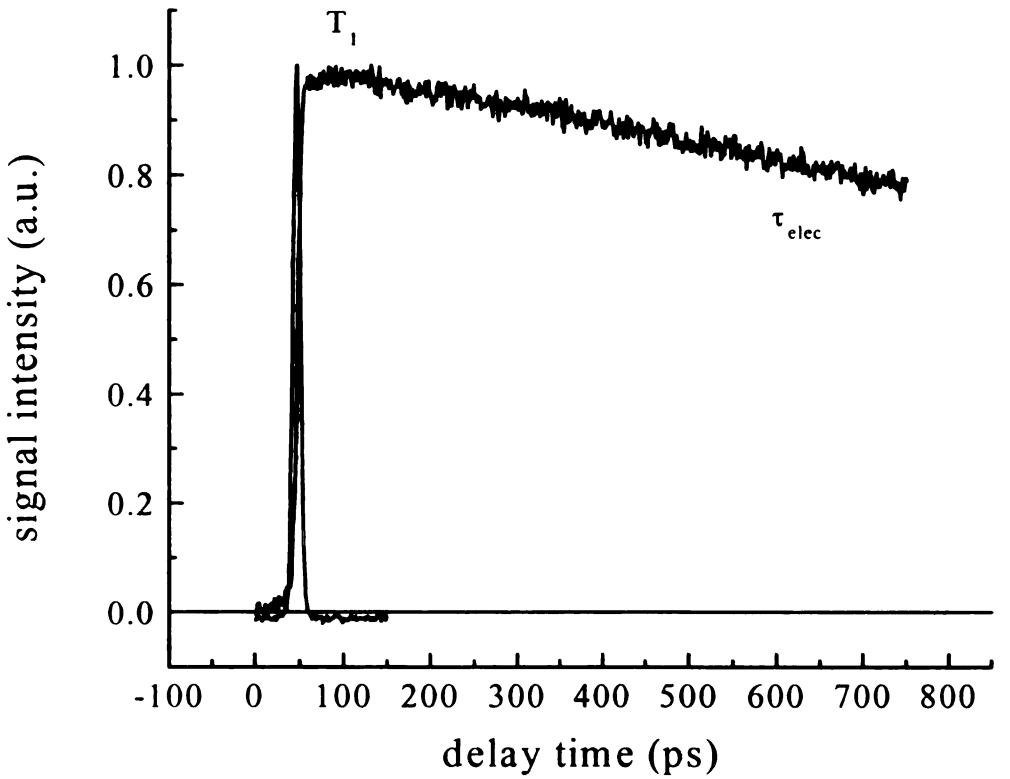

Figure 7 – Magic angle data for perylene in methanol with instrument response function.

ground state population by detecting the transient change in absorption of the probe pulse resulting from excitation by the pump laser pulse, to sense changes in the local environment in the photoresist thin films.

Chapter 1 of this dissertation outlines two procedures attempted in our laboratory to synthesize 1-methylperylene, one of the solute chromophores studied in chapters 2 and 3. We compare the methods of Ziegler[83] and Peake[84] *et al.* and provide our results using their procedures, with characterization and purification data.

Chapters 2 and 3 of this dissertation examine the rotational diffusion and vibrational population dynamics of perylene and 1-methylperylene in a series of normal aliphatic alcohols and a series of aldehydes and selected ketones. We have found that the presence of a labile proton that can facilitate hydrogen bonding in alcohols and aldehydes has a greater effect on the local organization in the condensed phase than dipole-induced dipole interactions, such as those found in the ketones.

Chapters 4 and 5 of this dissertation deal with the characterization of photoresist materials used in the semiconductor industry. We describe a methodology to quantify the production of acid molecules in a photoresist material used in the microlithographic production of semiconductors using the probe molecule crystal violet in Chapter 4. In Chapter 5, we use the same probe molecule to examine the interactions between solute (probe molecule) and the solvent (photoresist) as a function of processing step.

Chapter 6 provides some final conclusions as well as some suggestions for future work in both the solution phase characterization of perylene and 1-methylperylene and the continued characterization of photoresist materials used in microlithographic applications.

In the appendix, a description of the hardware used and the function of each of the parts of the virtual instrument created to operate the pump-probe laser spectrometer instrument used in most of the experiments of this dissertation is recorded for future reference.

Literature Cited

1. Shapiro, S. L.; Winn, K. R.; *Chem. Phys. Lett.*, **1980**, *71*, 440.
2. Maroncelli, M.; Fleming, G. R.; *J. Chem. Phys.*, **1987**, *86*, 6221.
3. Huppert, D.; Ittah, V.; Kosower, E.; *Chem. Phys. Lett.*, **1989**, *159*, 267.
4. Chapman, C. F.; Fee, R. S.; Maroncelli, M.; *J. Phys. Chem.*, **1990**, *94*, 4929.
5. Huppert, D.; Ittah, V.; *Chem. Phys. Lett.*, **1990**, *173*, 496.
6. Jarzeba, W.; Walker, G. C.; Johnson, A. E.; Barbara, P. F.; *Chem. Phys.*, **1991**, *152*, 57.
7. Wagener, A.; Richert, R.; *Chem. Phys. Lett.*, **1991**, *176*, 329.
8. Fee, R. S.; Milsom, J. A.; Maroncelli, M.; *J. Phys. Chem.*, **1991**, *95*, 5170.
9. Yip, R. W.; Wen, Y. X.; Szabo, A. G.; *J. Phys. Chem.***1993**, *97*, 10458.
10. Fee, R. S.; Maroncelli, M.; *Chem. Phys.*, **1994**, *183*, 235.
11. Sanders, M. J.; Wirth, M. J.;*Chem. Phys. Lett.*, **1983**, *101*, 361.
12. Gudgin-Templeton, E. F.; Quitevis, E. L.; Kenney-Wallace, G. A.; *J. Phys. Chem.*, **1985**, *89*, 3238.
13. Von Jena, A.; Lessing, H. E.; *Chem. Phys.*, **1979**, *40*, 245.
14. Von Jena, A.; Lessing, H. E.; *Ber. Bunsen-Ges. Phys. Chem.*, **1979**, *83*, 181.
15. Von Jena, A.; Lessing, H. E.; *Chem. Phys. Lett.*, **1981**, *78*, 187.
16. Eisenthal, K. B.; *Acc. Chem. Res.*, **1975**, *8*, 118.
17. Fleming, G. R.; Morris, J. M.; Robinson, G. W.; *Chem. Phys.*, **1976**, *17*, 91.
18. Shank, C. V.; Ippen, E. P.; *Appl. Phys. Lett.*, **1975**, *26*, 62.
19. Millar, D. P.; Shah, R.; Zewail, A. H.; *Chem. Phys. Lett.*, **1979**, *66*, 435.
20. Gudgin-Templeton, E. F.; Kenney-Wallace, G. A.; *J. Phys. Chem.*, **1986**, *90*, 2896.
21. Blanchard, G. J.; Wirth, M. J.; *J. Phys. Chem.*, **1986**, *90*, 2521.

22. Blanchard, G. J.; *J. Chem. Phys.*, **1987**, *87*, 6802.

23. Blanchard, G. J.; Cihal, C. A.; *J. Phys. Chem.*, **1988**, *92*, 5950.

24. Blanchard, G. J.; *J. Phys. Chem.*, **1988**, *92*, 6303.

25. Blanchard, G. J.; *J. Phys. Chem.*, **1989**, *93*, 4315.

26. Blanchard, G. J.; *Anal. Chem.*, **1989**, *61*, 2394.

27. Alavi, D. S.; Hartman, R. S.; Waldeck, D. H.; *J. Phys. Chem.*, **1991**, *95*, 6770.

28. Hartman, R. S.; Alavi, D. S.; Waldeck, D. H.; *J. Phys. Chem.*, **1991**, *95*, 7872.

29. Jiang, Y.; Blanchard, G. J.; *J. Phys. Chem.*, **1994**, *98*, 6436.

30. Brocklehurst, B.; Young, R. N.; *J. Phys. Chem.*, **1995**, *99*, 40.

31. Pauls, S. W.; Hedstrom, J. F.; Johnson, C. K.; *Chem. Phys.*, **1998**, *237*, 205.

32. Elsaesser, T.; Kaiser, W.; *Annu. Rev. Phys. Chem.*, **1991**, *42*, 83.

33. Lingle, R., Jr.; Xu, X.; Yu, S. C.; Zhu, H.; Hopkins, J. B.; *J. Chem. Phys.*, **1990**, *93*, 5667.

34. Anfinrud, P. A.; Han, C.; Lian, T.; Hochstrasser, R. M.; *J. Phys. Chem.*, **1990**, *94*, 1180.

35. Heilweil, E. J.; Casassa, M. P.; Cavanagh, R. R.; Stephenson, J. C.; *Ann. Rev. Phys. Chem.*, **1989**, *40*, 143.

36. Heilweil, E. J.; Cavanagh, R. R.; Stephenson, J. C.; *Chem. Phys. Lett.*, **1987**, *134*, 181.

37. Heilweil, E. J.; Cavanagh, R. R.; Stephenson, J. C.; *J. Chem. Phys.*, **1989**, *89*, 230.

38. Heilweil, E. J.; Casassa, M. P.; Cavanagh, R. R.; Stephenson, J. C.; *J. Chem. Phys.*, **1986**, *85*, 5004.

39. Hambir, S. A.; Jiang, Y.; Blanchard, G. J.; *J. Chem. Phys.*, **1993**, *98*, 6075.

40. Jiang, Y.; Blanchard, G. J.; *J. Phys. Chem.*, **1994**, *98*, 9411.

41. Jiang, Y.; Blanchard, G. J.; *J. Phys. Chem.*, **1994**, *98*, 9417.

42. Jiang, Y.; Blanchard, G. J.; *J. Phys. Chem.*, **1995**, *99*, 7904.

43. McCarthy, P. K.; Blanchard, G. J.; *J. Phys. Chem.*, **1995**, *99*, 17748.

44. McCarthy, P. K.; Blanchard, G. J.; *J. Phys. Chem.*, **1996**, *100*, 5182.

45. Agmon, N.; *J. Phys. Chem.*, **1990**, *94*, 2959.

46. Maroncelli, M.; Fee, R. S.; Chapman, C. F.; Fleming, G. R.; *J. Phys. Chem.*, **1991**, *95*, 1012.

47. Blanchard, G. J.; *J. Chem. Phys.*, **1991**, *95*, 6317.

48. Jiang, Y.; McCarthy, P. K.; Blanchard, G. J.; *Chem. Phys.*, **1994**, *183*, 249.

49. Flory, W. C.; Blanchard, G. J.; *Appl. Spec.*, **1998**, *52*, 82.

50. Castner, E. W.; Maroncelli, M.; Fleming, G. R.; *J. Chem. Phys.*, **1987**, *86*, 1090.

51. Jessop, J.L.; Goldie, S.N.; Scranton, A.B.; Blanchard, G.J.; Rangarajan, B.; Capodieci, L.; Subramanian, R.; Templeton, M.K. *SPIE Proc.* **1999**, *3678*, 914.

52. Haugland, R. P. In *Handbook of Fluorescent Probes and Research Chemicals*, 6th ed.; Spence, M. T. Z; Johnson, I. D. Eds.; Molecular Probes: USA, **1996**.

53. Slavik, J.; *Fluorescent Probes in Cellular and Molecular Biology*, CRC Press, Inc.: Ann Arbor, MI, 1994.

54. Pohlers, G.; Scaiano, J.C.; Sinta, R.; *Chem. Mater.* **1997**, *9*, 3222.

55. Pohlers, G.; Virdee, S.; Scaiano, J.C.; Sinta, R.; *Chem. Mater.* **1996**, *8*, 2654.

56. Dentinger, P.M.; Lu, B.; Taylor, J.W.; Bukofsky, S. J.; Feke, G.D.; Hessman, D.; Grober, R.D.; *J. Vac. Sci. Technol. B*, **1998**, *16*, 3767.

57. Okoroanyanwu, U.; Byers, J.D.; Cao, T.; Webber, S.E. Willson, C.G.; *Micro and Nano-patterning Polymers*; Ito, H.; Reichmanis, E.; Nalamasu, O.; Ueno, Y. Eds.; American Chemical Society: Washington, D.C., 1998, 174.

58. Wang, F.W.; Lowry, R.E.; Grant, W.H.; *Polymer*, **1984**, *25*, 690.

59. Moorjani, S.K.; Rangarajan, B.; Scranton, A.B.; "Effect of viscosity on the rate of photosensitization of diaryliodonium salts by anthracene," In *Photopolymerization: Fundamentals and Applications*; Scranton, A.B.; Bowman, C.N.; Peiffer, R.W. Eds. American Chemical Society: Washington, D.C., **1997**, 95.

60. Victor, J.G.; Torkelson, J.M.; *Macromolecules*, **1987**, *20*, 2241.

61. Jiang, Y.; Hambir, S. A.; Blanchard, G. J.; *Opt. Commun.*, **1993**, *99*, 216.

62. Bado, P.; Wilson, S. B.; Wilson, K. R., *Rev. Sci. Instrum.* **1982**, *53*, 606.

63. Andor, L.; Lorincz, A.; Siemion, J.; Smith, D. D.; Rice, S. A., *Rev. Sci. Instrum.* **1984**, *55*, 64.

64. Blanchard, G. J.; Wirth, M. J.; *Anal. Chem.* **1986**, *56,* 532.

65. Labhart, H.; Pantke, E. R. *Chem. Phys. Lett.* **1973**, *23*, 482.

66. Zinsli, P. E. *Chem. Phys.* **1977**, *20*, 299.

67. Klein, U. K. A.; Haar, H. P. *Chem. Phys. Lett.* **1979**, *63*, 40.

68. Christensen, R. L.; Drake, R. C.; Phillips, D. *J. Phys. Chem.* **1986**, *90*, 5960.

69. Ben-Amotz, D. Scott, T. W. *J. Chem. Phys.* **1987**, *87*, 3739.

70. Debye, P. *Polar Molecules*; Chemical Catalog Co.: New York, 1929; 84.

71. Perrin, F. *J. Phys. Radium* **1936**, *7*, 1.

72. Chuang, T. J.; Eisenthal, K. B. *J. Chem. Phys.* **1972**, *57*, 5094-5097.

73. Hu, C. M.; Zwanzig, R. *J. Chem. Phys.* **1974**, *60*, 4354.

74. Youngren, G. K.; Acrivos, A. *J. Chem. Phys.* **1975**, *63*, 3846.

75. Zwanzig, R.; Harrison, A. K. *J. Phys. Chem.* **1985**, *83*, 5861.

76. Yardley, J. T. *Introduction to Molecular Energy Transfer*; Academic: New York, 1980.

77. Förster , T. *Ann. Phys. (Liepzig)* **1948**, *2*, 55.

78. Akins, P. W. *Physical Chemistry*, 4th ed.; Freeman: New York, 1990.

79. Förster, T. In *Comparative Effects of Radiation;* Burton, M., Kirby-Smith, J. S., Magee J. C., Ed.; Wiley: New York, 1960; p 300.

80. Cotton, F. A. *Chemical Applications of Group Theory*, 3rd ed. Wiley: New York, 1990.

81. Ben-Amotz, D.; Harris, C. B.; *J. Chem. Phys.* **1987**, *86*, 4856.

82. Ben-Amotz, D.; Harris, C. B.; *J. Chem. Phys.* **1987**, *86*, 5433.

83. Zieger, H. E.; Laski, E. M. *Tetrahedron Lett.* **1966**, *32*, 1966

84. Peake, D. A.; Oyler, A. R.; Heikkila, K. E; Liukkonen, R. J; Engroff, E. C.; Carlson, R. M. *Synth. Commun.* **1983**, *13*, 21.

Chapter 1

SYNTHETIC PATHWAYS TO 1-METHYLPERYLENE

Introduction

Much of the work in this dissertation concerns the behavior of perylene and 1-methylperylene in solution. These two probe molecules were chosen for examination because perylene is well characterized[1-8] and the ease of synthesis of 1-methylperylene, a molecule with similar electronic spectroscopic properties, but lower symmetry. The lower symmetry of 1-methylperylene affects the linear response, vibrational population relaxation times and rotational diffusion, (*vide infra*). These changes can help to elucidate information about the solution phase behavior of these chromophores, which has yet to be resolved satisfactorily in the literature.

Perylene is a member of the D_{2h} point group. The addition of a single methyl group in the **1** position reduces the symmetry of 1-methylperylene to the C_1 point group, removing the center of inversion. The methyl group on 1-methylperylene causes the two naphthalene moieties to be twisted out of planarity by ~ 20°.[9,10] The methyl group added to form 1-methylperylene results in a reduction in the conjugation of the π-system, which causes a blue shift, relative to the linear response of perylene. The reduction in symmetry also causes additional vibrational transitions to become allowed. These additional transitions are important to our understanding of these data for several reasons. Under our two-pulse measurement scheme for vibrational population relaxation, used in many experiments in this dissertation, molecules possessing a center of inversion, such as perylene, the lowest order multipole moment that can be modulated using our excitation

scheme is the quadrupole moment. The solute donor mode will couple to the solvent bath modes through quadrupole-dipole interactions, assuming an IR-active acceptor mode. This coupling mechanism depends on donor-acceptor spacing as r^{-8}.[5] For a donor that does not possess a center of inversion, such as 1-methylperylene, the excited vibrational resonance is a dipolar modulation and the donor-acceptor coupling will depend on intermolecular distance as r^{-6}. The Stokes shift of 1-methylperylene relative to perylene is indicative of a small but finite permanent dipole moment in 1-methylperylene. PM3 semi-empirical calculations indicate $\mu \sim 0.24$ D in the S_0 and 0.53 D in the S_1 for 1-methylperylene.[11]

Measurement of the vibrational population relaxation, T_1, of perylene and 1-methylperylene as a function of solvent identity can provide information on the spatial proximity and relative orientation of the donor and acceptor species.[5,12] Quadrupole-dipole and dipole-dipole coupling processes operate over different length scales (r^{-8} vs. r^{-6}) and thus it is not possible to compare results directly. Despite the differences of length scale, the solvent-dependent trends observed in the T_1 data for the two molecules provide insight into the average spatial relationship between donor and acceptor functionalities in solution.

Perylene and 1-methylperylene have ring breathing modes at ~1375 cm^{-1}. The terminal methyl groups of the alkanols, aldehydes and ketones used in this work exhibit rocking motions at ~1378 cm^{-1}, essentially degenerate with the solvent mode. In addition to this donor/acceptor system, the donor solute molecules also possess a vibrational mode near ~1730 cm^{-1}. This mode is degenerate with the carbonyl-stretching mode in the aldehydes and ketones (~1727 and 1716 cm^{-1}, respectively). These donor/acceptor

modes will be examined throughout this work to understand the role of molecular structure and functionality in mediating solution phase vibrational excitation transport.

To simplify the treatment of our rotational diffusion data, we assign a coordinate system to each chromophore such that the *x*-axis resides in approximately in the *xy* plane of the π-system and it is coincident with the long, in-plane axis of the chromophore. The *z*-axis in our coordinate system is perpendicular to the π-system plane, shown in Figure 8.

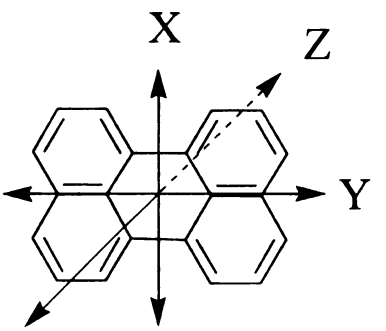

Figure 8 – Laboratory coordinate system applied to perylene. A similar laboratory coordinate system was applied to 1-methylperylene.

The *x*-axis also coincides with the absorption transition moment of perylene because of its high symmetry, but this does not apply for 1-methylperylene it is not since the π-system for this chromophore is non-planar. Comparing the reorientation behavior of perylene with that of 1-methylperylene allows us to evaluate whether or not measurable contributions from weak dipolar solvation effects are present in addition to the dominant van der Waals interactions.

1-Methylperylene ($C_{21}H_{14}$, FW = 266.34) can be synthesized from perylene in one of two ways. The first method used in our laboratory, developed by Zieger and Laski,[13] involved the addition of methyl lithium to perylene in benzene with heating to obtain a reported yield of 33%. The second method, by Peake, *et al.*[14], contrasts the first method

by cooling to -78°C, in dry tetrahydrofuran (THF) in an attempt to slow the kinetics of the alkyl addition. The reported yield of this second synthesis scheme was 85 ± 5%. Both methods were attempted in our laboratory, and the method reported by Peake *et al.* was preferred, because of higher yield and "one-pot" (single reaction vessel) procedure. The experimental schemes, procedures, and our results are outlined here. Spectroscopic data and separation techniques are also supplied in an attempt to provide a more complete synthetic procedure.

Synthesis Scheme 1

Scheme 1 – Synthesis of 1-methylperylene through alkylation of perylene with methyllithium.

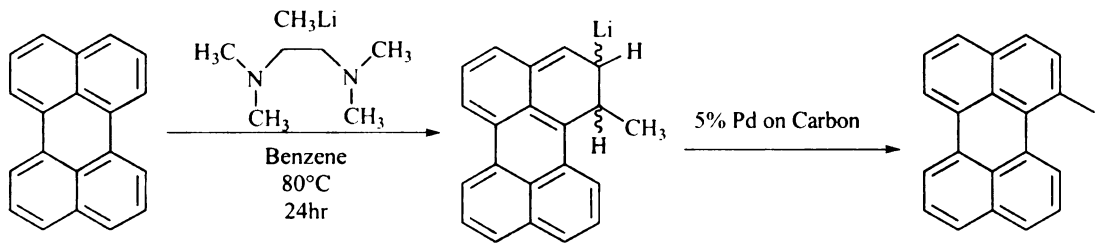

Scheme 1 illustrates the method of Zieger and Laski.[13] In this method, a 500mL, three necked round bottom flask is equipped with a condensor sealed with a rubber septum and a second rubber septum equipped with a nitrogen inlet, and an addition funnel. A magnetic stir bar, heating mantel and magnetic stirring plate were also used. The reaction vessel is charged with perylene (5 g, $C_{20}H_{14}$, FW = 252.31, 20 mmol) in 400 mL of benzene and purged with nitrogen for 30 min. 5 mL of methyl lithium in benzene (1.4 M, 7 mmol) was added through the septum in the condensing column using a nitrogen-purged syringe. 10 mL of N, N, N', N'-tetramethylethylenediamine (FW = 116.21, 66 mmol) was added to the reaction using a nitrogen-purged syringe, to serve as an electron donor. The solution color turned to a dark green upon the addition of the N,

N, N', N'-tetramethylethylenediamine. The reaction was refluxed under nitrogen for 24 h, with stirring. The reaction subsequently quenched using 100 mL of 2 M HCl. The organic layer was then separated, dried using sodium sulfate, and concentrated. The crude product was crystallized from hexane and ethanol. Subsequent recrystallization from ethanol, afforded an orange solid. This powder was redissolved in ethanol and heated. To this orange colored solution, ~0.3 g of 5% wt. palladium on activated carbon was added to the solution and stirred for 30 min. The carbon was removed through vacuum filtration. The orange solution was observed to have turned yellow in color. Concentration of this solution afforded a dark orange solid. ^{1}H NMR of the recovered solid showed that a peak at 2.9 ppm (s, 3H) indicative of the methyl group added to the perylene system.

Separation of the product and the starting material was not a trivial task. The change in the polarity from perylene to 1-methylperylene is not significant enough to achieve baseline resolution between the two peaks in any of the chromatographic separation schemes attempted in our laboratory. Thin layer chromatography was attempted using a series of solvent systems suggested through consultations with the members of the MSU Organic area. Hexane/ethyl acetate, cyclohexane/ethyl acetate, and petroleum ether/ethyl acetate were examined, along with reverse phase thin layer chromatography, with 95/5 (v/v) acetonitrile/water as the mobile phase. 95/5 (v/v) cyclohexane/ethyl acetate together with extended elution times had the best results for thin layer chromatography. This process is labor intensive, and the recovered product for each separation is very small. Several hundred milligrams are required for the rotational diffusion and vibrational population relaxation measurements in this dissertation, and the

throughput, coupled with the reported and observed low yields was insufficient to produce enough material in a timely manner. A suggestion was made from the MSU Organic area to attempt to separate the 1-methylperylene and perylene using column chromatography. A 97/3 (v/v) petroleum ether/ethyl acetate mobile phase were found to work best for with 200-mesh silica gel as the stationary phase. Because the crude product was only slightly soluble in petroleum ether, the sample was added to the column by creating a slurry with a minimal amount of tetrahydrofuran (THF), and silica gel and dried under vacuum. This was deposited at the top of the column, and then eluted with the solvent system specified above. Because the reaction has an inherent low yield, separation of the product from the starting material was still difficult, and did not produce sufficient quantities of material for the spectroscopic experiments. Consultations with the MSU Organic area resulted in another literature search for additional information about a more efficient methodology.

The challenges associated with the method of Zieger and Laski[13] are numerous. The low yield and separation make it a labor intensive, inefficient process. With this methodology, the introduction of water anywhere in the system will react with the methyl lithium and quench it. The system must be devoid of all water, including solvents, glassware, and syringes used. Proper handling of air sensitive reagents must be maintained. Failure to do so will adversely affect the yield, as shown here. Few of these techniques were observed during the first attempt using the procedure of Zieger and Laski, and this resulted in a lower yield being obtained in our laboratory than what was reported in the literature, and contributed to the inability to recover any useful product.

Synthesis Scheme 2

With these challenges, a second search for alkylation methodology was performed. A second method, developed by Peake *et al.*[14] was found, and is presented in Scheme 2. This method, was reported to have a higher yield than the Zieger and Laski[13] method (85 ± 5% vs. 33%), and was performed in a single reaction vessel, an improvement over the first method.

Scheme 2 - The alkylation of perylene using methyl lithium/lithium bromide to form 1-methylperylene.

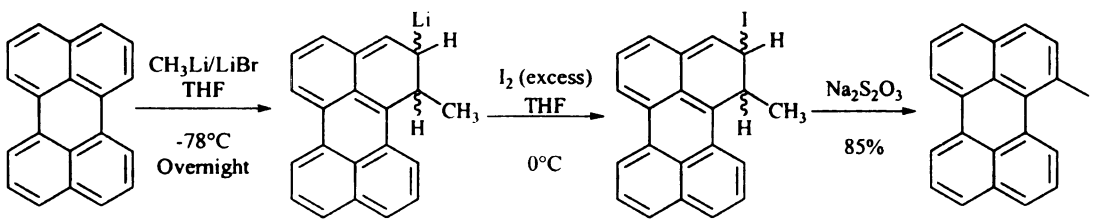

In this method, a 1000 mL oven-dried three necked round bottom flask is charged with perylene (2 g, $C_{20}H_{14}$, FW = 252.31, 8 mmol) in 500 mL of dry tetrahydrofuran (THF). The THF was distilled from sodium metal and benzophenone ketyl. The reaction vessel is equipped with three rubber septa, and a magnetic stir bar with a magnetic stirrer. A positive pressure of nitrogen was maintained throughout the experimental procedure. The reaction was cooled to ~ -78°C using a dry ice/acetone bath. 11 mL of methyl lithium/lithium bromide complex (1.5 M, 20 mmol) was added using a dry, purged syringe and a syringe pump over the course of 1 hr with stirring. The solution color turned to a dark green upon addition of the lithium complex. 1 hr after the addition of the lithium complex, the cooling bath was removed. The reaction vessel was allowed to slowly warm to room temperature overnight, with stirring. The reaction was then cooled to 0°C and 7 g of iodine was added in one portion. The reaction continued to stir for 6.75

h after the iodine addition. This is much longer than the specified procedure[14] of 15 min. The time was extended as ^{1}H NMR of initial experiments (not shown) indicated the existence of possible intermediates that could have been reacted with longer decomposition times.

The solution was then diluted with 500 mL CH_2Cl_2 to minimize the size of the emulsion that will form with THF/water mixtures. To decompose any excess iodine, the solution was washed with saturated aqueous sodium thiosulfate (2x 400 mL). The recovered organic phase was then washed with water (2x 200 mL), and brine solution (2x 200 mL). The organic phase dried over $MgSO_4$ and concentrated. The crude product was then purified using silica gel column chromatography. The solvent system of 70/30 (v/v) hexane/methylene chloride suggested by Peake *et al.*[14] did not separate the products satisfactorily. Testing determined that a better solvent system for the column chromatography was 95/5 (v/v) petroleum ether/ethyl acetate.

The fractions containing the desired product were then combined, and concentrated. ^{1}H NMR of the concentrated product indicated the desired singlet at 2.9 ppm, attributed to the methyl group and the multiplet between 7.37 and 8.18 ppm, in the aromatic region had the appropriate integration of 10.73. The crude product was then recrystallized twice from hexane and ethanol affording the desired product as yellow/orange plates, 0.3185 g, 16% yield. The difference in yield to that reported[14] is attributed to the difference in ability level of the members of our laboratory and the research team of Peake *et al.*

The ^{1}H NMR for pure perylene and the purified 1-methylperylene product are presented in Figure 9 and Figure 10, respectively. The melting point of the purified

product was determined to be 116-120°C, in accordance with published values for 1-methylperylene.[13] Mass spectrometry of the purified 1-methylperylene product shows a parent peak at m/z = 266.2 and a peak at 252.2 in a 7.25:1 ratio. These peaks are in accordance with published data.[13] A typical absorption/emission set for perylene and 1-methylperylene in methanol respectively, are provided in Figure 11 and Figure 12 for reference. The absorption and emission maxima were observed to be 433.5 and 435.5 nm for perylene in methanol, and 425.5 and 436.0 nm for 1-methylperylene in methanol. These values are within experimental agreement with similar solvents.[13,15] The linear response is also observed to be broader for 1-methylperylene than for perylene in the same solvent.

The second synthetic scheme of Peake *et al.*[14] was applied in our laboratory to obtain a sufficient amount of desired product in a short amount of time. The single reaction vessel, and straightforward purification procedure provided for a reasonable throughput so that these probe molecules can be used with sufficient specificity and purity in the spectroscopic experiments outlined elsewhere in this work.

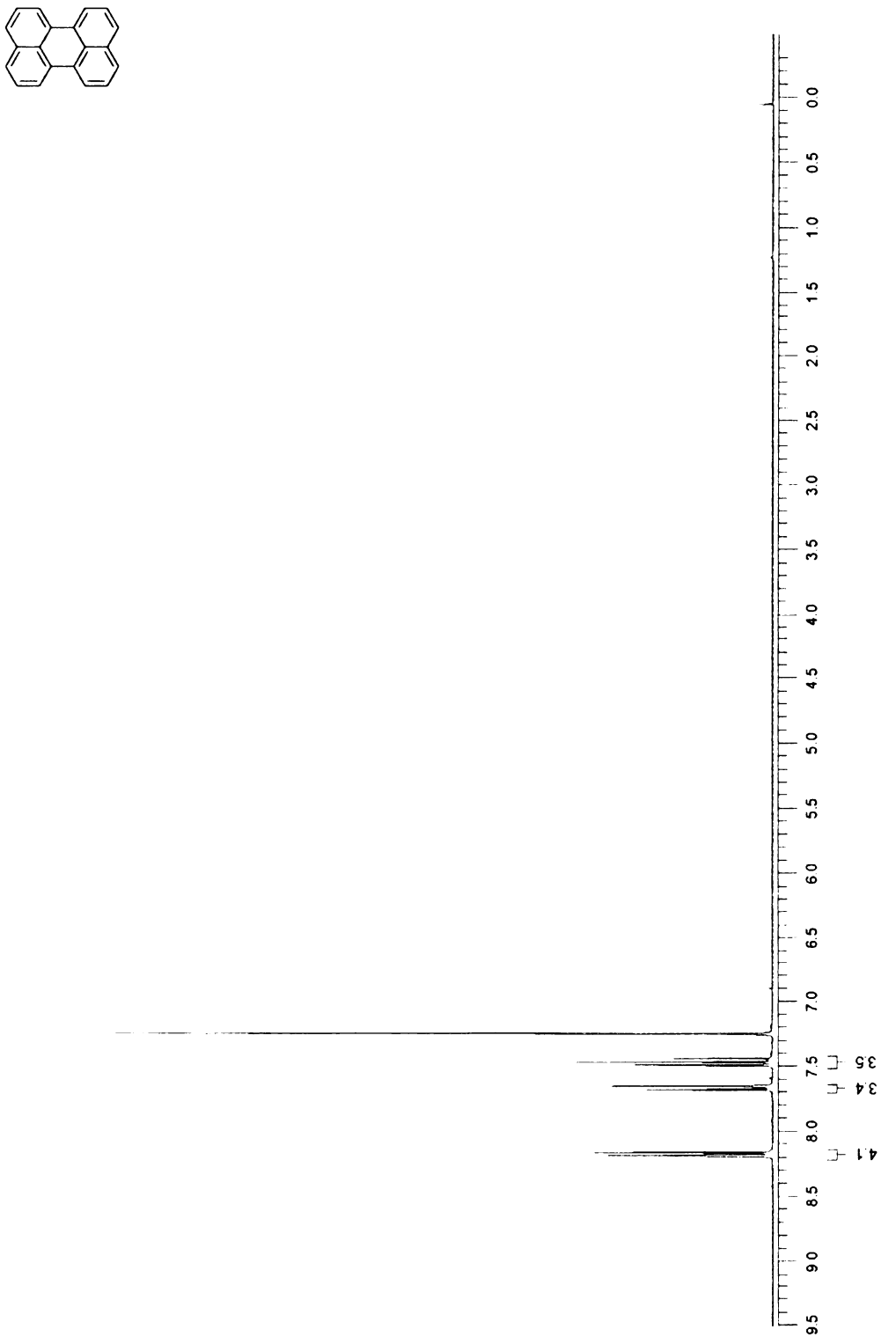

Figure 9 – 300 MHz ^{1}H NMR of perylene in d-CH_2Cl_2. The structure of the perylene molecule is shown in the inset.

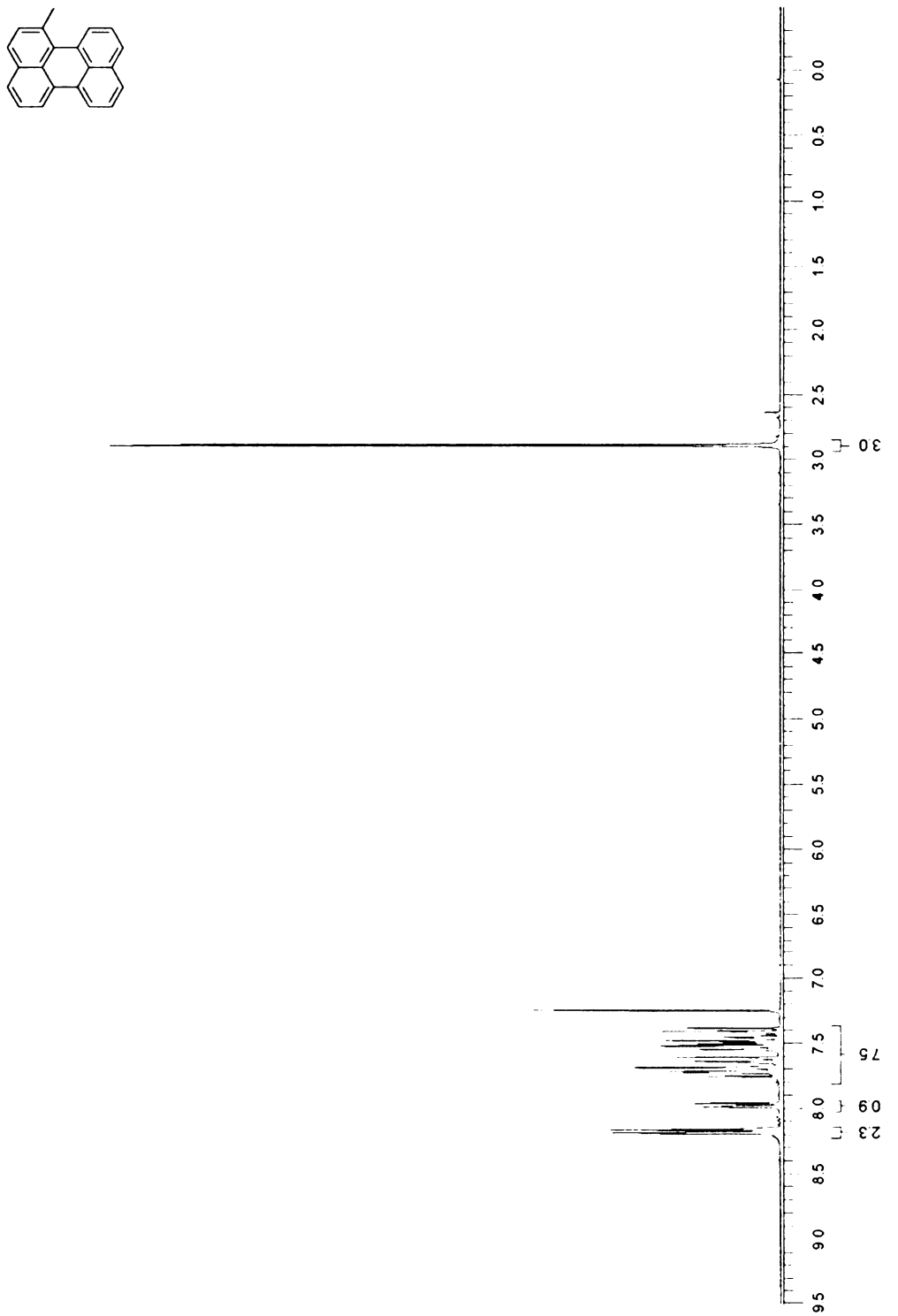

Figure 10 – 300 MHz ^{1}H NMR of 1-methylperylene in d-CH_2Cl_2. The structure of the 1-methylperylene molecule is shown in the inset.

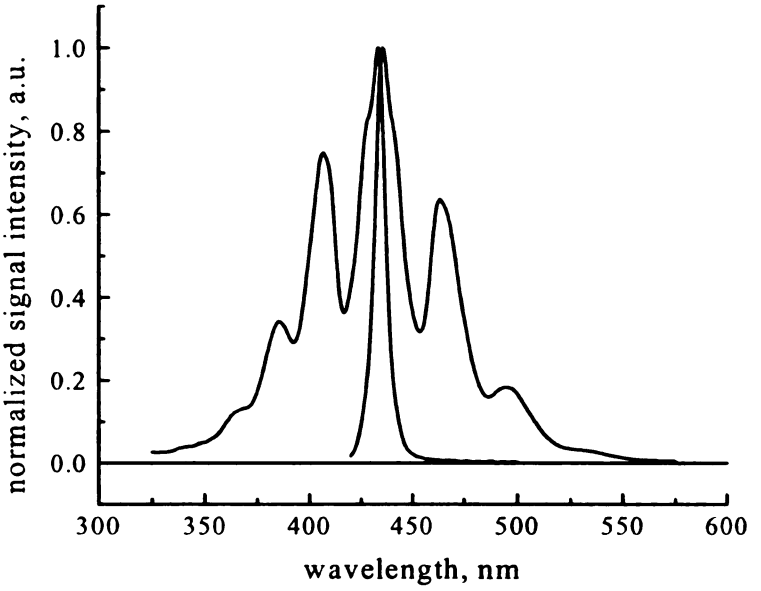

Figure 11 – Absorbance and emission spectra for perylene in methanol. Data has been normalized for presentation.

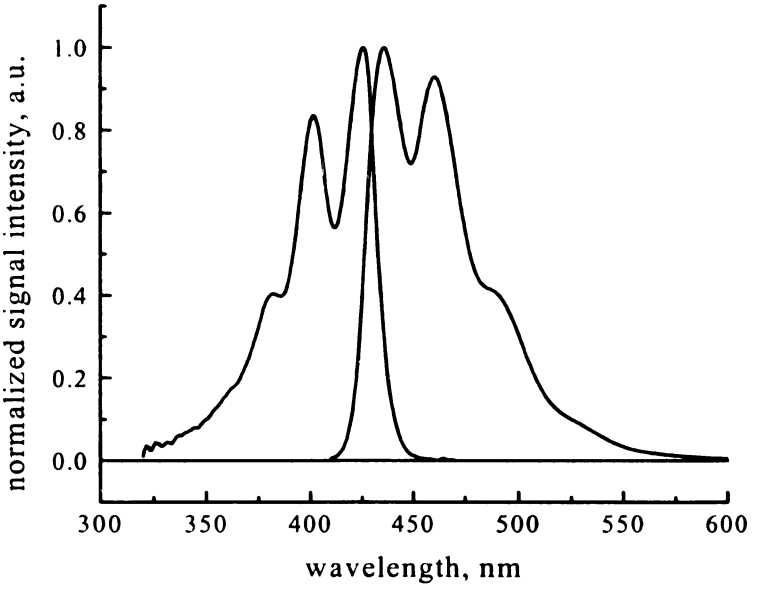

Figure 12 – Absorption and emission spectra for 1-methylperylene in methanol. Data has been normalized for presentation.

Literature Cited

1. Jiang, Y.; Blanchard, G. J.; *J. Phys. Chem.*, **1994**, *98*, 6436.
2. Brocklehurst, B.; Young, R. N.; *J. Phys. Chem.*, **1995**, *99*, 40.
3. Pauls, S. W.; Hedstrom, J. F.; Johnson, C. K.; *Chem. Phys.*, **1998,** *237,* 205
4. Hambir, S. A.; Jiang, Y.; Blanchard, G. J.; *J. Chem. Phys.*, **1993**, *98*, 6075.
5. Jiang, Y.; Blanchard, G. J.; *J. Phys. Chem.*, **1994**, *98*, 9411.
6. Jiang, Y.; Blanchard, G. J.; *J. Phys. Chem.*, **1994**, *98*, 9417.
7. McCarthy, P. K.; Blanchard, G. J.; *J. Phys. Chem.*, **1995**, *99*, 17748.
8. McCarthy, P. K.; Blanchard, G. J.; *J. Phys. Chem.*, **1996**, *100*, 5182.
9. Lewitzka, L.; Lohmannsroben, H.-G.; Strauch, M.; Luttke, W.; *J. Photochem. Photobiol. A: Chem.*, **1991**, *61*, 191.
10. Grimme, S.; Lohmannsroben, H.-G.; *J. Phys. Chem.*, **1992**, *96*, 7005.
11. Calculated using Hyperchem V 4.0.
12. Jiang, Y.; Blanchard, G. J. *J. Phys. Chem.* **1995**, *99*, 7904.
13. Zieger, H. E.; Laski, E. M. *Tetrahedron Lett.* **1966**, *32*, 1966
14. Peake, D. A.; Oyler, A. R.; Heikkila, K. E; Liukkonen, R. J; Engroff, E. C.; Carlson, R. M. *Synth. Commun.* **1983**, *13*, 21.
15. Campbell, A. D.; Elder, R. S.; Emerson, C. W. *J. Chem. Soc.* **1959**, 3526.

Chapter 2

ORIENTATIONAL AND VIBRATIONAL RELAXATION DYNAMICS OF PERYLENE AND 1-METHYLPERYLENE IN *N*-ALKANOLS: SUBTLE DIFFERENCES IN SOLVENT-SOLUTE INTERACTIONS[1]

Introduction

Understanding the details of interactions between solvents and solutes has received a great deal of attention by the chemistry community because of the importance of these interactions in determining properties such as chemical reaction yield and kinetics, or the ability to isolate one compound from another. Interactions between solutes and their surrounding solvent molecules are difficult to resolve because, unlike solids, the spatial relationships between the molecules are not fixed on time scales that can be accessed using structural measurements such as X-ray diffraction or multidimensional NMR spectrometry. Intermolecular interactions in the liquid phase are more complex than those in the gas phase because of their characteristic strength, the property that gives rise to the liquid phase and at the same time prevents a simple statistical description of collisional interactions from providing adequate insight. For these reasons, time domain spectroscopies have found particular favor in the investigation of solvation processes.

There are essentially three time-resolved spectroscopic approaches to the measurement of solvent-solute interactions. These are measurement of the time-delayed fluorescence Stokes shift (TDFSS) of selected solutes,[2-11] rotational diffusion[12-32] and vibrational population relaxation.[33-45] Of these, TDFSS measurements have provided the most insight into the early-time separation of inertial and diffusive contributions to

solvent reorganization about excited solute molecules, and at the same time these reports have proven to be the most controversial in terms of their interpretation.[46-50] Perhaps the most significant issue that needs to be addressed regarding TDFSS measurements is the lack of generality of the effect. Despite the broad conclusions drawn from these experimental results, only a handful of chromophores with complicated spectroscopic responses are known to exhibit resolvable transient Stokes shifts.[2,51] The two other approaches to the measurement of solvent-solute interactions do not offer the same time-resolution as the TDFSS measurements, but the phenomena of rotational diffusion and vibrational relaxation are not limited to a few chromophores - these are general effects, and the characteristic time scales over which they proceed are consonant with chemical reaction processes. We concentrate here on the rotational diffusion and vibrational population relaxation dynamics of perylene and 1-methylperylene in the *n*-alkanols methanol through *n*-decanol. We have chosen these probe molecules because they are relatively well characterized[30-32,40-45] and because literature reports on their solution phase dynamical behavior leave open some significant questions.

Perylene has been studied more extensively than 1-methylperylene. Several reports on the reorientation dynamics of perylene point to solvents in which a two-component anisotropy decay is seen[31,32] and others where there is only a single decay.[30] It is important to understand the fundamental basis for these results and the data we present here provide some insight into this matter. Comparing the reorientation behavior of perylene with that of 1-methylperylene allows us to evaluate whether or not there is a measurable contribution from (weak) dipolar solvation effects in additional to the dominant van der Waals interactions. We reported previously that the reorientation of

perylene in *n*-alkanes pentane through hexadecane yielded single exponential anisotropy decays[30] and the nature of the solvent-solute frictional interactions changed as the length of the solvent molecule became similar to that of the solute. For 1-methylperylene in these same solvents, we found that there was a clear break in the anisotropy behavior at the same point, but the measured change was not simply a change in the frictional boundary condition, but a shift in the functionality of the anisotropy decay from single to double exponential.[43] Such a change is consistent with a substantial alteration of the way in which the 1-methylperylene chromophore reorients in the longer alkane solvents. These data point to a qualitative change in the nature of solvent-solute interactions that depends on the relative lengths of the molecules, but a broader picture of the solvation of these two molecules has yet to emerge.

We have measured vibrational population relaxation from the ~1375 cm^{-1} ring breathing modes of perylene and 1-methylperylene to understand the role of "structural" factors in mediating solution phase vibrational excitation transport. We have found that both the spatial separation between vibrational donor and acceptor moieties and their relative orientation are important in mediating vibrational excitation transport.[45] Interestingly, it is not the acceptor density that determines the efficiency of transport. The ability of the donor and acceptor vibrational coordinates to align with one another mediates vibrational excitation transport for 1-methylperylene in the alkanes. In contrast to the reorientation measurements, the vibrational population relaxation dynamics of these two chromophores cannot be compared directly because the efficiency of donor-acceptor coupling is determined by the symmetry of the chromophores.[43] Using our two-pulse measurement scheme, systems that possess a center of inversion, such as perylene,

will necessarily couple to the solvent bath modes according to the modulation of the solute's quadrupole moment. For donors without a center of inversion, such as 1-methylperylene, the modulation of the solute dipole moment by vibrational motion mediates excitation transport. These two coupling processes operate over different length scales (r^{-8} vs. r^{-6}) and thus it is not possible to compare results directly. Despite the differences of scale, the solvent-dependent trends observed in the T_1 data for the two molecules provide insight into the average spatial relationship between donor and acceptor functionalities in solution.

Comparison of the reorientation and vibrational population relaxation dynamics we report here for perylene and 1-methylperylene in the *n*-alkanols yields significant information on the nature of the solvent-solute interactions the chromophores experience. A key difference between the *n*-alkanes and *n*-alkanols is the extent to which solvent self-association determines their properties.[22,52] We find from the reorientation measurements that self-association of the alcohols determines the immediate environment of the chromophores to a significant extent, especially for the longer *n*-alkanes. The vibrational population relaxation data suggest that, for the longer *n*-alkanols, perylene appears to associate with the non-polar aliphatic chains while the more polar 1-methylperylene interacts with the solvent alcohol functionality. These results are not surprising but do reveal the point at which solvent size, relative to the chromophore, becomes important for amphiphilic systems.

Experimental

Laser system: The picosecond pump-probe laser spectrometer used for both the reorientation and vibrational population relaxation measurements has been described in detail previously,[53] and we present only a brief outline of its performance characteristics here. A mode-locked CW Nd:YAG laser (Coherent Antares 76-S) produces 30 W of average power (1064 nm, 100 ps pulses, 76 MHz repetition rate). The output of this laser is frequency-tripled to produce ~1.3 W of average power at 354.7 nm. The third harmonic light is used to excite two cavity-dumped dye lasers (Coherent 702) synchronously. Both lasers operate with Stilbene 420 laser dye (Exciton). The output of each laser is ~100 mW average power at 8 MHz repetition rate with a pulse that produces a 7 ps FWHM autocorrelation trace using a three plate birefringent filter. The pump laser wavelength was set between 429.7 nm and 438.9 nm, depending on the chromophore and solvent, while the probe laser was set in the range of 456.7 nm to 463.1 nm. The pump wavelength was chosen to access the 0-0 transition of the chromophore and the probe wavelength to stimulate emission from the $S_1^{v=0}$ state to the $S_0^{v=1}$ state, where the vibrational resonance of interest is the 1375 cm^{-1} v=1 ring breathing mode. These wavelengths were used for the vibrational relaxation and the reorientation measurements. Our previous work has demonstrated that the ground state and excited state reorientation behavior of perylene are identical[30] and we assume that this is also the case for 1-methylperylene. The probe laser polarization was set alternately to 0° and 90° relative to the pump laser polarization for the reorientation measurements, and to 54.7° for the vibrational relaxation measurements. The time resolution of this system, ~10 ps, is determined by the cross-correlation between the pump and probe laser pulse trains.

Detection of the transient signals was accomplished using a radio and audio frequency triple-modulation scheme, with synchronous demodulation detection.[54-56] Each reported time constant is the average of at least six individual determinations that are themselves the average of seven to ten time-scans.

Steady State Spectroscopy: The steady state absorption spectra of both chromophores in the *n*-alkanols were recorded with 1 nm resolution using a Hitachi U-4001 spectrometer. The spontaneous emission spectra for the same solutions was obtained with 1 nm resolution using a SPEX Fluorolog2 Model F111AT spectrometer. These data were used to determine the appropriate laser wavelengths for each chromophore/solvent pair. The absorption and emission spectra for perylene and 1-methylperylene in *n*-pentanol are shown in Figure 13 and Figure 14. We understand the details of these spectral profiles and describe them in the next section.

Chemicals and Sample Handling: Perylene (99.5%, sublimed) was obtained from Aldrich Chemical Company and used as received. 1-Methylperylene was synthesized by using the procedure of Peake *et al.*,[57] which is selective for methylation at the 1-position, and outlined in Chapter 1 of this dissertation. All other solvents were obtained from Aldrich Chemical Company at the highest purity possible, and used as received. To minimize thermal lensing considerations, sample solutions were flowed through a 1 mm path length quartz flow cell. The sample temperature was controlled at 300 ± 0.1 K using a thermostated bath.

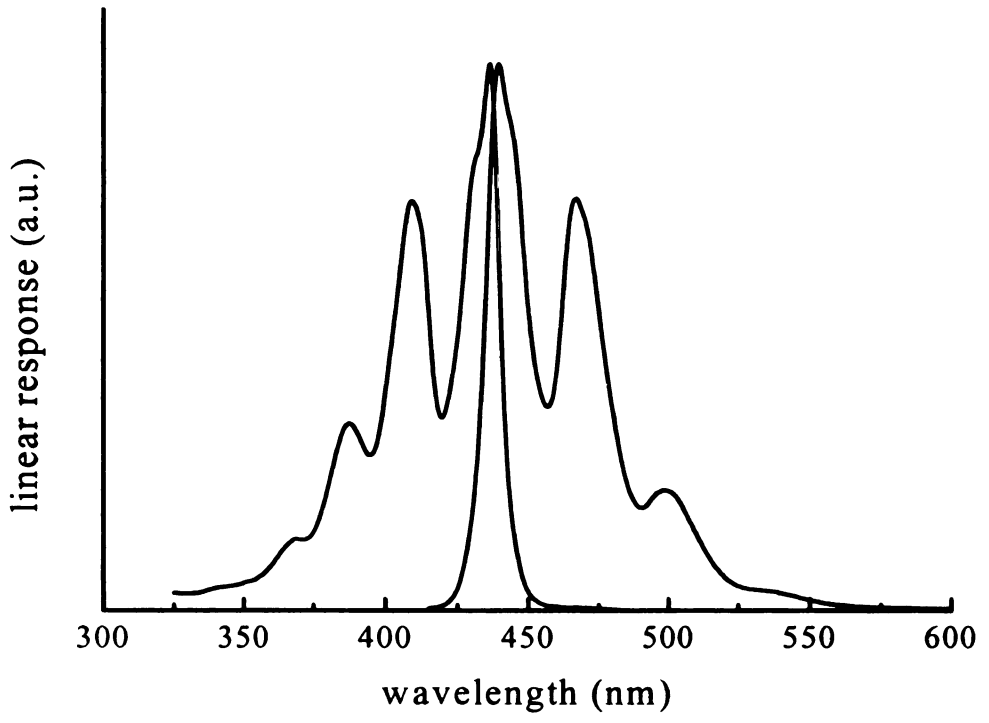

Figure 13 – Absorption and emission spectra for perylene in *n*-pentanol. Data has been normalized for presentation.

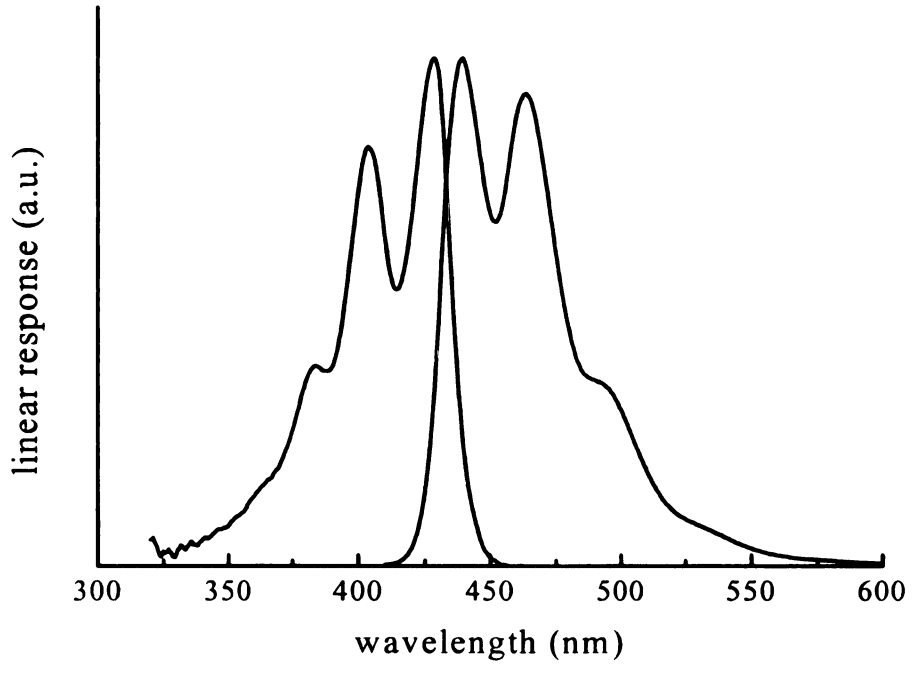

Figure 14 – Absorption and emission spectra for 1-methylperylene in *n*-pentanol. Data has been normalized for presentation.

Results and Discussion

The focus of this chapter is on understanding the solvent-solute interactions of perylene and 1-methylperylene in the *n*-alkanols. Placing our results in the context of previous work on these same chromophores will allow us to gain insight into the dominant intermolecular interactions of these probe molecules. While the majority of the information on the solvation behavior of these probes is obtained from the time domain measurements, it is important to understand their steady state optical responses because they are reflective of the average environment they experience.

Steady State Linear Spectroscopy. Among the reasons for using perylene and 1-methylperylene for these studies is the well-behaved optical response of each molecule. The quasi-mirror image absorption and emission spectra demonstrate the relatively small role that vibronic coupling plays in these data[58] and the Stokes shift of 1-methylperylene compared to that of perylene points to the presence of a small but finite permanent dipole moment in 1-methylperylene. PM3 semi-empirical calculations indicate $\mu \sim 0.24$ D in the S_0 and 0.53 D in the S_1 for 1-methylperylene.[59]

The linear responses of solutes can provide significant insight into the dielectric properties of the solvent. For example, the absorption maximum of the polar chromophore oxazine 725 exhibits a solvent polarity-dependent red shift in *n*-alkanol solvents up to *n*-heptanol.[25] Comparison of those data to the oxazine 725 absorption maximum in DMSO reveals that at least one contribution to the polarity-dependent spectral shift is solvent H-bonding. For the chromophores we use here, H-bonding almost certainly does not play the same role, but it is clear that there is a solvent-dependence to their absorption maxima. Before considering this point, we need to

account for the differences in the linear response of perylene and 1-methylperylene. The absorption maximum of perylene is red shifted from 1-methylperylene for a given solvent and the individual features in the 1-methylperylene spectra are less well-defined. We understand these differences as arising from the fact that the methyl group on 1-methylperylene causes the two naphthalene moieties to be cocked at ~ 20° with respect to one another.[60,61] The resulting slight break in conjugation causes the blue shift and the reduction in symmetry causes additional vibrational resonances to become allowed, adding to the greater width of the absorption and emission spectral features. The solvent dependence of the absorption maxima of perylene and 1-methylperylene are shown in Figure 15. First, we note that the solvent-dependence for perylene and 1-methylperylene appear to be identical and, if plotted in terms of relative shift with respect to the band position in methanol (not shown) the results for the two chromophores are identical. We understand these shifts in the context of the chromophore ground and excited states being solvated more efficiently with increasing aliphatic chain length of the alkanol solvent. The excited states of the chromophores are solvated more efficiently than the ground states, presumably because van der Waals interactions between the solvent aliphatic chains and the chromophore π^* states are stronger than those for the ground state. These data are reminiscent of those for oxazine 725 in the same solvents, except that we do not see a saturation in the spectral red shift with increasing aliphatic chain length. We interpret this difference in terms of the affinity for the ionic dye oxazine 725 for the alcohol functionality and the preference of perylene and 1-methylperylene for the aliphatic portion of the solvent. These data suggest that the balance of interactions

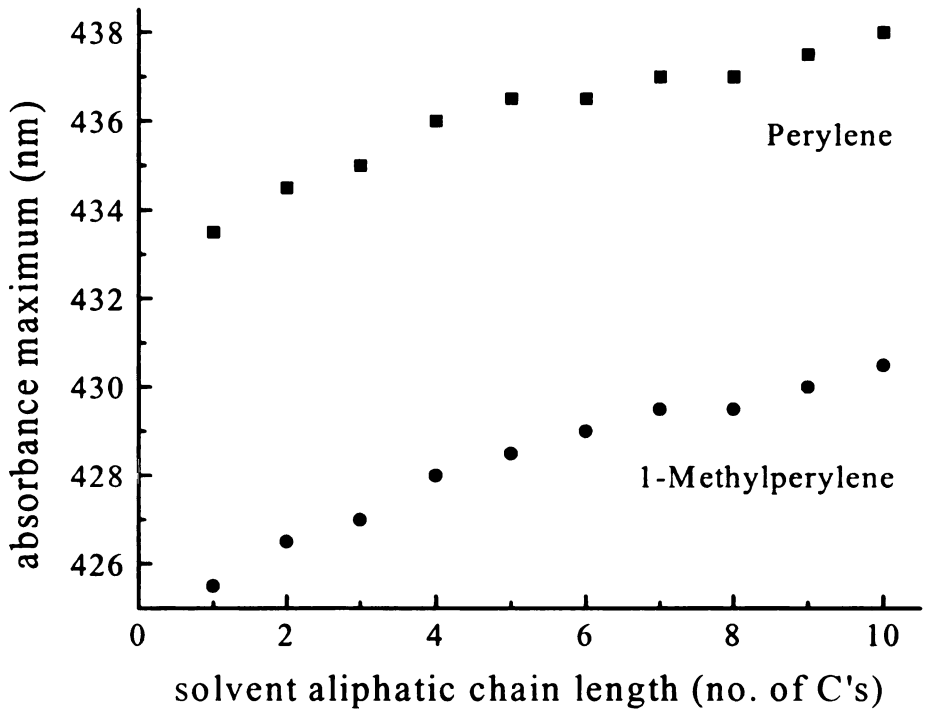

Figure 15 – Dependence of perylene and 1-methylperylene absorption maxima on solvent aliphatic chain length. When normalized for wavelength shift relative to their absorption spectra in methanol, the solvent dependencies are identical for both chromophores.

between the different functionalities of these solvents will be important in understanding the transient data we consider next.

Molecular reorientation. Of the time domain spectroscopies used in the study of solvent-solute interactions, molecular reorientation measurements are supported best by a theoretical framework for the interpretation of the experimental data.[62-67] The starting point for relating reorientation data to solvent and solute properties is the modified Debye-Stokes-Einstein (DSE) equation,[62,63,65-67]

$$\tau_{OR} = \frac{\eta V f}{k_B T S} \qquad (6)$$

In Equation (6), η is the solvent viscosity, V the solute hydrodynamic volume (225 $Å^3$ for perylene and 243 $Å^3$ for 1-methylperylene),[68] f is a frictional interaction term to account for frictional contributions to solvent-solute interactions, k_B is the Boltzmann constant, T is the temperature and S is a shape factor to account for the non-spherical shape of the solute. The DSE equation is clearly not intended to account for specific molecular-level interactions between molecules, and it is clear that any description of solvation phenomena based on solvent bulk properties must be incomplete. These limitations notwithstanding, the modified DSE model provides remarkably close agreement with many experimental results and it thus serves as a useful starting point in any discussion of reorientation measurements.

Experimentally, the time-dependencies of the stimulated gain signal on the probe beam, polarized parallel ($I_{\parallel}(t)$) and perpendicular ($I_{\perp}(t)$) to the pump beam, are used to extract information on the re-randomization of the anisotropic distribution of chromophores selected by the pump pulse, Equation (7):

$$R(t) = \frac{I_{\parallel}(t) - I_{\perp}(t)}{I_{\parallel}(t) + 2I_{\perp}(t)} \qquad (7)$$

The most common result for reorientation measurements is to recover an experimental R(t) function that decays as a single exponential, with the time constant of this decay being taken as τ_{OR}. Such data are often interpreted in the context of Equation (6). There are a number of experiments, however, where R(t) is found to decay with a multiple exponential functionality,[23,31,42,69] or depends on the manner in which the chromophore is excited.[12,32] In these cases, Equation (6) is clearly not sufficient. Chuang and Eisenthal have formulated the relationship between R(t) and solute properties such as the angle between the excited and probed one photon transition moments and the actual anisotropy in the diffusion constant.[64] They found that R(t) can decay with as many as five exponential components, although the most common case is that of a single exponential. In cases where more than one decay component is resolved, it is possible to interpret the details of the reorientation dynamics in substantial detail.

For the purposes of the following discussion, we consider that the chromophores have their π-system in the approximate *xy* plane with *x* being the long, in-plane axis, and *z* is perpendicular to the π-system plane. For each chromophore our intention was to assign the coordinate system such that the *x*-axis coincides with the absorption transition moment. For perylene this assignment is coincident with specific bond axes because of its high symmetry while for 1-methylperylene it is not since the π-system for this chromophore is non-planar. Using these approximations and Chuang and Eisenthal's equations,[64] we can relate the experimental reorientation times to the shape of the volume swept out by the rotating molecule. We describe this volume in terms of ellipsoids,

where a prolate ellipsoid, Equation (8) and Figure 16, is characterized by rotation primarily about its long in-plane axis, $D_x > D_y \sim D_z$ and an oblate ellipsoid, Equation (9) and Figure 17, by is characterized by rotation about the axis perpendicular to the chromophore π-system, $D_z > D_x \sim D_y$.

Prolate: $R(t) = 0.4\exp(-6D_z t)$ (8)

Oblate: $R(t) = 0.3\exp(-(2D_x + 4D_z)t) + 0.1\exp(-6D_x t)$ (9)

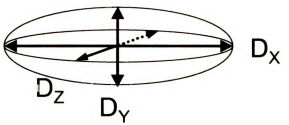

Figure 16 – Prolate ellipsoid with Cartesian coordinate system superimposed. See text for discussion.

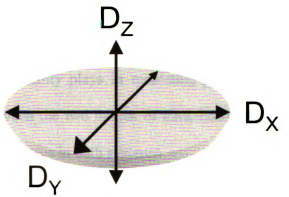

Figure 17 – Oblate ellipsoid with Cartesian coordinate system superimposed. See text for a discussion.

For both perylene and 1-methylperylene in the *n*-alkanols, we measure experimental R(t) functions that are fit best by the sum of two exponential decays (Table 1, Table 2, Figure 18, and Figure 19.) The solvent dependence of the fitted times is presented in Figure 20. Using Equation (8) to interpret our data, we can obtain the quantities D_z and D_x. We show the diffusion constants as a function of solvent aliphatic chain length in Figure 21, and their ratio in Figure 22. These data on 1-methylperylene are consistent with those reported in the *n*-alkanes because, in both cases, they trend toward an increasing ellipsoidal aspect ratio with increasing solvent aliphatic chain length. In our previous work,[43] for *n*-alkanes octane and shorter, we recovered ratio $D_z/D_x < 1$ and in this work, D_z/D_x ranges from ~4 to ~8.5. Also, in the *n*-alkanes, we see that the ellipsoid aspect ratio saturates at ~ 8.5 for sufficiently long alkanes.[43] For 1-methylperylene in *n*-decanol, $D_z/D_x \sim 8.5$. It is not clear that this is a saturation value because we have not used longer *n*-alkanols because *n*-dodecanol has been shown to form a mesophase between 24°C and 30°C.[22] Clearly the data on 1-methylperylene in the two families of solvents are not identical but this is not surprising because of the important role that the alcohol functionality plays in mediating persistent organization.[52,70] The close correspondence between the two bodies of data, however, suggests that the same fundamental physics are operative in both systems.

The data on perylene in the alkanes and alkanols provide less in the way of direct correspondence. For *n*-alkanes up to *n*-hexadecane,[32] methanol and ethanol we recover a single exponential decay and for *n*-alkanols propanol through decanol we find a two component anisotropy decay. Perylene reorients as a prolate rotor in alkanes and as an

Table 1 – Reorientation times and zero-time anisotropies for perylene in the *n*-alkanols. The data are the best fit results of the data to the function $R(t) = R_1(0)\exp(-t/\tau_1) + R_2(0)\exp(-t/\tau_2)$. Times are given in ps and the uncertainties listed are standard deviations ($\pm 1\sigma$) for at least six determinations of each quantity.

Solvent	$R_1(0)$	τ_1 (ps)	$R_2(0)$	τ_2 (ps)
CH_3OH	0.23±0.06	17±2	--	--
C_2H_5OH	0.11±0.02	30±6	--	--
C_3H_7OH	0.20±0.05	16±4	0.10±0.03	59±17
C_4H_9OH	0.17±0.05	27±8	0.06±0.03	101±39
$C_5H_{11}OH$	0.19±0.09	21±7	0.11±0.03	82±16
$C_6H_{13}OH$	0.19±0.07	28±6	0.11±0.03	110±22
$C_7H_{15}OH$	0.22±0.05	35±7	0.10±0.03	168±29
$C_8H_{17}OH$	0.21±0.04	32±5	0.11±0.01	157±15
$C_9H_{19}OH$	0.20±0.05	33±15	0.14±0.04	146±23
$C_{10}H_{21}OH$	0.20±0.05	37±7	0.15±0.02	217±45

Table 2 – Reorientation times and zero-time anisotropies for 1-methylperylene in the *n*-alkanols. The data are the best fit results of the data to the function $R(t) = R_1(0)\exp(-t/\tau_1) + R_2(0)\exp(-t/\tau_2)$. Times are given in ps and the uncertainties listed are standard deviations ($\pm 1\sigma$) for at least six determinations of each quantity.

Solvent	$R_1(0)$	τ_1 (ps)	$R_2(0)$	τ_2 (ps)
CH_3OH	0.16±0.04	11±2	0.06±0.01	34 ± 5
C_2H_5OH	0.25±0.05	17±2	0.07±0.03	53 ± 13
C_3H_7OH	0.28±0.03	18±2	0.09±0.03	62 ± 6
C_4H_9OH	0.19±0.05	17±3	0.12±0.04	69 ± 14
$C_5H_{11}OH$	0.19±0.06	21±7	0.12±0.05	81 ± 27
$C_6H_{13}OH$	0.21±0.04	23±7	0.13±0.04	107 ± 26
$C_7H_{15}OH$	0.23±0.03	29±4	0.14±0.02	139 ± 15
$C_8H_{17}OH$	0.18±0.02	29±5	0.14±0.02	133 ± 15
$C_9H_{19}OH$	0.16±0.04	28±5	0.17±0.03	132 ± 20
$C_{10}H_{21}OH$	0.21±0.02	40±6	0.11±0.02	206 ± 21

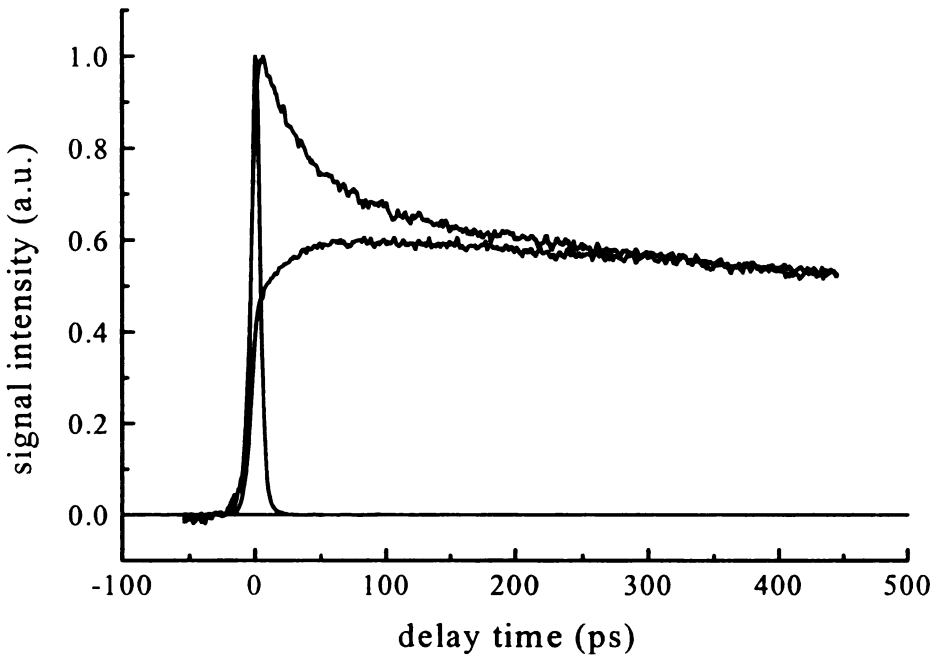

Figure 18 – Experimental $I_{\parallel}(t)$ and $I_{\perp}(t)$ scans for 1-methylperylene in *n*-pentanol, along with the instrumental response function. These data are typical of those recorded for reorientation measurements.

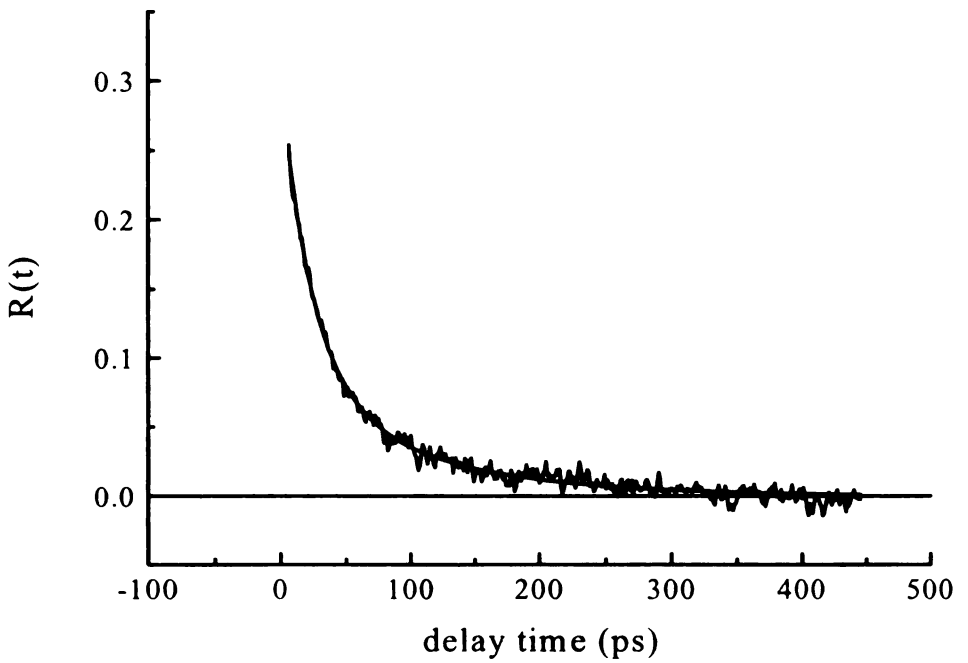

Figure 19 – Anisotropy function, R(t), for the data shown in Figure 18. The decay is fit to the function $R(t) = R_1(0)\exp(-t/\tau_1) + R_2(0)\exp(-t/\tau_2)$

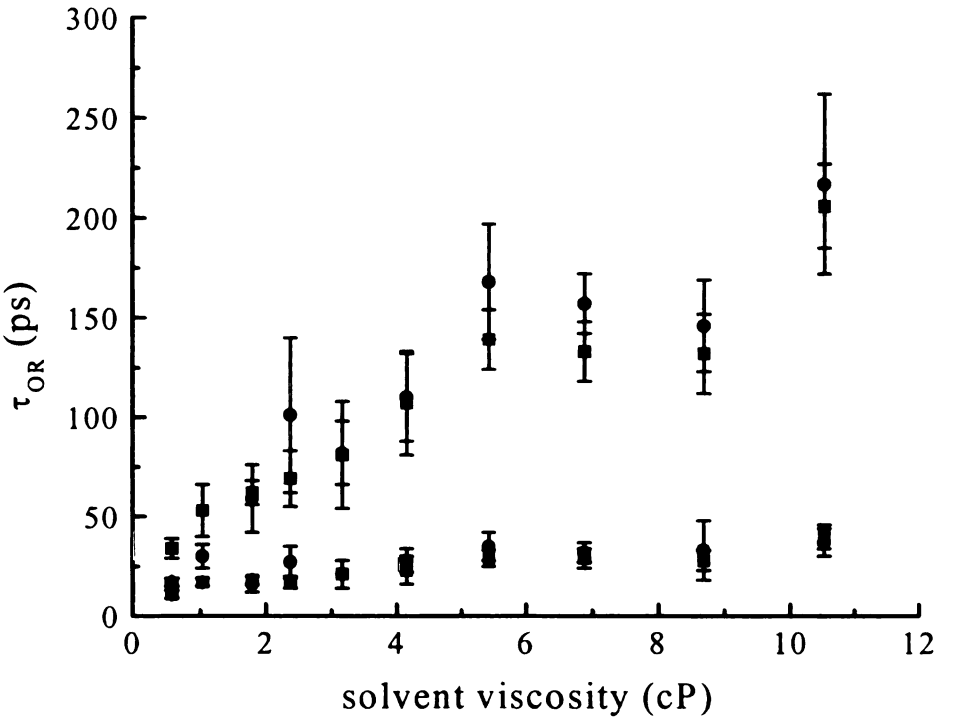

Figure 20 – Reorientation time constants plotted as a function of solvent viscosity for perylene (•) and 1-methylperylene (■). The reorientation time constants are identical to within the experimental uncertainty for the two chromophores in the solvents used. The fast reorientation time is essentially solvent viscosity independent and the dependence of the slow reorientation time does not depend linearly on viscosity.

Table 3 – Cartesian components of the rotational diffusion constant, D, for perylene in the *n*-alkanols. These quantities and their uncertainties are derived from the fitted time constants shown in Table 1.

Solvent	D_x (GHz)	D_z (GHz)	D_z/D_x
CH_3OH	--	9.8 ± 1.2	< 1
C_2H_5OH	--	5.6 ± 1.1	< 1
C_3H_7OH	2.8 ± 0.8	14.2 ± 3.6	5.0 ± 0.4
C_4H_9OH	1.7 ± 0.6	8.4 ± 2.5	5.1 ± 0.5
$C_5H_{11}OH$	2.0 ± 0.4	10.9 ± 3.6	5.4 ± 0.4
$C_6H_{13}OH$	1.5 ± 0.3	8.2 ± 1.8	5.4 ± 0.3
$C_7H_{15}OH$	1.0 ± 0.2	6.7 ± 1.3	6.7 ± 0.3
$C_8H_{17}OH$	1.1 ± 0.1	7.3 ± 1.1	6.9 ± 0.2
$C_9H_{19}OH$	1.1 ± 0.2	7.0 ± 3.2	6.1 ± 0.5
$C_{10}H_{21}OH$	0.8 ± 0.2	6.4 ± 1.2	8.3 ± 0.3

Table 4 – Cartesian components of the rotational diffusion constant, D, for 1-methylperylene in the *n*-alkanols. These quantities and their uncertainties are derived from the fitted time constants shown in Table 2.

Solvent	D_x (GHz)	D_z (GHz)	D_z/D_x
CH_3OH	4.9 ± 0.7	20.3 ± 0.7	4.1 ± 0.2
C_2H_5OH	3.2 ± 0.8	13.1 ± 1.5	4.2 ± 0.3
C_3H_7OH	2.7 ± 0.3	12.5 ± 1.4	4.7 ± 0.1
C_4H_9OH	2.4 ± 0.5	13.5 ± 2.4	5.6 ± 0.3
$C_5H_{11}OH$	2.1 ± 0.7	10.9 ± 3.6	5.3 ± 0.5
$C_6H_{13}OH$	1.6 ± 0.4	10.1 ± 3.1	6.5 ± 0.4
$C_7H_{15}OH$	1.2 ± 0.1	8.0 ± 1.1	6.7 ± 0.2
$C_8H_{17}OH$	1.3 ± 0.1	8.0 ± 1.4	6.4 ± 0.2
$C_9H_{19}OH$	1.3 ± 0.1	8.3 ± 1.5	6.6 ± 0.2
$C_{10}H_{21}OH$	0.8 ± 0.1	5.8 ± 0.9	7.2 ± 0.2

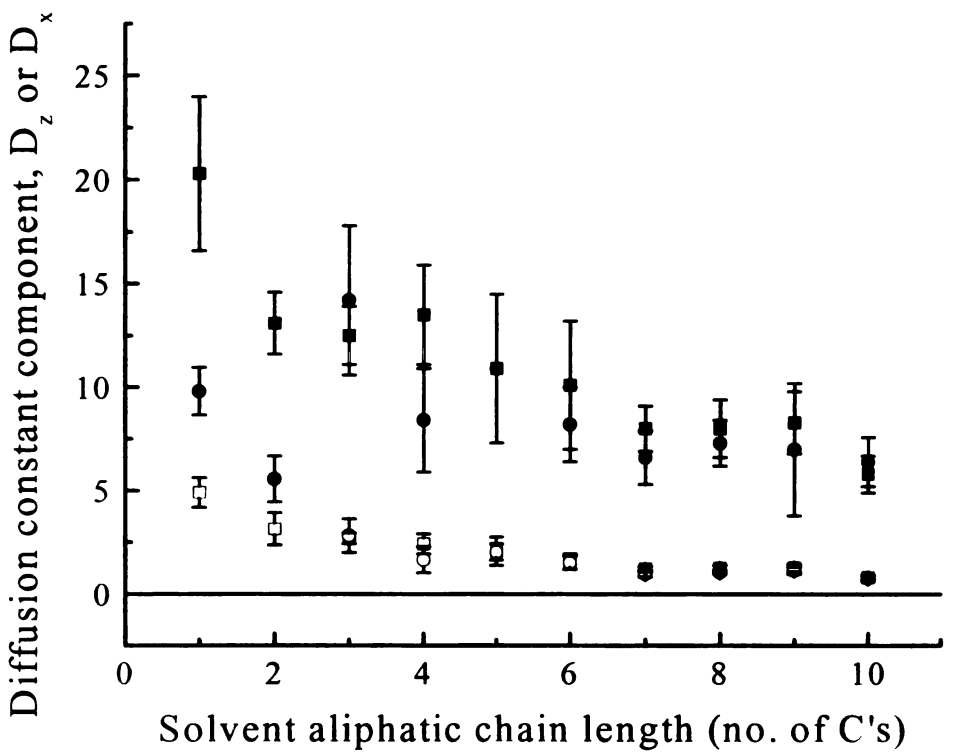

Figure 21 – Cartesian components of the rotational diffusion constant as a function of solvent aliphatic chain length for perylene (D_z = ●, D_x = ○) and 1-methylperylene (D_z = ■, D_x = □) in the *n*-alkanols.

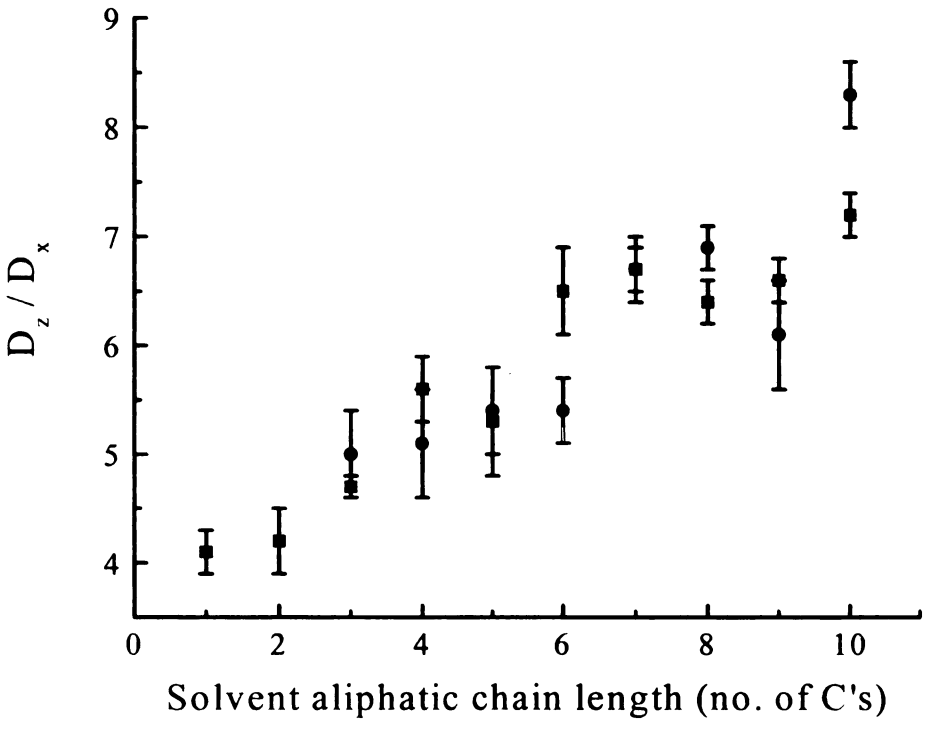

Figure 22 – The ratio D_z/D_x as a function of solvent chain length for perylene (●) and 1-methylperylene (■). These data indicate that the environment experienced by both chromophores is essentially identical and the structural anisotropy in the solvent cage increases with solvent aliphatic chain length.

oblate rotor in the alkanols *n*-propanol and longer. In methanol and ethanol, we recover what appears to be a single exponential decay, and note that our ability to distinguish between a fast second component and a single decay is limited by temporal resolution and signal-to-noise ratio. The apparently discontinuous change in D_z for perylene in ethanol and *n*-propanol (Table 3) suggests that we have not resolved the fast second component in R(t) for the smaller solvents. We measure $D_z/D_x \sim 8.5$ for perylene in *n*-decanol and $D_z/D_x < 1$ for perylene in *n*-decane. This remarkable difference in aspect ratios for one chromophore in the different solvents underscores the important role that the presence of the alcohol group plays in the organization of the solvent.

It is interesting to note that, for both chromophores, the increasingly anisotropic environment formed with increasing solvent aliphatic chain length is characterized by a strong dependence of D_z on solvent identity and a much weaker solvent-dependence of D_x (Figure 21). The dominant constraint imposed on the chromophores is for reorientation out of plane, suggesting a layered or quasi-lamellar environment. This finding is consistent with our results on 1-methylperylene in the *n*-alkanes and the fact that we observe this phenomenon in all solvents argues for persistent local organization over a length-scale that is at least on the order of the chromophore (*vide infra*). We note also that this result is in excellent agreement with a recent report by the Johnson group on two photon excitation induced anisotropy decays, where the form of the R(t) function was found to depend measurably on the excitation polarization conditions.[32]

It is clear that the reorientation behavior of these two chromophores depends sensitively on the solvent in which they are dissolved. With only the reorientation data, it is possible to draw correlations between bulk solvent properties and microscopic

reorientation behavior, but the extent to which these correlations can provide real insight into the relevant intermolecular interactions is limited. For this reason we have also studied the vibrational population relaxation behavior of these chromophores in the same alkanol solvents. Those data, in conjunction with the reorientation measurements, provide additional insight into the average organization of solvents about the solutes.

Before we discuss our vibrational population relaxation data, we consider what is known about the solvent alcohols. NMR experiments have shown that, at room temperature, the dominant form of the *n*-alkanols is the trimer,[52] which is believed to exist in a ring-bound configuration.[22] This finding indicates that the solvent bath mode is heterogeneous on the length scale sensed by the solvent. Such local heterogeneity can, in principle, be sensed by vibrational population relaxation as we discuss below. Another significant implication of the presence of trimers in solution is that it makes the dominant form of the solvent have a hydrodynamic volume three times larger than that predicted from calculations of monomer solvent.[68] This is true in the limit of the characteristic lifetime of the solvent trimers being on the same order as the dynamics we measure. For the alkanols, the longitudinal relaxation time, τ_L, ranges from tens of ps to hundreds of ps as the aliphatic chain length increases.[70] With the larger effective solvent species, it is reasonable to expect more restriction of the chromophores, consistent with our findings of an effective oblate rotor shape in the *n*-alkanols and in the longer *n*-alkanes for 1-methylperylene.

Vibrational population relaxation measurements. Vibrational population relaxation measurements provide information that is complementary to reorientation measurements. While these two measurements sense fundamentally different

phenomena, both depend on the properties of the chromophore local environment. The reorientation data we present here indicate that, in the *n*-alkanols, both perylene and 1-methylperylene exist in environments that are restricted in such a way as to allow chromophore rotation primarily about an axis perpendicular to the π-system plane. The type of solvent local organization most consistent with these findings is that of a quasi-lamellar medium. As we had mentioned above, the alkanol solvents likely exist primarily as H-bonded trimers, and such a configuration will likely give rise to a micro-heterogeneous environment. With this picture in mind, we present our T_1 data.

We have focused on the vibrational relaxation behavior of the perylene 1375 cm^{-1} and the 1-methylperylene 1370 cm^{-1} ring-breathing modes.[40-45] We have chosen these modes because the terminal CH_3 group on the alkanol exhibits a rocking motion at ~1378 cm^{-1}, essentially degenerate with the solute donor mode. In this manner, measurement of T_1 as a function of alkanol identity can provide information on the spatial proximity and relative orientation of the donor and acceptor vibrational coordinates. The details of how the experimental technique operates have been presented elsewhere[40,71,72] and we forego a discussion of this point here. The vibrational population relaxation time constants we report here are significantly longer for perylene than for 1-methylperylene in methanol through *n*-heptanol. We understand this effect in the context of the nature of the coupling between the donor and acceptor.[41,43] For molecules possessing a center of inversion, the lowest order multipole moment that can be modulated using our excitation scheme is the quadrupole moment. Assuming an IR-active acceptor mode, the intermolecular coupling will decay with donor-acceptor spacing as r^{-8}.[41] For a donor that does not possess a center of inversion, the excited vibrational resonance will modulate the dipole moment and the

donor-acceptor coupling will depend on intermolecular distance as r^{-6}.[43] We have synthesized and use 1-methylperylene precisely because it is of lower symmetry than perylene, and we have shown that the coupling between the ring breathing mode and the solvent bath will be stronger than it is for perylene. Because the theoretical framework for the interpretation of vibrational population relaxation in liquids is not well developed, we do not attempt to extract solvent-solute interaction information from single T_1 data points. Rather, we are interested in the solvent-dependent behavior of these time constants (Table 5 and Figure 23.)

We observe a break in the T_1 trend for both chromophores at *n*-octanol. For 1-methylperylene, we see an abrupt increase in T_1 with increasing alkanol chain length. We interpret this effect as a change in the proximity of the solvent acceptor mode relative to the solute donor mode. This finding suggests the association of the 1-methylperylene chromophore with the solvent alcohol functionalities. We can rationalize this assertion based on the fact that 1-methylperylene has a non-zero dipole moment and dipolar interactions must therefore contribute to the solvent-solute interactions at some level. When the alkanol chain becomes long enough that the terminal CH_3 group can, on average, be relatively isolated from the 1-methylperylene chromophore, the donor-acceptor coupling weakens, accounting for our experimental findings.

For perylene, the situation is not directly comparable. This is because the functionality of the population relaxation dynamics data changes for *n*-octanol through *n*-decanol. For solvents methanol through *n*-heptanol, we recover the expected form of the signal shown in Figure 24 and Equation (10),

$$S(t) = a\exp(-t/\tau_{ste}) - b\exp(-t/T_1) \qquad (10)$$

but for the longer alkanols the signal functionality changes to be a sum of exponentials, shown in Figure 25 and Equation (11).

$$S(t) = a\exp(-t/\tau_{ste}) + b\exp(-t/\tau_2) \qquad (11)$$

where τ_2 is the fast decay time. We have encountered this solvent-dependent change-over previously for tetracene in *n*-hexadecane,[44] and understand it in the context of the solvent-solute interactions providing or mediating an additional non-radiative decay pathway. In the previous work, we conjectured that intersystem crossing was responsible for the observed solvent-dependent change in the functionality of S(t) because tetracene has a relatively low ϕ_{fl} and a modest ϕ_{ISC}.[44,73,74] For perylene, ϕ_{fl} is ~ 0.94 and depends only weakly on solvent.[75] Intersystem crossing is thus less likely to account for our result here. Because the origin of this new relaxation pathway is not known, there is ambiguity in the assignment of the physical meaning of the recovered time constant. We therefore will not attempt to cloud the discussion presented here with speculative interpretations of these data. The fact that we see a change in the interactions between perylene and its immediate environment at the same point that we observe a change for 1-methylperylene indicates that perylene is sensing either the same local environment as 1-methylperylene or its complement. For 1-methylperylene, the T_1 data are consistent with a measurable contribution from dipole-dipole solvent-solute interactions, but for perylene, there is no permanent dipole moment, precluding the contribution of such interactions. The complement to the environment sensed by 1-methylperylene would be for perylene to interact most strongly with the aliphatic portion of the solvent, and this

Table 5 – Vibrational population relaxation times, T_1, for perylene and 1-methylperylene in the *n*-alkanols. Relaxation times are determined from at least six individual data sets and the uncertainties are standard deviations. Times are values from fits of the experimental data to Equation (10) and are given in ps. Times marked with an asterisk are the results of fits to Equation (11).

	Perylene	1-methylperylene
Solvent	T_1 (ps)	T_1 (ps)
CH_3OH	209 ± 68	40 ± 18
C_2H_5OH	374 ± 109	31 ± 7
C_3H_7OH	443 ± 111	48 ± 11
C_4H_9OH	389 ± 119	126 ± 20
$C_5H_{11}OH$	397 ± 109	36 ± 11
$C_6H_{13}OH$	180 ± 52	60 ± 11
$C_7H_{15}OH$	439 ± 109	41 ± 12
$C_8H_{17}OH$	*54 ± 24**	160 ± 41
$C_9H_{19}OH$	*72 ± 16**	214 ± 25
$C_{10}H_{21}OH$	*185 ± 74**	99 ± 38

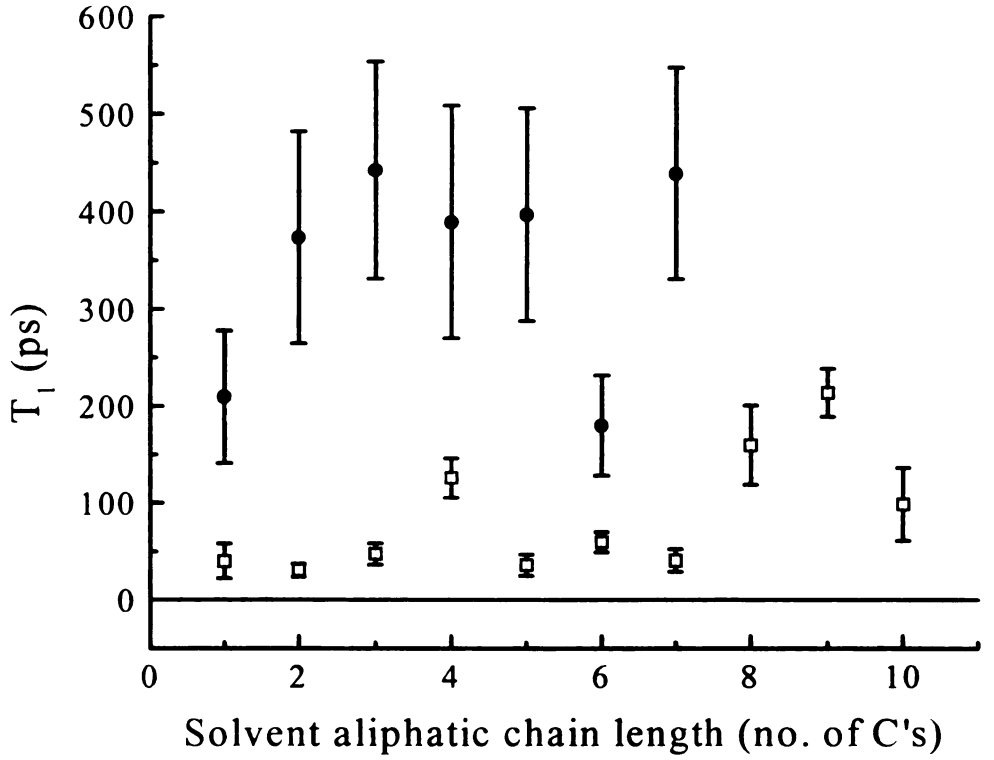

Figure 23 – Vibrational population relaxation times for perylene (●) and 1-methylperylene (□) as a function of solvent aliphatic chain length.

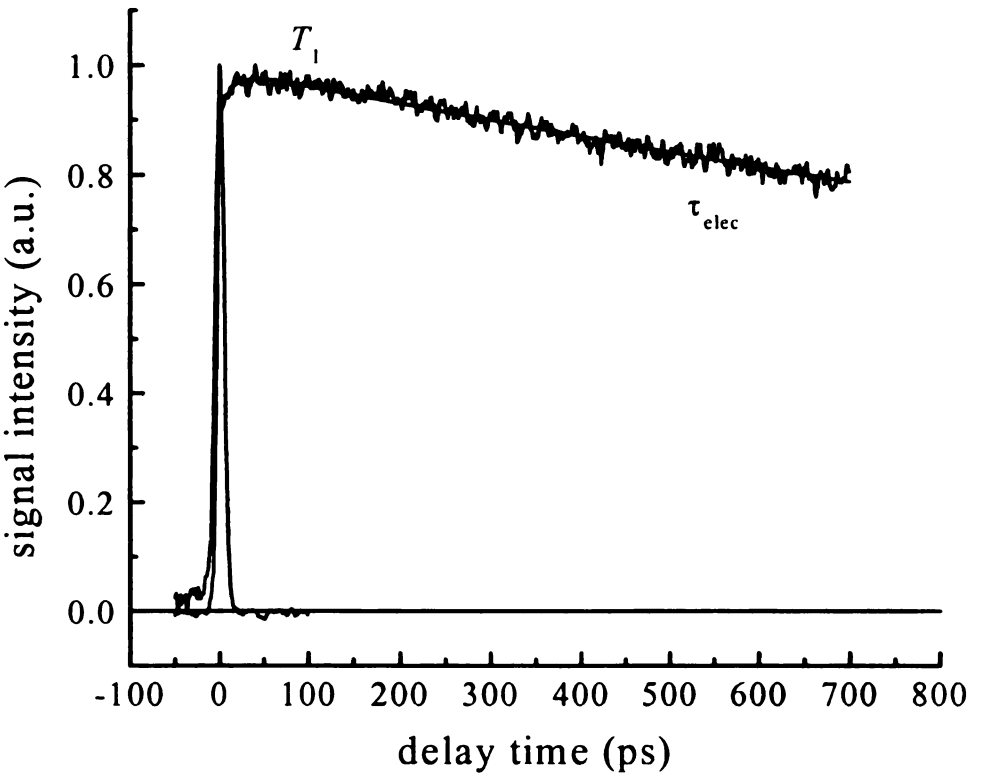

Figure 24 – Magic angle data for perylene in *n*-pentanol with instrument response function. See text for a discussion.

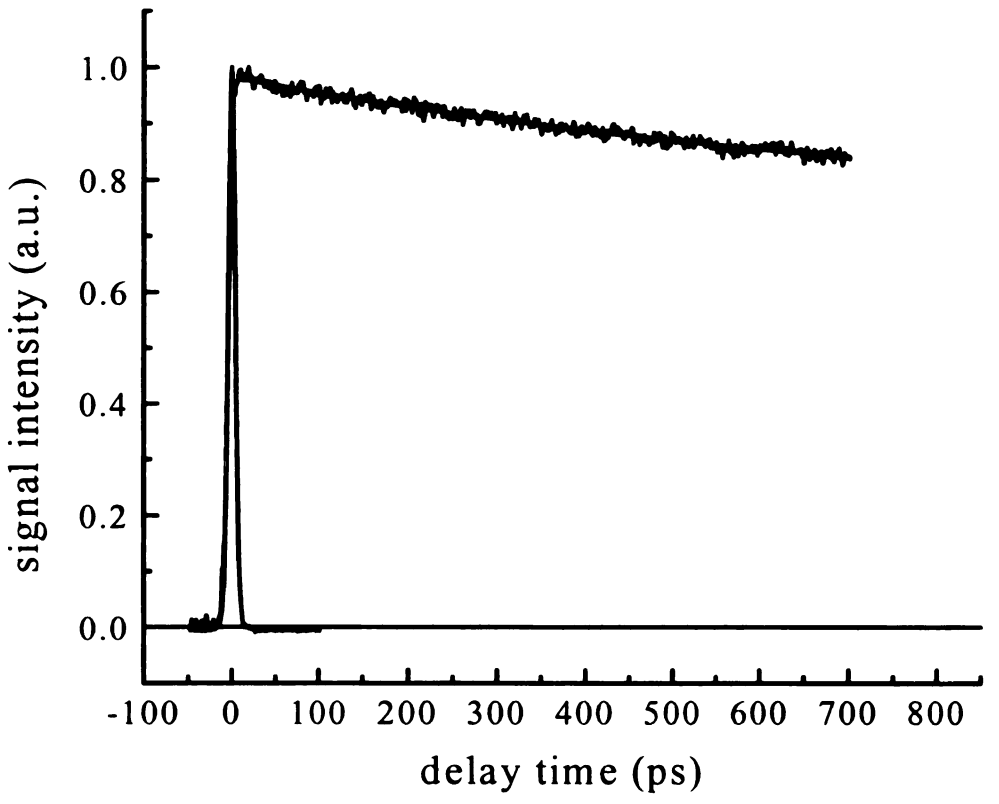

Figure 25 – Magic angle data for perylene in *n*-decanol. Note the difference in the functionality of the population decay. See text for a discussion.

suggestion is in intuitive agreement with the dominance of van der Waals interactions between (symmetric) PAHs and aliphatic solvents. Indeed, we observe this same behavior for tetracene only in long-chain aliphatic solvents.

Taken collectively, the reorientation and vibrational population relaxation data for perylene and 1-methylperylene in the alkanols point to the importance of solvent self-organization in determining solvent-solute interactions. Alcohols are known to form persistent H-bonded networks with the lifetime of the network being proportional to the aliphatic chain length.[52,71] NMR data point to the dominance of H-bonded trimers in solution,[52] and with the assumption that the characteristic time constant of the H-bonded network is the same as the average lifetime for the trimers, it is likely that these species dominate the solvent-solute interaction dynamics we sense. The reorientation data suggest that both chromophores are constrained to reorient in an environment that is best described as quasi-lamellar.[43] The presence of solvent trimers implies structural heterogeneity on the length scale of the solvent molecules, with relatively hydrophobic and hydrophilic microenvironments in close spatial proximity. The vibrational population relaxation measurements suggest that 1-methylperylene associates with the more closely with polar portions of the solvent and this segregation becomes pronounced for sufficiently large alkanol solvents. For perylene, it is likely that the chromophore associates with the less polar environment, although it would be necessary to assign some specific physical meaning to the second exponential decay seen for *n*-octanol through *n*-decanol to augment this assertion.

Conclusions

We have studied the rotational diffusion and vibrational population relaxation dynamics for perylene and 1-methylperylene in a series of *n*-alcohols from methanol through *n*-decanol. We find evidence for solvent local organization, consistent with the relatively long-lived hydrogen bonded complexes that characterize the alkanol solvents. This local organization constrains the chromophores to reorient as oblate ellipsoids. The reorientation times measured in each *n*-alkanol are the same for both chromophores. We conclude that in these systems, the specific characteristics of the chromophore have less of an effect on the rotor shape than the hydrogen bond-mediated solvent transient structure.

The vibrational population relaxation times for perylene indicate that vibrational energy transfer is less efficient than it is for 1-methylperylene in *n*-alkanols. This is an expected result and we understand it based on the differences in the nature of donor-acceptor coupling for the two chromophores. For the alkanols, it is the strong persistent solute-solute interactions that mediate the solvent-solute interactions we measure. For alkanes, the interactions between solvent and solute are on the same order as solute-solute interactions, allowing the structure of the solute to play a more deterministic role in the form of the recovered transient optical responses. We expect that, in systems where dipole-dipole interactions are significant but where H-bonding interactions are largely mitigated, the difference in dynamics between these two chromophores will become more pronounced.

Literature Cited

1. This work was previously published - Goldie, S. N.; Blanchard, G. J. *J. Phys. Chem. A.* **1999**, *103*, 999.

2. Shapiro, S. L.; Winn, K. R.; *Chem. Phys. Lett.*, **1980**, *71*, 440.

3. Maroncelli, M.; Fleming, G. R.; *J. Chem. Phys.*, **1987**, *86*, 6221.

4. Huppert, D.; Ittah, V.; Kosower, E.; *Chem. Phys. Lett.*, **1989**, *159*, 267.

5. Chapman, C. F.; Fee, R. S.; Maroncelli, M.; *J. Phys. Chem.*, **1990**, *94*, 4929.

6. Huppert, D.; Ittah, V.; *Chem. Phys. Lett.*, **1990**, *173*, 496.

7. Jarzeba, W.; Walker, G. C.; Johnson, A. E.; Barbara, P. F.; *Chem. Phys.*, **1991**, *152*, 57.

8. Wagener, A.; Richert, R.; *Chem. Phys. Lett.*, **1991**, *176*, 329.

9. Fee, R. S.; Milsom, J. A.; Maroncelli, M.; *J. Phys. Chem.*, **1991**, *95*, 5170.

10. Yip, R. W.; Wen, Y. X.; Szabo, A. G.; *J. Phys. Chem.***1993**, *97*, 10458.

11. Fee, R. S.; Maroncelli, M.; *Chem. Phys.*, **1994**, *183*, 235.

12. Sanders, M. J.; Wirth, M. J.;*Chem. Phys. Lett.*, **1983**, *101*, 361.

13. Gudgin-Templeton, E. F.; Quitevis, E. L.; Kenney-Wallace, G. A.; *J. Phys. Chem.*, **1985**, *89*, 3238.

14. Von Jena, A.; Lessing, H. E.; *Chem. Phys.*, **1979**, *40*, 245.

15. Von Jena, A.; Lessing, H. E.; *Ber. Bunsen-Ges. Phys. Chem.*, **1979**, *83*, 181.

16. Von Jena, A.; Lessing, H. E.; *Chem. Phys. Lett.*, **1981**, *78*, 187.

17. Eisenthal, K. B.; *Acc. Chem. Res.*, **1975**, *8*, 118.

18. Fleming, G. R.; Morris, J. M.; Robinson, G. W.; *Chem. Phys.*, **1976**, *17*, 91.

19. Shank, C. V.; Ippen, E. P.; *Appl. Phys. Lett.*, **1975**, *26*, 62.

20. Millar, D. P.; Shah, R.; Zewail, A. H.; *Chem. Phys. Lett.*, **1979**, *66*, 435.

21. Gudgin-Templeton, E. F.; Kenney-Wallace, G. A.; *J. Phys. Chem.*, **1986**, *90*, 2896.

22. Blanchard, G. J.; Wirth, M. J.; *J. Phys. Chem.*, **1986**, *90*, 2521.

23. Blanchard, G. J.; *J. Chem. Phys.*, **1987**, *87*, 6802.

24. Blanchard, G. J.; Cihal, C. A.; *J. Phys. Chem.*, **1988**, *92*, 5950.

25. Blanchard, G. J.; *J. Phys. Chem.*, **1988**, *92*, 6303.

26. Blanchard, G. J.; *J. Phys. Chem.*, **1989**, *93*, 4315.

27. Blanchard, G. J.; *Anal. Chem.*, **1989**, *61*, 2394.

28. Alavi, D. S.; Hartman, R. S.; Waldeck, D. H.; *J. Phys. Chem.*, **1991**, *95*, 6770.

29. Hartman, R. S.; Alavi, D. S.; Waldeck, D. H.; *J. Phys. Chem.*, **1991**, *95*, 7872.

30. Jiang, Y.; Blanchard, G. J.; *J. Phys. Chem.*, **1994**, *98*, 6436.

31. Brocklehurst, B.; Young, R. N.; *J. Phys. Chem.*, **1995**, *99*, 40.

32. Pauls, S. W.; Hedstrom, J. F.; Johnson, C. K.; *Chem. Phys.*, **1998**, *237*, 205.

33. Elsaesser, T.; Kaiser, W.; *Annu. Rev. Phys. Chem.*, **1991**, *42*, 83.

34. Lingle, R., Jr.; Xu, X.; Yu, S. C.; Zhu, H.; Hopkins, J. B.; *J. Chem. Phys.*, **1990**, *93*, 5667.

35. Anfinrud, P. A.; Han, C.; Lian, T.; Hochstrasser, R. M.; *J. Phys. Chem.*, **1990**, *94*, 1180.

36. Heilweil, E. J.; Casassa, M. P.; Cavanagh, R. R.; Stephenson, J. C.; *Ann. Rev. Phys. Chem.*, **1989**, *40*, 143.

37. Heilweil, E. J.; Cavanagh, R. R.; Stephenson, J. C.; *Chem. Phys. Lett.*, **1987**, *134*, 181.

38. Heilweil, E. J.; Cavanagh, R. R.; Stephenson, J. C.; *J. Chem. Phys.*, **1989**, *89*, 230.

39. Heilweil, E. J.; Casassa, M. P.; Cavanagh, R. R.; Stephenson, J. C.; *J. Chem. Phys.*, **1986**, *85*, 5004.

40. Hambir, S. A.; Jiang, Y.; Blanchard, G. J.; *J. Chem. Phys.*, **1993**, *98*, 6075.

41. Jiang, Y.; Blanchard, G. J.; *J. Phys. Chem.*, **1994**, *98*, 9411.

42. Jiang, Y.; Blanchard, G. J.; *J. Phys. Chem.*, **1994**, *98*, 9417.

43. Jiang, Y.; Blanchard, G. J.; *J. Phys. Chem.*, **1995**, *99*, 7904.

44. McCarthy, P. K.; Blanchard, G. J.; *J. Phys. Chem.*, **1995**, *99*, 17748.

45. McCarthy, P. K.; Blanchard, G. J.; *J. Phys. Chem.*, **1996**, *100*, 5182.

46. Agmon, N.; *J. Phys. Chem.*, **1990**, *94*, 2959.

47. Maroncelli, M.; Fee, R. S.; Chapman, C. F.; Fleming, G. R.; *J. Phys. Chem.*, **1991**, *95*, 1012.

48. Blanchard, G. J.; *J. Chem. Phys.*, **1991**, *95*, 6317.

49. Jiang, Y.; McCarthy, P. K.; Blanchard, G. J.; *Chem. Phys.*, **1994**, *183*, 249.

50. Flory, W. C.; Blanchard, G. J.; *Appl. Spec.*, **1998**, *52*, 82.

51. Castner, E. W.; Maroncelli, M.; Fleming, G. R.; *J. Chem. Phys.*, **1987**, *86*, 1090.

52. Makarov, M. G.; Gus'kov, A. K.; Shvets, V. F.; *Zh. Fiz. Khim.*, **1982**, *56*, 71.

53. Jiang, Y.; Hambir, S. A.; Blanchard, G. J.; *Opt. Commun.*, **1993**, *99*, 216.

54. Bado, P.; Wilson, S. B.; Wilson, K. R. *Rev. Sci. Instrum.* **1982**, *53*, 706.

55. Andor, L.; Lorincz, A.; Siemion, J.; Smith, D. D.; Rice, S. A.; *Rev. Sci. Instrum.* **1984**, *55*, 64

56. Blanchard, G. J.; Wirth, M. J.; *Anal. Chem.*, **1986**, *56*, 532.

57. Peake, D. A.; Oyler, A. R.; Heikkila, K. E.; Liukkonen, R. J.; Engroff, E. C.; Carlson, R. M. *Synth. Commun.* **1983**, *13*, 21.

58. Karpovich, D. S.; Blanchard, G. J.; *J. Phys. Chem.*, **1995**, *99*, 3951.

59. Calculated using Hyperchem V 4.0.

60. Lewitzka, L.; Lohmannsroben, H.-G.; Strauch, M.; Luttke, W.; *J. Photochem. Photobiol. A: Chem.*, **1991**, *61*, 191.

61. Grimme, S.; Lohmannsroben, H.-G.; *J. Phys. Chem.*, **1992**, *96*, 7005.

62. Debye, P. *Polar Molecules*; Chemical Catalog Co.: New York, 1929; p. 84.

63. Perrin, F. *J. Phys. Radium* **1936**, *7*, 1.

64. Chuang, T. J.; Eisenthal, K. B. *J. Chem. Phys.* **1972**, *57*, 5094.

65. Hu, C. M.; Zwanzig, R. *J. Chem. Phys.* **1974**, *60*, 4354.

66. Youngren, G. K.; Acrivos, A. *J. Chem. Phys.* **1975**, *63*, 3846.

67. Zwanzig, R.; Harrison, A. K. *J. Chem. Phys.* **1985**, *83*, 5861.

68. Edward, J. T.; *J. Chem. Ed.*, **1970**, *47*, 261.

69. Piston, D. W.; Bilash, T.; Gratton, E.; *J. Phys. Chem.*, **1989**, *93*, 3963.

70. Garg, S. K.; Smyth, C. P.; *J. Phys. Chem.*, **1965**, *69*, 1294.

71. Blanchard, G. J.; *Rev. Sci. Instrum.*, **1996**, *67*, 4085.

72. Blanchard, G. J.; *Anal. Chem.*, **1997**, *69*, 351A.

73. Birks, J. B.; *Photophysics of Aromatic Molecules*, Wiley-Interscience, London (1970).

74. Douris, R. G.; *Ann. Chim.*, **1959**, *31*, 479.

75. Berlman, I. B.; Handbook of Fluorescence Spectra of Aromatic Molecules, 2nd Edition, Academic Press, 1971, p. 399.

Chapter 3

ORIENTATIONAL AND VIBRATIONAL RELAXATION DYNAMICS OF PERYLENE AND 1-METHYLPERYLENE IN ALDEHYDES AND KETONES[1]

Introduction

Over the past three decades, the scientific community has made enormous strides in understanding intermolecular interactions in the liquid phase. Despite these gains, our understanding of liquids lags behind that of solids and gases because of the associative and dynamic nature of the liquid phase. Indeed, for a given solvent-solute system, there are many solvent cage configurations that lie within a very narrow energetic window, capable of interconversion on a fast timescale. Because of this intrinsic complexity, gaining an understanding of the average environment that a solute molecule experiences in a given solvent system is not a simple matter.

With the advent of picosecond lasers, the study of liquids expanded greatly because many of the dynamics relevant to solvation processes proceed on the picosecond or longer timescale, especially in polar, strongly associative systems. There have been many methods devised for studying intermolecular interactions in solution and among the most successful has been the measurement of probe molecule rotational motion. The study of molecular reorientation has been aided by the existence of a well-established theoretical framework for the interpretation of experimental data, and much insight into solvent-solute interactions has been gained through such studies.[2-22] One limitation of rotational diffusion measurements lies in the amount of information that is available from typical experimental data and also that the probe molecules used in such studies are invariably larger than the length scale over which any solvent organization persists. As a

result of these limitations we have shown that by comparing the results of reorientation and vibrational population relaxation measurements, we can gain additional insight into the details of intermolecular interactions.[23-35] This is because, for many systems, dipolar and/or hydrogen-bonding interactions dominate both the reorientation and vibrational population relaxation events, but vibrational population relaxation operates over characteristically shorter distances than are sensed by the reorientation measurements.

Of central importance to gaining an understanding of intermolecular interactions is the appropriate choice of probe molecule. There have been many chromophores examined in such studies, with many of them being polar or ionic dye molecules. The information gained from such work is useful but in many cases less than ideal because of the strength of the solvent-solute interactions. In an attempt to use a limited number of relatively well-characterized chromophores in selected solvent systems, we have reported recently on the reorientation and vibrational population relaxation dynamics of perylene and 1-methylperylene in a variety of non-polar and amphiphilic solvents. We have used these two probe molecules because of their symmetries. Perylene is of D_{2h} symmetry, possessing a center of inversion. It thus has no permanent dipole moment and, for the vibrational population relaxation measurements we report here, the coupling between solvent and solute is expected to scale as r^{-8} in the absence of substantial perturbation of the chromophore by the solvent.[36] 1-Methylperylene is a probe molecule that is structurally and spectroscopically similar to perylene, but because of the presence of the methyl group at the 1- position, the center of inversion has been lifted and all vibrational modes in this molecule are both infrared- and Raman-active. Consequently, intermolecular coupling processes are expected to scale with r^{-6} for this molecule.[36]

Using both molecules allows us, in principle, to examine intermolecular interactions over a range of length scales while the reorientation dynamics of the two remains very similar in most solvent systems.

As part of our ongoing effort to understand intermolecular interactions in the liquid phase, we report here on the reorientation and vibrational population relaxation dynamics of perylene and 1-methylperylene in a series of aliphatic aldehydes and ketones. These two probe molecules exhibit relaxation dynamics that are the same for a given solvent system, but their behavior in the different families of solvents provides substantial insight into the dominant forces responsible for solvation of these molecules. The reorientation of these probes in the aldehydes is reminiscent of their behavior in the *n*-alcohols while the ketones data offer qualitative similarities to that seen in the *n*-alkanes. From these findings, in conjunction with the vibrational population relaxation measurements, we consider that longer-lived associative interactions between solvent molecules (*e.g.* H-bonding) play a greater role than solvent dipole moment in determining the dynamics of these probes.

In examining the data we report here, it is important to place the interpretation in the context of other data that exist for these molecules. Our prior work on perylene and 1-methylperylene in *n*-alcohols showed that both molecules yielded the same dynamics to within the experimental uncertainty for *n*-propanol through *n*-decanol, characterized by a double exponential decay of the induced orientational anisotropy. Perylene and 1-methylperylene behaved differently in the *n*-alkanes. For 1-methylperylene we observed a change in dynamical behavior between C_8 and C_9, as we see here for the ketones. We also report here that the aldehydes and ketones exhibit a break in their dynamical

response at C_5, whereas for the *n*-alcohols, the analogous break is seen either between C_2 and C_3 (perylene) or is not seen (1-methylperylene). We view these data as indicating that the ketones and alkanes behave similarly, as do the aldehydes and *n*-alcohols. The aldehydes and *n*-alcohols both possess a relatively labile proton capable of substantial intermolecular interaction, although the aldehyde proton is less labile than the *n*-alcohol proton. The presence of the labile protons in these solvents provides the opportunity for significant intermolecular interactions and thus more persistent solvent local organization. Because the ketones and alkanes do not possess analogous protons, the interactions between solvent molecules are weaker, thereby providing less confinement of the solute. A key finding of this work is that the solvent dipole moment plays a relatively less important role than the presence of labile protons for the solvation of essentially nonpolar species.

Experimental

Laser system: The picosecond pump-probe laser spectrometer used for both the reorientation and vibrational population relaxation measurements has been described in detail previously,[37] and we present only a brief outline of its properties here. A mode-locked CW Nd:YAG laser (Coherent Antares 76-S) produces 30 W of average power (1064 nm, 100 ps pulses, 76 MHz repetition rate). The output of this laser is frequency-tripled to produce ~1.2 W of average power at 355 nm. The third harmonic light is used to excite two cavity-dumped dye lasers (Coherent 702-3) synchronously. Both lasers operate with Stilbene 420 laser dye (Exciton). The output of each laser is ~60 mW average power at 8 MHz repetition rate with a pulse that produces a 7 ps FWHM autocorrelation trace using a three plate birefringent filter. The pump laser wavelength

was set between 433.0 nm and 440.1 nm, depending on the chromophore and solvent, while the probe laser was set in the range of 460.8 nm to 468.4 nm for vibrational population relaxation measurements of the solute ~1375 cm^{-1} ring breathing modes, and 468.5 nm to 476.5 nm for measurements that examined the solute ~1733 cm^{-1} combination modes. The pump wavelength was chosen to access the 0-0 transition of the chromophore and the probe wavelength to stimulate emission from the $S_1^{v=0}$ state to the $S_0^{v=1}$ state of interest. The same wavelengths were used for both vibrational population relaxation and reorientation measurements. Our previous work has demonstrated that the ground state and excited state reorientation behavior of perylene are identical[30] and we take this to be the case for 1-methylperylene as well. The probe laser polarization was set alternately to 0° and 90° relative to the pump laser polarization for the reorientation measurements, and to 54.7° for the vibrational population relaxation measurements. The time resolution of this system, ~10 ps, is determined by the cross-correlation between the pump and probe laser pulse trains. Detection of the transient signals was accomplished using a radio and audio frequency triple-modulation scheme, with synchronous demodulation detection.[38-40] Each reported time constant is the average of at least five individual determinations that are themselves the average of ten to twenty-five time-scans.

Steady State Spectroscopy: The steady state absorption spectra of both chromophores in the aldehydes and ketones were recorded with 1 nm resolution using a Hitachi U-4001 spectrometer. The spontaneous emission spectra for the same solutions were obtained with 1 nm resolution using a Hitachi F-4500 spectrometer. These data were used to determine the appropriate laser wavelengths for each chromophore/solvent

pair. The absorption and emission spectra for perylene and 1-methylperylene in 3-octanone are shown in Figure 26 and Figure 27.

Chemicals and Sample Handling: Perylene (99.5%, sublimed) was obtained from Aldrich Chemical Company and used as received. 1-Methylperylene was synthesized using the procedure of Peake *et al.*,[41] which is more than 95% selective for methylation at the 1-position, described in Chapter 1 of this disseration. All chemicals used in the synthesis were purchased from Aldrich in the highest purity grade available.

Solvents used in this work were obtained from Aldrich in the highest purity grade available. Solutions ($\sim 10^{-4}$ M) were made fresh before each set of experiments to minimize oxidative effects. A 1 cm quartz cuvette with a magnetic stir bar was used to contain and mix the sample during analysis, to eliminate the effects of thermal lensing. A jacketed brass cuvette holder connected to a re-circulating water bath (300.0 ± 0.1K), fabricated in house, was used to maintain the sample temperature. Results from previous experiments in our laboratory show no discernable difference between this sample handling method and the use of a flowing sample cell.

Results and Discussion

The focus of this work is on understanding the solvent-solute interactions of perylene and 1-methylperylene in selected aldehydes and ketones, and to place these results in context with respect to the behavior of these same probe molecules in other solvent systems. In this work, it is the functionality of the induced orientational anisotropy decay function, R(t), and in particular, how R(t) varies with the identity of the solvent, that provides insight into the intermolecular interactions experienced by these

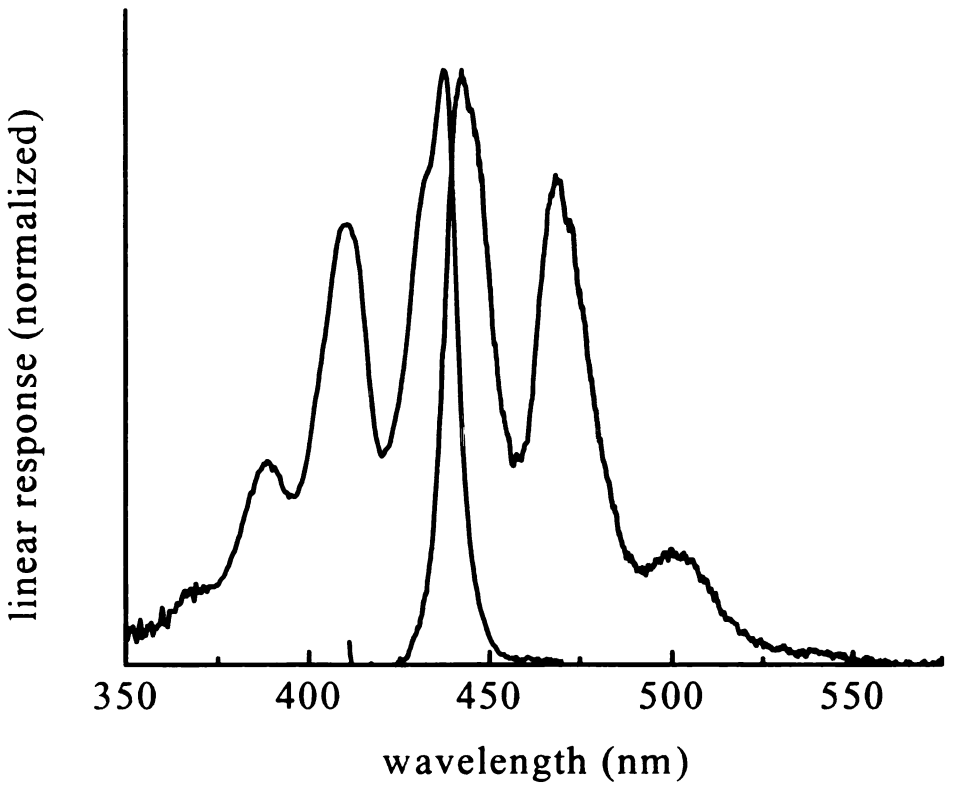

Figure 26 – Normalized absorption and emission spectra of perylene in 3-octanone.

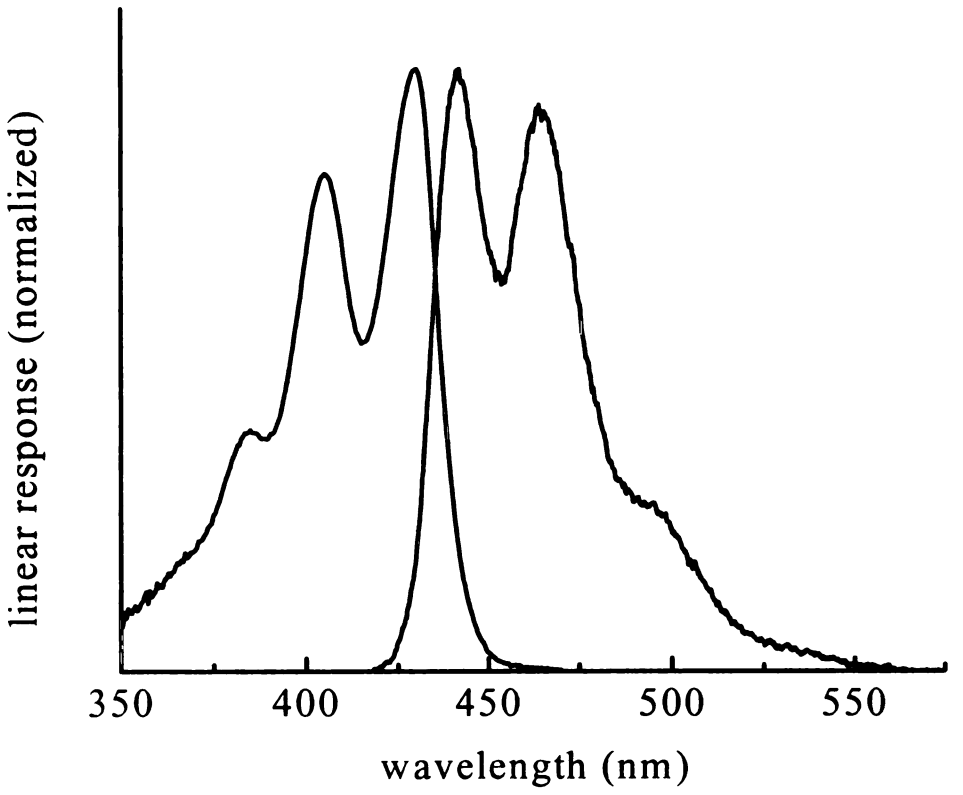

Figure 27 – Normalized absorption and emission spectra of 1-methylperylene in 3-octanone.

probe molecules. Vibrational population relaxation data indicate strong solvent-solute interactions for both probe molecules. Before considering the dynamical data, we review the linear responses of the probe molecules.

Steady State Linear Spectroscopy. Perylene is of D_{2h} symmetry with the ground electronic state being of ^1A_g symmetry and the first excited singlet state being of $^1B_{3u}$ symmetry.[42] 1-Methylperylene, by virtue of the presence of the methyl group, is of C_1 symmetry, with all states having A character. These molecules exhibit qualitatively similar linear responses; the quasi-mirror image absorption and emission spectra (Figure 26 and Figure 27) indicate that vibronic coupling plays a minor role in determining their linear responses.[43] 1-Methylperylene exhibits a slightly larger Stokes shift than perylene, reflecting the presence of a small permanent dipole moment. Semi-empirical calculations indicate that $\mu \sim 0.2$ D in the S_0 and ~ 0.5 D in the S_1 for 1-methylperylene.[57] The absorption maximum of perylene is red-shifted from 1-methylperylene in a given solvent, and the individual features in the 1-methylperylene spectra are less well defined. These differences result from the presence of the methyl group on 1-methylperylene, which causes the two naphthalene moieties to be cocked at ~20° with respect to one another.[44,45] The resulting slight break in conjugation causes the blue shift and the reduction in symmetry causes additional vibrational resonances to become allowed, adding to the greater width of the absorption and emission features. To within the experimental resolution (1 nm), the absorption responses of both perylene and 1-methylperylene are solvent-independent for the solvents studied here.

Rotational diffusion measurements. Rotational diffusion has been used extensively as a tool for understanding intermolecular interactions in solution.[12-30] One

reason for our use of this technique is that it is supported by a sound theoretical framework for the interpretation of the experimental data.[46-51] The modified Debye-Stokes-Einstein (DSE) (Equation (12)) is the usual starting point for relating reorientation data to solvent and solute properties,[62,63,65-67]

$$\tau_{OR} = \frac{\eta V f}{k_B T S} \qquad (12)$$

where η is the solvent viscosity, V the solute hydrodynamic volume (225 $Å^3$ for perylene and 243 $Å^3$ for 1-methylperylene),[52] f is a frictional interaction term to account for frictional contributions to solvent-solute interactions,[65,66] k_B is the Boltzmann constant, T is the temperature and S is a shape factor to account for the non-spherical shape of the solute.[63] In this model, a single exponential decay of the induced orientational anisotropy, R(t), is expected. For cases where a more complicated functionality is seen in R(t), it is clear that this simplistic but remarkably useful model cannot describe the data adequately.

The experimental stimulated gain signal transients, polarized parallel ($I_{\parallel}(t)$) and perpendicular ($I_{\perp}(t)$) to the pump beam, are related to the function R(t) through Equation (13), and representative experimental $I_{\parallel}(t)$, $I_{\perp}(t)$ and R(t) data are shown in Figure 28 and Figure 29.

$$R(t) = \frac{I_{\parallel}(t) - I_{\perp}(t)}{I_{\parallel}(t) + 2I_{\perp}(t)} \qquad (13)$$

The typical result for reorientation measurements is to recover an experimental R(t) function that decays as a single exponential. There are a number of experiments, however, where R(t) is found to decay with a multiple exponential functionality,[23,43,53,54] or the measured decay is found to depend on the pump and/or probe wavelengths.[12,55,56]

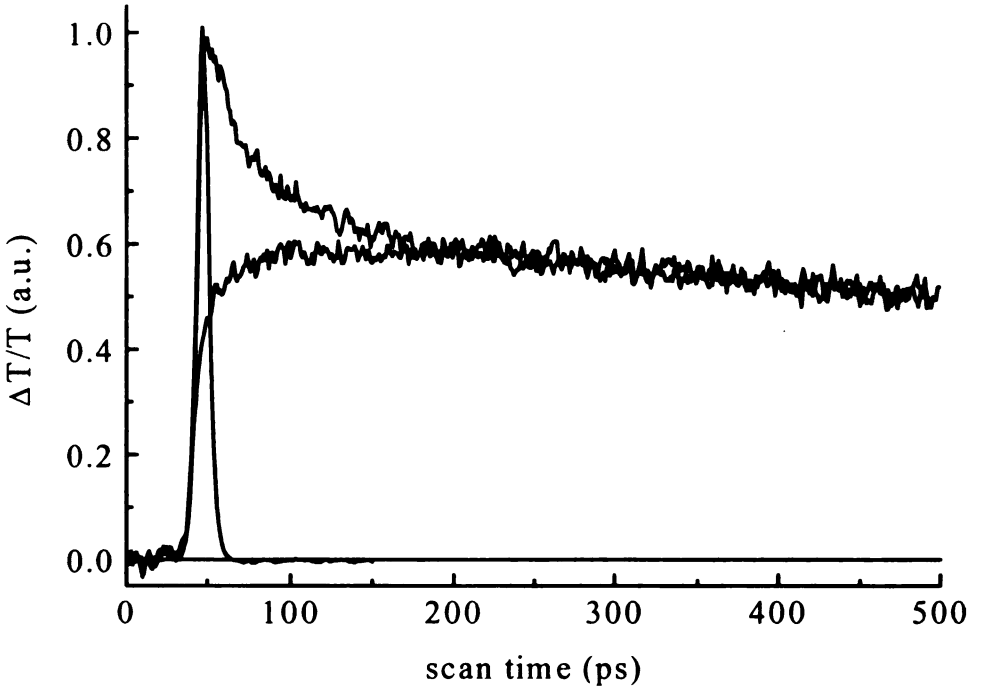

Figure 28 – Experimental $I_{\parallel}(t)$ and $I_{\perp}(t)$ scans for 1-methylperylene in 2-nonanone, along with the instrumental response function.

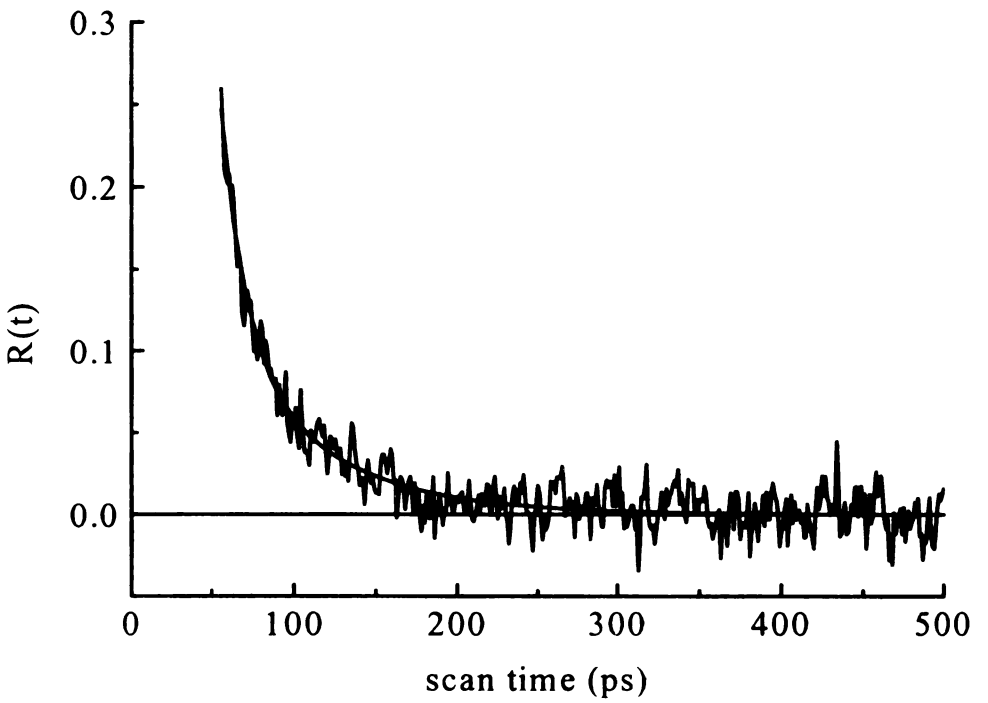

Figure 29 – Anisotropy function, R(t), generated from the raw data shown in Figure 28. The decay is fit to the function $R(t) = R_1(0)\exp(-t/\tau_1) + R_2(0)\exp(-t/\tau_2)$, with the results of the fit given in Figure 28.

In these cases, a more thorough study of the anisotropy decay dynamics is required. Chuang and Eisenthal have derived expressions for $I_{\parallel}(t)$ and $I_{\perp}(t)$ that depend on the angle between the excited and probed transition dipole moments and the Cartesian components of the rotational diffusion constant.[64] R(t) can decay with as many as five exponential components, and in cases where more than one decay component is resolved, it is possible to interpret the reorientation dynamics in substantial detail.

To facilitate the treatment of our experimental data using Chuang and Eisenthal's formulation, we assign the Cartesian axes as follows: The chromophore π-systems are in the (approximate) *xy* plane and *z* is perpendicular to the *xy* plane. The *x*-axis coincides with the absorption transition dipole moment. For perylene this assignment is coincident with specific bond axes, consistent with its D_{2h} symmetry. For 1-methylperylene, the assigned *x*-axis is not necessarily coincident with any bonds because the π-system for this chromophore is non-planar and the presence of the methyl group at the 1- position will affect the orientation of the transition dipole moment relative to the molecular framework. Using these approximations with Chuang and Eisenthal's equations,[64] we can relate the experimental reorientation times to the shape of the volume swept out by the rotating molecule. Because the experimental data do not possess sufficient information to separate the three Cartesian components of the rotational diffusion constant unambiguously, we describe this volume in terms of prolate or oblate ellipsoids. For a prolate ellipsoid, characterized by rotation primarily about its long in-plane axis, $D_x > D_y = D_z$. An oblate ellipsoid is characterized by rotation about the axis perpendicular to the chromophore π-system, $D_z > D_x = D_y$. Using these geometric approximations, we

obtain expressions for R(t) that can be used directly in the interpretation of our experimental data.

Oblate: $R(t) = 0.3\exp(-(2D_x + 4D_z)t) + 0.1\exp(-6D_x t)$ (14)

Prolate: $R(t) = 0.4\exp(-6D_z t)$ (15)

Where the excited and probed transition dipole moments are assumed to be parallel and lie along the *x*-axis (*vide infra*). In our previous work on the reorientation dynamics of perylene and 1-methylperylene in alkanes and *n*-alcohols, we have interpreted much of the data in the context of Equations (14) and (15). We found that, for reorientation of perylene in alkanes, we always recovered a single exponential anisotropy decay, but the nature of the frictional contributions to the reorientation of the chromophore (*f* in Equation (12)) decreased with increasing solvent aliphatic chain length.[30] The reorientation of 1-methylperylene in the alkanes appears to be significantly different.[43] We observed a single exponential anisotropy decay in pentane, hexane, heptane and octane. For nonane, we observed a two-component R(t) decay, and interpreted these results in terms of a solvent-dependent change in the effective rotor shape of the chromophores. As the solvent aliphatic chain length increased, we quantitated the aspect ratio of the ellipsoid of rotation, D_z/D_x, saturated at a value of ~8.5, suggesting that, as the solvent increases in length, the confinement of the 1-methylperylene chromophore becomes more pronounced.

For the reorientation of perylene and 1-methylperylene in the *n*-alcohols, we observed a two-component decay of R(t) for all cases save for perylene in methanol and ethanol. We argued that the observation of a single component decay for these two solutions is the result of limited time resolution achievable with our system rather than an

explicit change in effective rotor shape. With this assertion, the results for probe reorientation in the *n*-alcohols suggest an oblate rotor shape in all cases and thus substantial solvent confinement of the probe. This interpretation is consistent with the known strong solvent-solvent interactions present in these solvents. As with the alkanes, for long chain *n*-alcohols we observe a saturation in the ratio D_z/D_x at ~8.5, arguing for substantial solute confinement. Our results for the reorientation of perylene and 1-methylperylene in aldehydes and ketones are consistent with our findings in the alkanes and *n*-alcohols and, when these bodies of information are viewed as a whole, it is clear that the role of labile solvent protons plays a more significant role in solvation processes than does solvent permanent dipole moment.

We present the reorientation time constants for perylene and 1-methylperylene in the aldehydes in Figure 30. The data show that the reorientation dynamics of the two probe molecules are identical in each aldehyde studied, to within our experimental uncertainty. We do not view this finding as surprising given the structural similarity of the two probes. Of perhaps greater significance is the clear change in behavior from single exponential to double exponential decay in going from pentanal to hexanal. As discussed above, these data indicate a change in the shape of the volume swept out by the probe molecule(s) from prolate to oblate. In contrast to our previous measurements, we observe that the D_z/D_x ratio does not change substantially in going from hexanal to decanal, and its limiting value in the aldehydes is ~ 5.5. These two findings, a change in effective rotor shape between C_5 and C_6, and a D_z/D_x ratio of ~5.5, suggests (but does not prove) the existence of substantial solvent-solvent interactions in the aldehydes. We will return to a discussion of this point later.

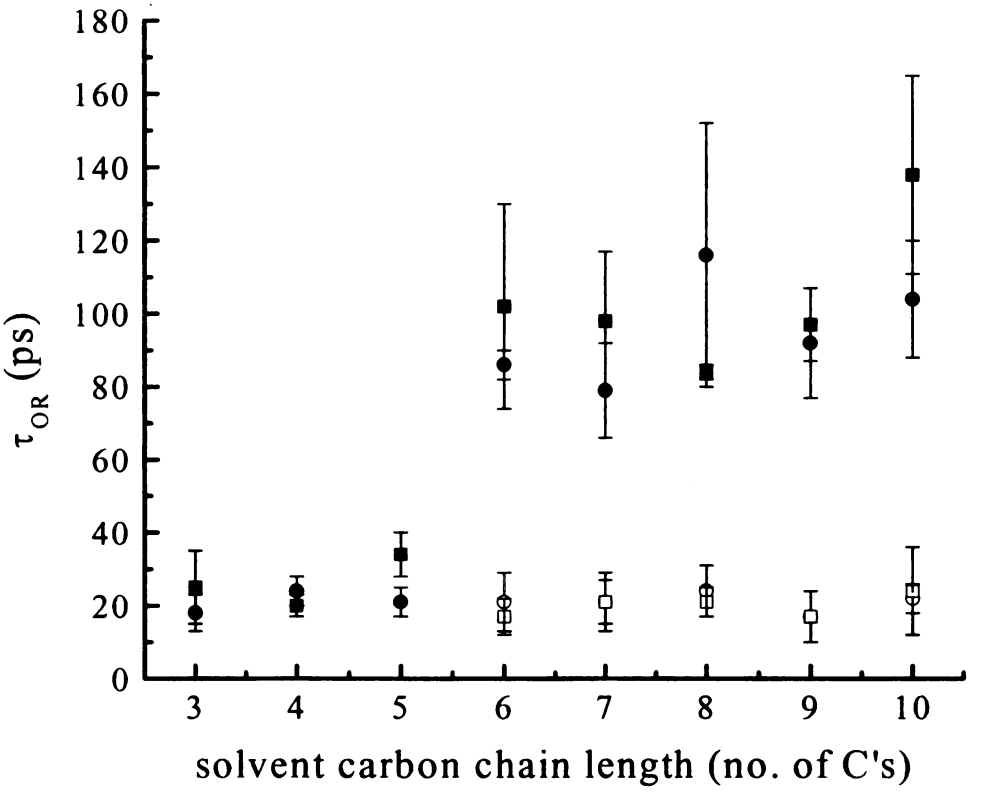

Figure 30 – Reorientation time constants plotted as a function of carbon chain length for perylene (●,○) and 1-methylperylene (■,□) in the aldehydes.

The reorientation dynamics of perylene and 1-methylperylene in selected ketones are shown in Figure 31. These data are for ketones of three different lengths; C_7, C_8 and C_9, and the chemical variable in this series of data is the location of the carbonyl functionality. As with the aldehydes, the reorientation behavior of both probe molecules is identical to within the experimental uncertainty for a given solvent. We note that, for the ketones, the reorientation behavior exhibits a change between C_8 and C_9 total solvent length, and this finding is reminiscent of the experimental reorientation data for 1-methylperylene in the *n*-alkanes. For the C_9 ketones, we find that the ratio of D_z/D_x does depend on the location of the carbonyl functionality, with 2-nonanone exhibiting a D_z/D_x ratio of ~4.5, substantially less than the $D_z/D_x \sim 5.5$ ratio seen for 3-, 4- and 5-nonanone (Table 4). While the ketones possess significant permanent dipole moments at their carbonyl functionality (calculated $\mu = 2.5$ D),[57] and this interaction appears to play a role in the carbonyl position-dependent D_z/D_x ratio seen for the ketones, we do not see evidence for strong solvent-solute interactions between the probe molecules and these solvents with the reorientation measurements.

Previous studies of the rotational dynamics of 1-methylperylene in *n*-alkanes exhibited similar behavior to what we have observed here.[43] The alkanes do, indeed, exert a substantial structural influence in the "free volume" that is accessible to the chromophore molecules. The break in behavior in going from C_8 to C_9 in both the alkanes and the ketones reflects the balance between the strength of solvent-solvent and solvent-solute interactions. The change in behavior from prolate rotor to oblate rotor is consistent with confinement of the probe molecules in a layered or quasi-lamellar environment.

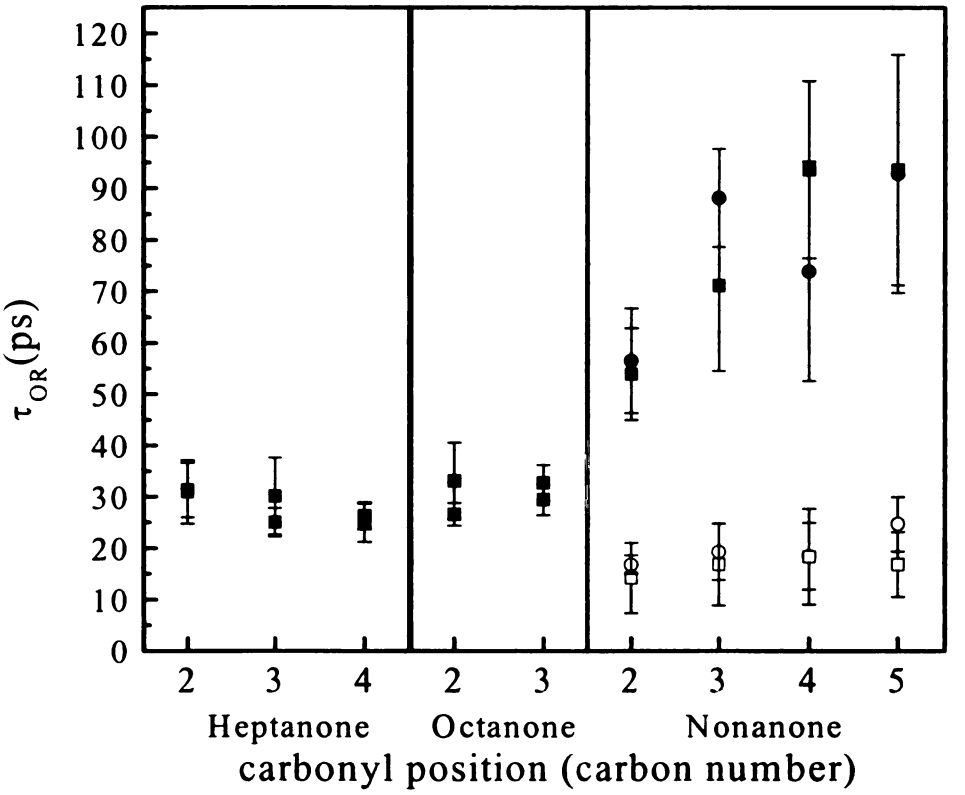

Figure 31 – Reorientation time constants plotted as a function of solvent viscosity for perylene (●,○) and 1-methylperylene (■,□) in the ketones. The boxed regions indicate specific solvent lengths.

The experimental anisotropy data provide information on both the reorientation and spectroscopic properties of the probe molecules. Equations (14) and (15) were derived with the assumption that the transition moments of the excited and probed transitions are parallel and lie along the *x*-axis. For these conditions, we expect a zero time anisotropy of 0.4 for an oblate rotor and zero-time components of 0.1 and 0.3 for an oblate rotor. Experimentally, we observe values close to the theoretical predictions (perylene in aldehydes: Table 6; 1-methylperylene in aldehydes: Table 7; perylene in ketones: Table 8; 1-methylperylene in ketones: Table 9), but there are noticeable deviations in the zero-time anisotropies in all cases. The Johnson group has noted similar results for the reorientation of perylene in 2-propanol and cyclohexane[42] and these data are consistent with our earlier reports.[30,43,59] Jas *et al.* argue that at least a portion of the experimental deviation of the R(0) values stems from contributions to the data from excited state absorption. This explanation is consistent with the known excited state absorption response of perylene.[58] Unfortunately, we do not have experimental data on the excited state absorption spectra of perylene or 1-methylperylene in the solvents we report on here and thus cannot infer the relative contribution of this effect.

We have touched upon the issue of diffusion constant ratio above, but a more detailed discussion of these data is in order. We present the calculated values for perylene (Table 6) and 1-methylperylene (Table 7) for the aldehydes and Table 8 and Table 9 for the ketones. It is useful to compare these results to our earlier data. For 1-methylperylene in *n*-alkanes octane and shorter, we recovered ratio $D_z/D_x < 1$, and a D_z/D_x approaching ~8.5 in the longer chain solvents, and found that this ellipsoid aspect

Table 6 – Reorientation Times and Zero-Time Anisotropies for Perylene in the n-Aldehydes.[a]

	Perylene			
Solvent	$R_1(0)$	τ_1 (ps)	$R_2(0)$	τ_2 (ps)
C_2H_5CHO	0.23±0.04	18±5	--	--
C_3H_7CHO	0.28±0.01	24±4	--	--
C_4H_9CHO	0.30±0.05	21±4	--	--
$C_5H_{11}CHO$	0.24±0.10	21±8	0.20±0.10	86±4
$C_6H_{13}CHO$	0.21±0.10	21±6	0.12±0.05	79±13
$C_7H_{15}CHO$	0.19±0.05	24±7	0.11±0.04	116±36
$C_8H_{17}CHO$	0.15±0.05	17±7	0.19±0.02	92±15
$C_9H_{19}CHO$	0.23±0.06	22±4	0.14±0.02	104±16

[a]The data are the best fit results of the data to the function $R(t) = R_1(0)\exp(-t/\tau 1)$ or $R(t) = R_1(0)\exp(-t/\tau 1) + R_2(0)\exp(-t/\tau 2)$. Times are given in ps and the uncertainties listed are standard deviations ($\pm 1\sigma$) for at least six determinations of each quantity.

Table 7 – Reorientation Times and Zero-Time Anisotropies for 1-Methylperylene in the n-Aldehydes.[a]

	1-Methylperylene			
Solvent	$R_1(0)$	τ_1 (ps)	$R_2(0)$	τ_2 (ps)
C_2H_5CHO	0.26±0.14	25±10	--	--
C_3H_7CHO	0.25±0.04	20±3	--	--
C_4H_9CHO	0.23±0.04	34±6	--	--
$C_5H_{11}CHO$	0.25±0.11	17±5	0.12±0.05	102 ± 28
$C_6H_{13}CHO$	0.26±0.08	21±8	0.10±0.06	98 ± 19
$C_7H_{15}CHO$	0.15±0.04	21±4	0.12±0.04	84 ± 2
$C_8H_{17}CHO$	0.16±0.07	17±7	0.20±0.02	97 ± 10
$C_9H_{19}CHO$	0.23±0.04	24±12	0.17±0.06	138 ± 27

[a]The data are the best fit results of the data to the function $R(t) = R_1(0)\exp(-t/\tau 1)$ or $R(t) = R_1(0)\exp(-t/\tau 1) + R_2(0)\exp(-t/\tau 2)$. Times are given in ps and the uncertainties listed are standard deviations ($\pm 1\sigma$) for at least six determinations of each quantity.

Table 8 – Reorientation Times and Zero-Time Anisotropies for Perylene in the Ketones.[a]

	Perylene			
Solvent	$R_1(0)$	τ_1 (ps)	$R_2(0)$	τ_2 (ps)
2-heptanone	0.24±0.05	31±5	--	--
3-heptanone	0.34±0.03	25±3	--	--
4-heptanone	0.20±0.01	26±3	--	--
2-octanone	0.19±0.03	27±2	--	--
3-octanone	0.20±0.02	33±3	--	--
2-nonanone	0.23±0.03	17±2	0.12±0.01	57±10
3-nonanone	0.29±0.09	19±5	0.09±0.04	88±10
4-nonanone	0.30±0.17	18±6	0.12±0.06	74±21
5-nonanone	0.31±0.12	25±5	0.09±0.05	93±23

[a]The data are the best fit results of the data to the function $R(t) = R_1(0)\exp(-t/\tau_1)$ or $R(t) = R_1(0)\exp(-t/\tau_1) + R_2(0)\exp(-t/\tau_2)$. Times are given in ps and the uncertainties listed are standard deviations ($\pm 1\sigma$) for at least six determinations of each quantity.

Table 9 – Reorientation Times and Zero-Time Anisotropies for 1-Methylperylene in the Ketones.[a]

	1-methylperylene			
Solvent	$R_1(0)$	τ_1 (ps)	$R_2(0)$	τ_2 (ps)
2-heptanone	0.27±0.05	11±2	--	--
3-heptanone	0.26±0.05	17±2	--	--
4-heptanone	0.24±0.03	18±2	--	--
2-octanone	0.27±0.05	17±3	--	--
3-octanone	0.34±0.06	21±7	--	--
2-nonanone	0.25±0.04	14±7	0.12±0.07	54 ± 9
3-nonanone	0.31±0.03	17±8	0.14±0.05	71 ± 17
4-nonanone	0.32±0.10	20±8	0.11±0.05	98 ± 15
5-nonanone	0.37±0.20	17±6	0.13±0.05	94 ± 22

[a]The data are the best fit results of the data to the function $R(t) = R_1(0)\exp(-t/\tau_1)$ or $R(t) = R_1(0)\exp(-t/\tau_1) + R_2(0)\exp(-t/\tau_2)$. Times are given in ps and the uncertainties listed are standard deviations ($\pm 1\sigma$) for at least six determinations of each quantity.

ratio saturates at ~ 8.5 for sufficiently long alkanes.[43] For both perylene and 1-methylperylene in the *n*-alcohols, we recovered D_z/D_x ranges from ~4 in methanol to ~8.5 in *n*-decanol.[59] It is not clear that $D_z/D_x \sim 8.5$ is a saturation value because we are limited in the length of the *n*-alcohols we can use. *n*-Dodecanol has been shown to form a mesophase between 24°C and 30°C,[60] and we must therefore expect similar phenomena for even longer chain *n*-alcohols near their freezing point. In the work we present here, we recover $D_z/D_x < 1$ for 1-methylperylene in aldehydes pentanal and smaller, and in the C_7 and C_8 ketones, regardless of carbonyl functionality position. In the longer chain aldehydes and ketones, the ratio of D_z/D_x does not reach the same level seen for 1-methylperylene in *n*-alkanes and *n*-alcohols, but does appear to saturate (Table 10, Table 11, Table 12, Table 13).

It is important to note that long-chain solvents are not the only ones that exhibit double exponential anisotropy decay behavior. In a recent study by Jas *et al.*,[42] perylene in cyclohexane and 2-propanol were shown to exhibit double exponential decay anisotropy decays, and the authors concluded that the fast reorientation about the *z*-axis resulted from confinement of the perylene molecule. Their conclusions are in full agreement with ours. The phenomenon of (planar or quasi-planar) solute confinement within solvent lamellar-like structures appears to be reasonably general and it will be important to elucidate the nature of the solvent-solvent intermolecular forces that give rise to this sort of solute confinement.

Despite the wealth of information available from reorientation measurements, we would like to achieve an understanding of solvent-solute interactions that these measurements alone cannot provide. In an attempt to garner further insight into solvation

Table 10 – Cartesian components of the rotational diffusion constant, D, for perylene in the aldehydes.[a]

	Perylene		
Solvent	D_x (GHz)	D_z (GHz)	D_z/D_x[b]
C_2H_5CHO	--	9.0 ± 2.6	< 1
C_3H_7CHO	--	7.0 ± 1.1	< 1
C_4H_9CHO	--	7.9 ± 1.4	< 1
$C_5H_{11}CHO$	1.9 ± 0.1	10.7 ± 4.2	5.5 ± 0.4
$C_6H_{13}CHO$	2.1 ± 0.3	10.9 ± 3.2	5.2 ± 0.3
$C_7H_{15}CHO$	1.4 ± 0.5	9.8 ± 2.8	6.8 ± 0.4
$C_8H_{17}CHO$	1.8 ± 0.3	13.9 ± 5.5	7.6 ± 0.4
$C_9H_{19}CHO$	1.6 ± 0.2	10.8 ± 2.0	6.7± 0.2

[a]These quantities and their uncertainties are derived from the fitted time constants shown in Table 6. [b]The uncertainties in the quantities D_z/D_x were calculated from the standard deviations in the D_z and the D_x data according to the formula $\sigma_{D_z/D_x} = (D_z/D_x)\sqrt{(\sigma_{D_x}/D_x)^2 + (\sigma_{D_z}/D_z)^2}$.

Table 11 – Cartesian components of the rotational diffusion constant, D, for 1-methylperylene in the aldehydes.[a]

	1-methylperylene		
Solvent	D_x (GHz)	D_z (GHz)	D_z/D_x[b]
C_2H_5CHO	--	6.6 ± 2.6	< 1
C_3H_7CHO	--	8.3 ± 1.2	< 1
C_4H_9CHO	--	4.9 ± 1.0	< 1
$C_5H_{11}CHO$	1.6 ± 0.4	13.6 ± 3.9	8.4 ± 0.4
$C_6H_{13}CHO$	1.7 ± 0.3	11.2 ± 4.5	6.6 ± 0.4
$C_7H_{15}CHO$	2.0 ± 0.1	11.0 ± 2.0	5.6 ± 0.2
$C_8H_{17}CHO$	1.7 ± 0.2	13.5 ± 5.1	7.9 ± 0.4
$C_9H_{19}CHO$	1.2 ± 0.2	9.8 ± 4.9	8.1 ± 0.5

[a]These quantities and their uncertainties are derived from the fitted time constants shown in Table 7. [b]The uncertainties in the quantities D_z/D_x were calculated from the standard deviations in the D_z and the D_x data according to the formula $\sigma_{D_z/D_x} = (D_z/D_x)\sqrt{(\sigma_{D_x}/D_x)^2 + (\sigma_{D_z}/D_z)^2}$.

Table 12 – Cartesian components of the rotational diffusion constant, D, for perylene in the ketones.[a]

	Perylene		
Solvent	D_x (GHz)	D_z (GHz)	D_z/D_x[b]
2-heptanone	--	5.3 ± 0.9	< 1
3-heptanone	--	6.7 ± 0.7	< 1
4-heptanone	--	6.3 ± 0.6	< 1
2-octanone	--	6.3 ± 0.5	< 1
3-octanone	--	5.1 ± 0.5	< 1
2-nonanone	3.0 ± 0.5	13.4 ± 1.4	4.5 ± 0.2
3-nonanone	1.9 ± 0.2	12.0 ± 3.4	6.4 ± 0.3
4-nonanone	2.3 ± 0.7	12.4 ± 4.4	5.5 ± 0.5
5-nonanone	1.8 ± 0.5	9.2 ± 2.0	5.1 ± 0.3

[a]These quantities and their uncertainties are derived from the fitted time constants shown in Table 8. [b]The uncertainties in the quantities D_z/D_x were calculated from the standard deviations in the D_z and the D_x data according to the formula $\sigma_{D_z/D_x} = (D_z/D_x)\sqrt{(\sigma_{D_x}/D_x)^2 + (\sigma_{D_z}/D_z)^2}$.

Table 13 – Cartesian components of the rotational diffusion constant, D, for 1-methylperylene in the ketones.[a]

	1-methylperylene		
Solvent	D_x (GHz)	D_z (GHz)	D_z/D_x[b]
2-heptanone	--	5.4 ± 1.1	< 1
3-heptanone	--	5.5 ± 1.4	< 1
4-heptanone	--	6.7 ± 1.0	< 1
2-octanone	--	5.0 ± 1.1	< 1
3-octanone	--	5.7 ± 0.6	< 1
2-nonanone	3.1 ± 0.5	16.0 ± 7.7	5.2 ± 0.5
3-nonanone	2.3 ± 0.6	13.6 ± 6.5	5.8 ± 0.5
4-nonanone	1.8 ± 0.3	12.7 ± 6.5	7.2 ± 0.5
5-nonanone	1.8 ± 0.4	14.0 ± 5.2	7.8± 0.4

[a]These quantities and their uncertainties are derived from the fitted time constants shown in Table 9. [b]The uncertainties in the quantities D_z/D_x were calculated from the standard deviations in the D_z and the D_x data according to the formula $\sigma_{D_z/D_x} = (D_z/D_x)\sqrt{(\sigma_{D_x}/D_x)^2 + (\sigma_{D_z}/D_z)^2}$.

processes in these systems, we consider the vibrational population relaxation dynamics of perylene and 1-methylperylene in the aldehydes and ketones next.

Vibrational population relaxation measurements. Vibrational population relaxation measurements provide information that is complementary to reorientation measurements. While reorientation and vibrational population relaxation sense fundamentally different phenomena, both depend on the properties of the chromophore local environment. We have focused on the vibrational population relaxation of the perylene 1375 cm^{-1} and the 1-methylperylene 1370 cm^{-1} ring breathing modes.[43] We have chosen these modes because the solvent terminal CH_3 groups exhibit a rocking motion at ~1390 cm^{-1} in the aldehydes, and ~1375 cm^{-1} in the ketones. In addition to this donor/acceptor pair, perylene and 1-methylperylene both possess a second ring-breathing mode, a combination mode (1375 cm^{-1} + 358 cm^{-1}), at ~1733 cm^{-1} and ~1730 cm^{-1}, respectively, that is essentially degenerate with the aldehyde and ketone carbonyl stretching modes at ~1727 cm^{-1} and ~1717 cm^{-1}, respectively. The measurement of T_1 as a function of solvent identity for these modes can provide information on the spatial proximity and relative orientation of the donor and acceptor vibrational coordinates. We have chosen the series of ketones to address the proximity of the C=O and -CH_3 solvent functionalities to the selected chromophore vibrational coordinates. The experimental details of this technique have been presented elsewhere[61,62] and we forego a discussion of this matter here. We show a representative T_1 data set and instrument response function in Figure 32. The vibrational population relaxation time constants we report here are similar for the two chromophores in each of the ketones studied. We present

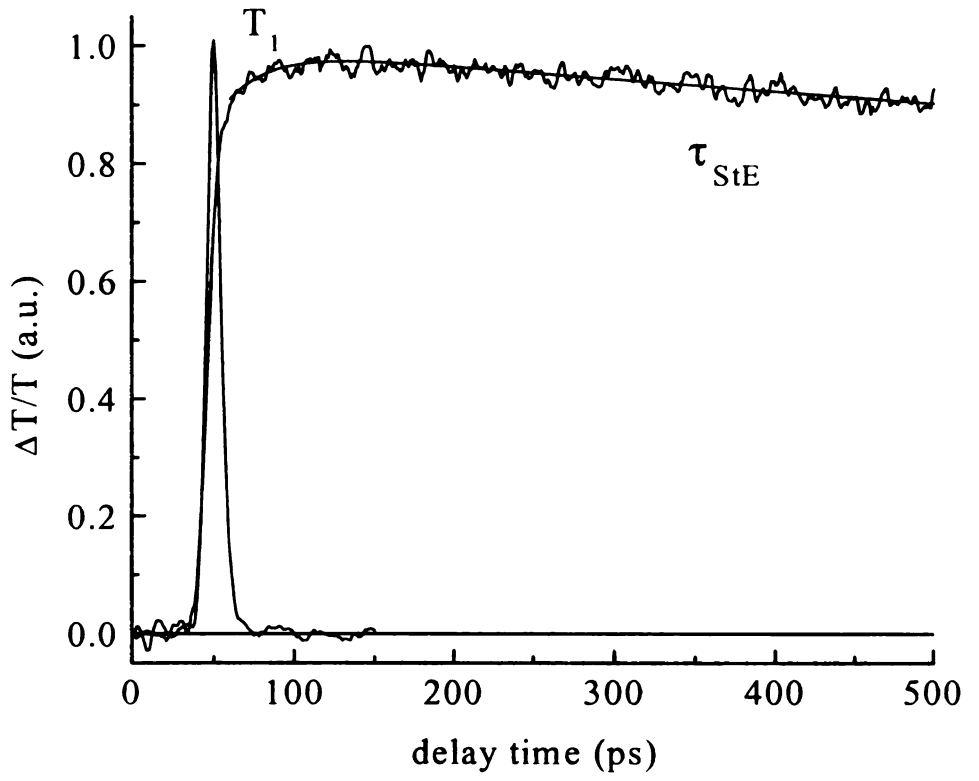

Figure 32 – Normalized vibrational population relaxation data (probe polarized at 54.7° with respect to the pump) and instrument response function for perylene in 3-octanone.

these T_1 values in Table 14 and Figure 33 and Figure 34. For all of the aldehydes examined, the T_1 times were unresolvably fast, implying strong solvent-solute coupling. For the ketones, the similarity of the T_1 data for the two probe molecules is unexpected because perylene possesses a center of inversion and 1-methylperylene does not. Molecules possessing a center of inversion couple with their immediate environment with a distance-dependence of r^{-8}, and molecules lacking a center of inversion couple with a distance-dependence of r^{-6}.[36] The fact that the T_1 values are so similar for the two probe molecules combined with the similarity in their reorientation times argues for a substantial perturbation of the chromophore symmetry by the solvent environment.

Because the theoretical framework for the interpretation of vibrational population relaxation in liquids is not well developed, we do not attempt to extract information on solvent-solute interactions from individual T_1 values. Rather, we are interested in the solvent-dependence of these time constants (Figure 33 and Figure 34). The observed trends for the ketone carbonyl acceptor mode closely follow those of the terminal methyl group acceptor mode, and this is an expected result since the donor mode (~1733 cm^{-1}) is a combination of the 1375 cm^{-1} ring breathing mode and the 358 cm^{-1} in-plane stretching mode. The ketone terminal methyl groups are in close proximity to the solute in all cases, and any additional coupling between the solute (donor) combination mode and the solvent carbonyl stretch is inefficient because of the facile pathway for relaxation through the 1375 cm^{-1} ring breathing mode.

The picture that emerges from the reorientation and T_1 data is that, for all of the ketones, the solvent terminal methyl groups remain in relatively close proximity to the solute; that

Table 14 – Vibrational population relaxation times, T_1, for perylene and 1-methylperylene in the ketones.

	Perylene		1-methylperylene	
Solvent	T_1 – 1370 cm^{-1}	T_1 – 1733 cm^{-1}	T_1 – 1375 cm^{-1}	T_1 – 1733 cm^{-1}
3-pentanone	15 ± 10	13 ± 6	11 ± 10	20 ± 14
3-heptanone	16 ± 6	40 ± 21	20 ± 11	22 ± 2
3-octanone	34 ± 17	47 ± 30	8 ± 5	50 ± 11
3-nonanone	21 ± 7	26 ± 14	35 ± 14	35 ± 13

Relaxation times are determined from at least six individual data sets and the uncertainties are standard deviations. Times are values from fits of the experimental data to the function:

$$f(t) = A_1 \exp(-t/\tau_{StE}) - A_2 \exp(-t/T_1)$$

where τ_{StE} is the stimulated emission decay time constant and T_1 is the vibrational population relaxation time constant. The T_1 times in are given in ps.

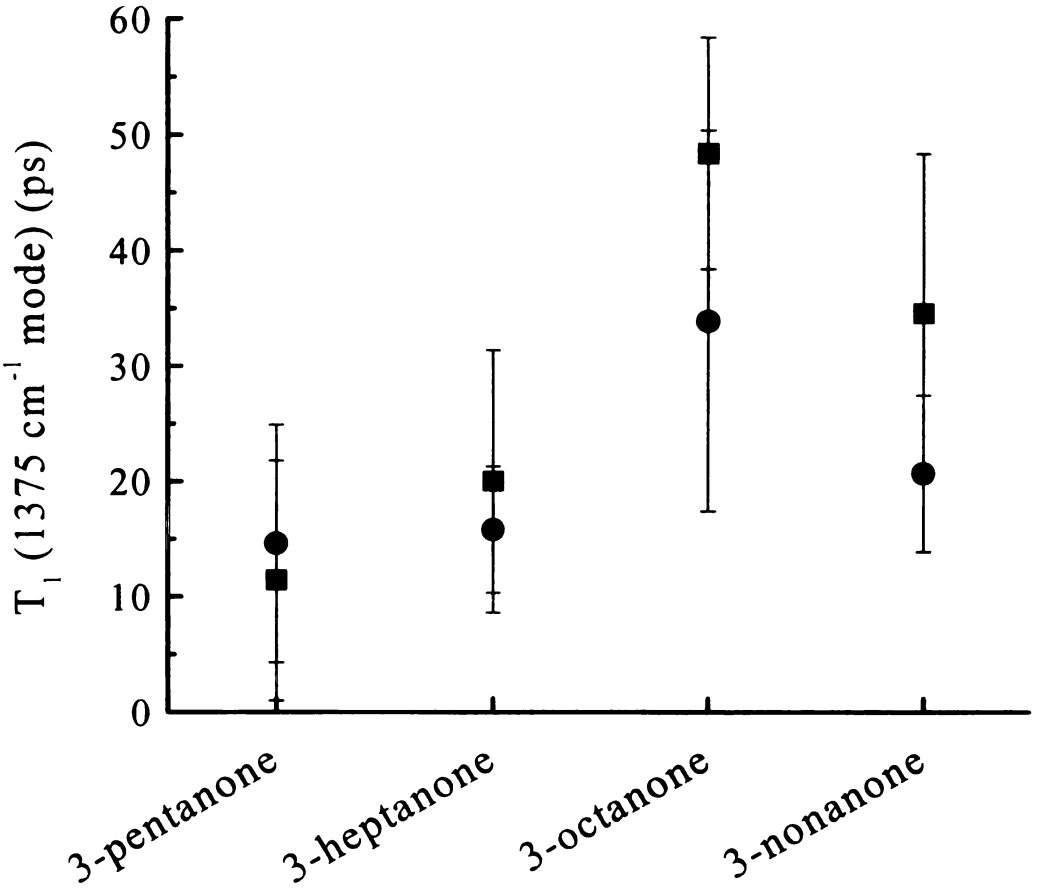

Figure 33 – Vibrational population relaxation times of the 1375 cm^{-1} mode for perylene (●) and 1-methylperylene (■) as a function of solvent aliphatic chain length in the ketones.

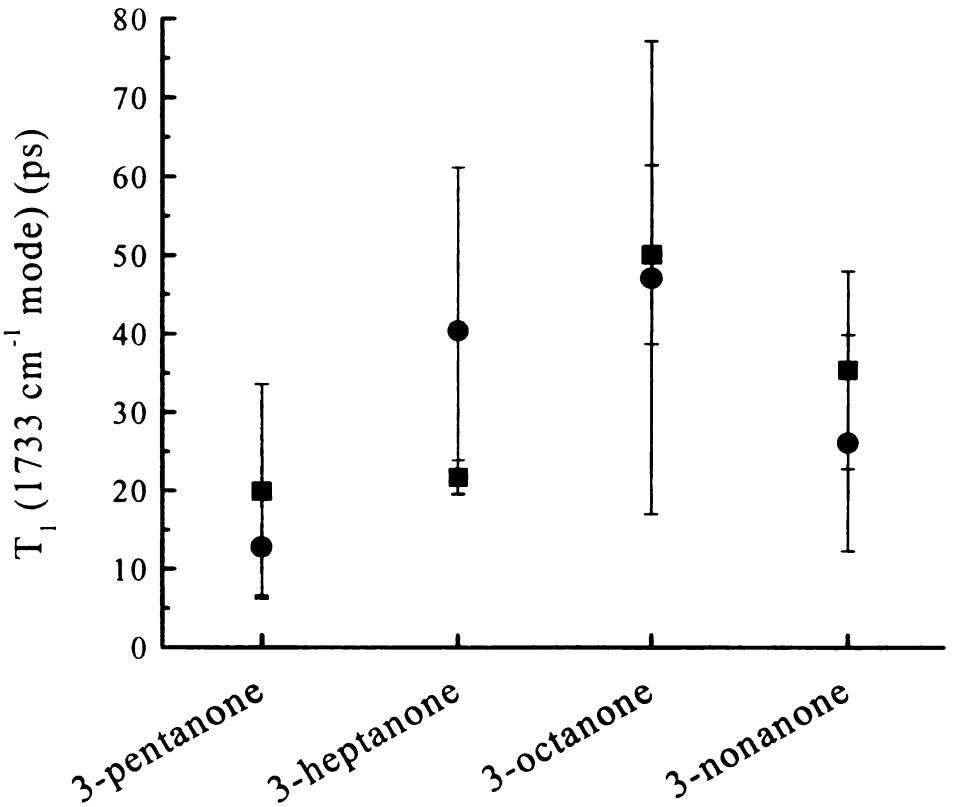

Figure 34 – Vibrational population relaxation times of the 1733 cm^{-1} mode for perylene (●) and 1-methylperylene (■) as a function of solvent aliphatic chain length in the ketones.

the interaction between the solute and solvent is of sufficient strength to effect a structural distortion that lifts the perylene center of inversion and that the solute is confined in a quasi-lamellar environment in solvents of sufficient length. It is important to note here that the extent of the distortion of the perylene molecule is not related in a linear fashion to the apparently large change in measured T_1 times relative to the unperturbed case.[41] Any break in the symmetry of the chromophore will give rise to stronger solvent-solute coupling. The proportionality between any such structural distortion and a change in T_1 has not been established. If the details of the putative structural distortion were known and the potential energy gradient for the solute along this coordinate were determined, then an estimate of the change in induced dipole moment as a function of distortion along the appropriate coordinate could be made. Given the limited information available, such an estimate is not possible. These findings do suggest, however, that the perylene chromophore is not as able to sequester itself away from the solvent polar group in the ketones to the extent that it can in the alcohols.

We now consider the T_1 results for perylene and 1-methylperylene in the aldehydes. For all cases we observe that the T_1 relaxation is fast, indicating high efficiency vibrational energy transfer from the solute to the solvent. We observe efficient solvent-solute coupling for both chromophores and, consistent with the data for the ketones, the strong coupling is necessarily due to the close proximity of the donor and acceptor moieties. These findings are consistent with the reorientation data. Because of the similarity of the perylene and 1-methylperylene reorientation data in the aldehydes and *n*-alcohols, substantial solvent-solvent interactions involving the terminal functionalities dominate the solvent organization that the chromophores sense. Our data

indicate that the aldehyde proton can H-bond efficiently with other solvent molecules, presumably at the C=O functionality.

The dynamical data for perylene and 1-methylperylene in the aldehydes are reminiscent of the behavior of these chromophores in the *n*-alcohols, and there is a similarity between the 1-methylperylene behavior in the alkanes and the ketones. For all cases, we see quasi-lamellar confinement of the probe molecules in longer solvents and the T_1 times for these systems are uniformly short. These data argue for strong solvent-solute interactions, and a central issue is the nature of these interactions. If dipole-induced dipole interactions were dominant, then we would expect to see similar behavior for these probe molecules in the aldehydes and ketones because of their similar dipole moments. We do not observe this experimentally. If H-bonding interactions were most significant, then the expected correspondence would be between the aldehydes and alcohols, and this is what we observe experimentally. The correspondence between the ketone and alkane data suggests that dipolar interactions are relatively unimportant for these probe molecules.

Conclusions

We have studied the rotational diffusion and vibrational population relaxation dynamics for perylene and 1-methylperylene in a series of aldehydes from propanal to decanal, and a series of ketones that have an aliphatic substituent similar in length to that of the major axis of the chromophore. We find evidence for solvent local organization in each solvent. In the aldehyde solvents, we observe changes in the rotational diffusion behavior that are consistent with hydrogen-bonding solvent-solvent interactions by virtue of the similarity of these data to the behavior of the same chromophores in *n*-alcohols.

For the ketones, we observe chromophore behavior that is reminiscent of that seen for these same molecules in *n*-alkanes. The central conclusions of this work are that the interactions between solvent and solute are sufficiently strong to perturb the symmetry of the chromophores, based on our T_1 data; the solvent-solvent interactions are sufficiently strong to provide a quasi-lamellar, confining environment for these chromophores, as manifested in the reorientation data. The balance of solvent-solvent and solvent-solute forces depends on the specific system studied, and for the chromophores perylene and 1-methylperylene, H-bonding solvent-solvent interactions are more important in determining solvation properties than dipole-induced dipole interactions.

Literature Cited

1. This work was submitted for review and publication to *J. Phys. Chem. A.*
2. Sanders, M. J.; Wirth, M. J.; *Chem. Phys. Lett.*, **1983**, *101*, 361.
3. Gudgin-Templeton, E. F.; Quitevis, E. L.; Kenney-Wallace, G. A.; *J. Phys. Chem.*, **1985**, *89*, 3238.
4. Von Jena, A.; Lessing, H. E.; *Chem. Phys.*, **1979**, *40*, 245.
5. Von Jena, A.; Lessing, H. E.; *Ber. Bunsen-Ges. Phys. Chem.*, **1979**, *83*, 181.
6. Von Jena, A.; Lessing, H. E.; *Chem. Phys. Lett.*, **1981**, *78*, 187.
7. Eisenthal, K. B.; *Acc. Chem. Res.*, **1975**, *8*, 118.
8. Fleming, G. R.; Morris, J. M.; Robinson, G. W.; *Chem. Phys.*, **1976**, *17*, 91.
9. Shank, C. V.; Ippen, E. P.; *Appl. Phys. Lett.*, **1975**, *26*, 62.
10. Millar, D. P.; Shah, R.; Zewail, A. H.; *Chem. Phys. Lett.*, **1979**, *66*, 435.
11. Gudgin-Templeton, E. F.; Kenney-Wallace, G. A.; *J. Phys. Chem.*, **1986**, *90*, 2896.
12. Blanchard, G. J.; Wirth, M. J.; *J. Phys. Chem.*, **1986**, *90*, 2521.
13. Blanchard, G. J.; *J. Chem. Phys.*, **1987**, *87*, 6802.
14. Blanchard, G. J.; Cihal, C. A.; *J. Phys. Chem.*, **1988**, *92*, 5950.
15. Blanchard, G. J.; *J. Phys. Chem.*, **1988**, *92*, 6303.
16. Blanchard, G. J.; *J. Phys. Chem.*, **1989**, *93*, 4315.
17. Blanchard, G. J.; *Anal. Chem.*, **1989**, *61*, 2394.
18. Alavi, D. S.; Hartman, R. S.; Waldeck, D. H.; *J. Phys. Chem.*, **1991**, *95*, 6770.
19. Hartman, R. S.; Alavi, D. S.; Waldeck, D. H.; *J. Phys. Chem.*, **1991**, *95*, 7872.
20. Jiang, Y.; Blanchard, G. J.; *J. Phys. Chem.*, **1994**, *98*, 6436.

21. Brocklehurst, B.; Young, R. N.; *J. Phys. Chem.*,**1995**, *99*, 40.

22. Pauls, S. W.; Hedstrom, J. F.; Johnson, C. K.; *Chem. Phys.*, **1998**, *237*, 205.

23. Elsaesser, T.; Kaiser, W.; *Annu. Rev. Phys. Chem.*, **1991**, *42*, 83.

24. Lingle, R., Jr.; Xu, X.; Yu, S. C.; Zhu, H.; Hopkins, J. B.; *J. Chem. Phys.*, **1990**, *93*, 5667.

25. Anfinrud, P. A.; Han, C.; Lian, T.; Hochstrasser, R. M.; *J. Phys. Chem.*, **1990**, *94*, 1180.

26. Heilweil, E. J.; Casassa, M. P.; Cavanagh, R. R.; Stephenson, J. C.; *Ann. Rev. Phys. Chem.*, **1989**, *40*, 143.

27. Heilweil, E. J.; Cavanagh, R. R.; Stephenson, J. C.; *Chem. Phys. Lett.*, **1987**, *134*, 181.

28. Heilweil, E. J.; Cavanagh, R. R.; Stephenson, J. C.; *J. Chem. Phys.*, **1989**, *89*, 230.

29. Heilweil, E. J.; Casassa, M. P.; Cavanagh, R. R.; Stephenson, J. C.; *J. Chem. Phys.*, **1986**, *85*, 5004.

30. Hambir, S. A.; Jiang, Y.; Blanchard, G. J.; *J. Chem. Phys.*, **1993**, *98*, 6075.

31. Jiang, Y.; Blanchard, G. J.; *J. Phys. Chem.*, **1994**, *98*, 9411.

32. Jiang, Y.; Blanchard, G. J.; *J. Phys. Chem.*, **1994**, *98*, 9417.

33. Jiang, Y.; Blanchard, G. J.; *J. Phys. Chem.*, **1995**, *99*, 7904.

34. McCarthy, P. K.; Blanchard, G. J.; *J. Phys. Chem.*, **1995**, *99*, 17748.

35. McCarthy, P. K.; Blanchard, G. J.; *J. Phys. Chem.*, **1996**, *100*, 5182.

36. McCarthy, P. K.; Blanchard, G. J.; *J. Phys. Chem.*, **1996**, *100*, 14592.

37. Jiang, Y.; Hambir, S. A.; Blanchard, G. J.; *Opt. Commun.*, **1993**, *99*, 216.

38. Bado, P.; Wilson, S. B.; Wilson, K. R. *Rev. Sci. Instrum.* **1982**, *53*, 706.

39. Andor, L.; Lorincz, A.; Siemion, J.; Smith, D. D.; Rice, S. A.; *Rev. Sci. Instrum.* **1984**, *55*, 64

40. Blanchard, G. J.; Wirth, M. J.; *Anal. Chem.*, **1986**, *56*, 532.

41. Peake, D. A.; Oyler, A. R.; Heikkila, K. E.; Liukkonen, R. J.; Engroff, E. C.; Carlson, R. M. *Synth. Commun.* **1983**, *13*, 21.

42. Jas, G. S.; Larson, E. J.; Johnson, C. K.; Kuczera, K.; *J. Phys. Chem. A*, **2000**, *104*, 9841.

43. Karpovich, D. S.; Blanchard, G. J. *J. Phys. Chem.* **1995**, *99*, 3951.

44. Lewitzka, L; Lohmannsroben, H.-G Strauch, M.; Luttke, W. *Photochem. Photobiol. A: Chem.* **1991**, *61*, 191.

45. Grimme, S.; Lohmannsroben, H.-G *J. Phys. Chem.* **1992**, *96*, 7005.

46. Debye, P. *Polar Molecules*; Chemical Catalog Co.: New York, 1929; p. 84.

47. Perrin, F. *J. Phys. Radium* **1936**, *7*, 1.

48. Chuang, T. J.; Eisenthal, K. B. *J. Chem. Phys.* **1972**, *57*, 5094.

49. Hu, C. M.; Zwanzig, R. *J. Chem. Phys.* **1974**, *60*, 4354.

50. Youngren, G. K.; Acrivos, A. *J. Chem. Phys.* **1975**, *63*, 3846.

51. Zwanzig, R.; Harrison, A. K. *J. Chem. Phys.* **1985**, *83*, 5861.

52. Edward, J. T.; *J. Chem. Ed.*, **1970**, *47*, 261.

53. Brocklehurst, B.; Young, R. N. *J. Chem. Phys.* **1995**, *99*, 40.

54. Piston, D. W.; Bilash, T.; Gratton, E.; *J. Phys. Chem.*, **1989**, *93*, 3963.

55. Blanchard, G. J.; Wirth, M. J.; *J. Chem. Phys.*, **1985**, *82*, 39.

56. Pauls, S. W.; Hedstrom, J. F; Johnson, C. K. *Chem. Phys.* **1998,** *237*, 205.

57. The permanent dipole moments for S_0 and S_1 1-methylperylene and for ground state solvent molecules was calculated using Hyperchem 6.0®, performing a semi-empirical calculation with PM-3 parameterization.

58. Matsunuma, S.; Akamatsu, N,; Kamisuki, T.; Adachi, Y.; *J. Chem. Phys.*, **1988,** *88*, 2956.

59. Goldie, S. N.; Blanchard, G. J. *J. Phys. Chem. A.* **1999,** *103*, 999.

60. Blanchard, G. J.; Wirth, M. J. *J. Phys. Chem.* **1986,** *90*, 2521.

61. Blanchard, G. J.; *Rev. Sci. Instrum.*, **1996,** *67*, 4085.

62. Blanchard, G. J.; *Anal. Chem.*, **1997,** *69*, 351A.

Chapter 4

IN-SITU QUANTIFICATION OF ACID GENERATION IN A DEEP UV PHOTORESIST THROUGH THE USE OF PROBE MOLECULES[1]

Introduction

One of the goals in the semiconductor industry is to increase the feature density of computer semiconductor chips. As feature density increases, so does the processing capability of these devices. To accomplish this goal, the microlithographic methods used today have been moving toward the use of shorter wavelengths, which translates to smaller features on a semiconductor chip. The circuit patterns of a microprocessor are transferred to silicon dioxide layers deposited on a silicon wafer using light and a quartz/chromium photomask. The intensity of commonly used short wavelength sources is characteristically low. In the manufacturing process, a single photon will at best result in a single photoevent. The limited number of short wavelength photons results in a low manufacturing efficiency.

There are two main problems that gave rise the development of chemically amplified resists. The first is the lack of photon flux in the deep UV (DUV) region of the spectrum of commonly used sources. The second problem is the relative insensitivity, or low quantum efficiency, of traditional resists and their photoactive compounds in the deep UV part of the spectral region.

To circumvent these problems, photoresists have been formulated with additives that will chemically amplify the number of photon absorbtion events in a polymeric matrix. One of these means is through the use of photoinitiators. These additives serve as catalysts in the amplification of the photons. A photoinitiator is activated by a photon.

which then dissociates to generate a photoacid molecule. In the polymer, the degradation process involves cleavage of pendant groups from the polymeric backbone through the use of this photoacid. (Scheme 3)

Scheme 3 – Deprotection reaction representative of photoresist exposure. The gases isobutylene and carbon dioxide are liberated, and the proton regenerated as a result of exposure to UV radiation.

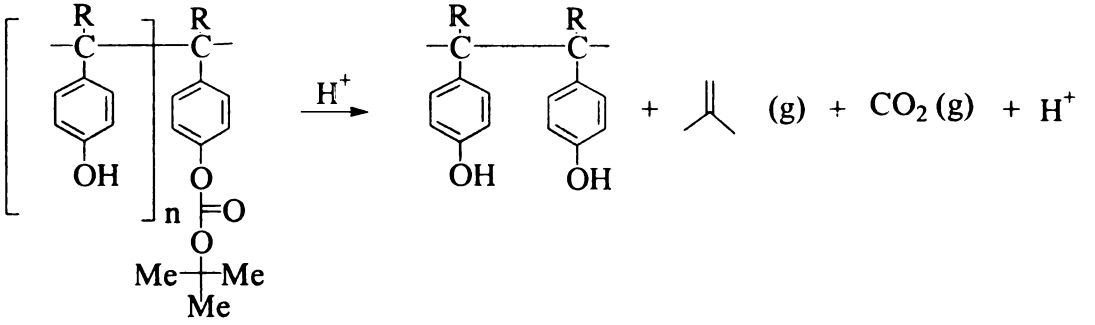

As a result of this process, carbon dioxide and isobutylene gases are generated and diffuse from the polymer. The photoacid is then regenerated and through a reaction-diffusion process causes many cleavage events to occur as the result of a single photon being absorbed. The cleavage of the pendant groups causes the polymer to be soluble in an alkaline solution, allowing it to be dissolved and removed, leaving a void where further chemical processing (*i.e.* etching, deposition) can occur. In a chemically amplified resist, the sensitivity to deep UV photons is increased. Instead of a single photoevent that results from a single photon, a single photon can result in several deprotection reactions.

Though this process enables the use of DUV photons for smaller feature sizes, it can cause another problem through the uncontrolled diffusion of the photoacid outside of the desired regions of the circuit paths. For this reason, it is important to understand the diffusional characteristics of the photoacid. The two processing steps that have the

greatest impact on the concentration and diffusional mobility of the photoacid are exposure and post exposure bake (PEB). The acid is produced by the photolysis of an onium salt photoacid generator (PAG). For a given PAG concentration, the exposure dose will dictate the amount of acid that is generated. The temperature and duration of the PEB both influence the diffusional mobility of the acid and the rate of the deprotection reaction. The PEB is the time in which the actual acid diffusion and deprotection reaction take place, and therefore the PEB conditions have the greatest impact on the resulting linewidth. Higher PEB temperatures increase the sensitivity of the resist but also increase the diffusivity of the acid, increasing susceptibility to process variations. Both reaction and diffusion are very sensitive to temperature and time, and even slight non-uniformity on hot plates or a delay in reaching a cool plate (and therefore a delay in quenching of the reaction) can cause significant changes in critical dimensions (CDs). These nonlinear interactions between exposure light intensity, chemical reaction and non-constant diffusion make optimizing and running a stable process a challenge. This creates non-uniform line shapes, which can result in incorrect or imperfect patterns on a chip. To understand and account for these processes, it is necessary to characterize the amount of acid generated and to determine the location of the photoacid with high resolution. We present a method here that will accomplish these tasks with relative ease and little equipment overhead.

Experimental

Steady State Spectroscopy – in-situ *samples*

APEX E-2408 DUV photoresist, (Shipley Co.), stored in the dark at 4°C, was doped with 0.1 wt% crystal violet (Sigma-Aldrich, used as received). This solution was spin coated at 2000 rpm onto 1" x 2" quartz slides using a PWM32 spinner (Headway Research Inc.) A film layer of ~1 μm thickness resulted. The slide was then heated at 90°C for 60 seconds (post application bake, PAB) to evaporate the solvent (propylene glycol mono-methyl ether acetate, PGMEA). The samples were then divided into exposed (subject to UV exposure and further processing) and control samples. Exposed samples were subjected to the output of a 200 W Hg(Xe) lamp (Oriel) for 30 seconds and then a post exposure bake (PEB) for 90 seconds at 90°C. Absorption measurements for all samples were obtained using a HP 8452-A diode array spectrometer, with a special sample holder manufactured in-house for film studies.

Steady State Spectroscopy – liquid phase samples

The steady state absorption spectra of crystal violet as a function of pH in aqueous solution were recorded with 1 nm resolution using a Hitachi U-4001 spectrometer. A constant crystal violet concentration of 6 x 10^{-6} M was maintained for all absorption measurements by dilution from a single stock solution. The pH of the solutions was set using a series of 0.2 M potassium chloride (Spectrum, used as received) and 0.2 M hydrochloric acid (Columbus Chemical Industries, used as received) buffer systems. Outside the buffer range of this acid/base pair, aqueous solutions of 0.2 M potassium chloride or 0.2 M hydrochloric acid were used to maintain the pH. A Fisher Scientific Accumet pH meter and combination electrode with automatic temperature correction was

used for all pH determinations. The final pH of the solutions ranged from 0.26 to 5.12; all pH measurements were performed after the absorption measurements. The ionic strength of our solutions was not explicitly controlled.

Results and Discussion

Crystal violet is a widely used and studied[2-8] acid/base indicator. The structure of crystal violet (Scheme 4) is characterized by three p-dimethylaniline rings, bonded to a central carbon atom. As the level of protonation increases on the amine

Scheme 4 - The structure of crystal violet, with protonation levels and equilibria. The native form of crystal violet is shown on the left. See text for further discussion.

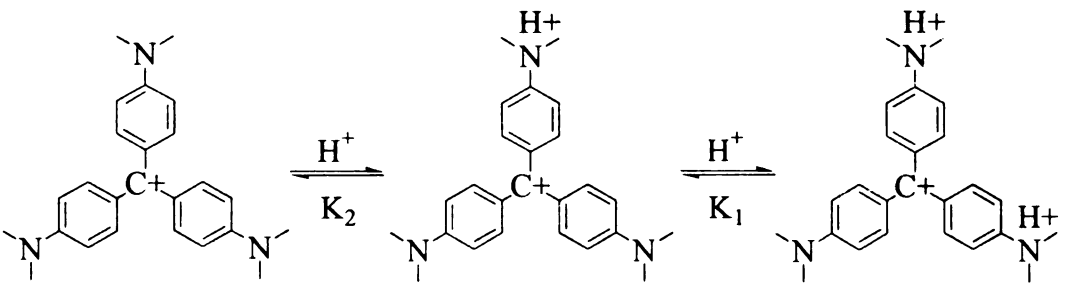

groups,[9] the steady state response of crystal violet changes. The native form of crystal violet (CV^+) is violet in color, with its $S_0 \rightarrow S_1$ absorption maximum centered about 590 nm. Protonation of one of the amino groups to form HCV^{2+} shifts the absorption maximum to 630 nm, which produces a solution that is green in color. Additional protonation to form H_2CV^{3+} produces a yellow solution, with the absorption maximum centered at 430 nm.

We were able to characterize the various forms of crystal violet in solution through the use of buffered pH systems[10] from pH~5 to pH~0, corresponding to proton concentration of 10^{-5} M to 1 M. The changes in absorption spectra are presented in Figure 35. We have found these absorption bands correspond to similar behavior

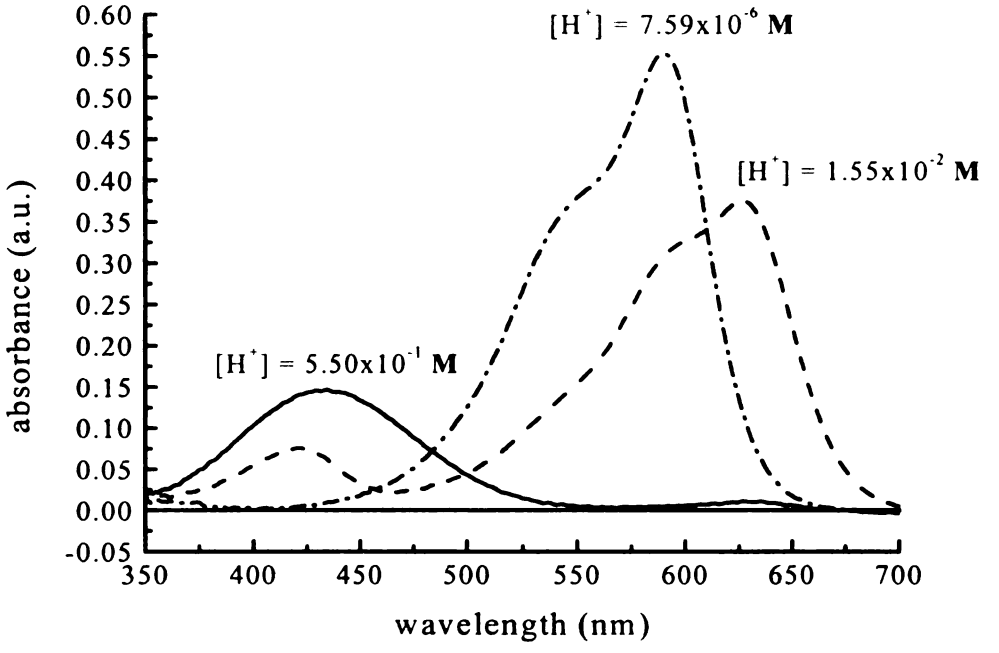

Figure 35 – The linear response of the three-protonation states of crystal violet. The acid concentration is presented near the maximum of each absorption spectrum.

of crystal violet *in-situ*. The native form of CV^+, present at low proton concentrations, absorbs strongly at 590 nm. As the pH decreases, and the proton concentration increases, the onset of a second absorption band centered at 630 nm is observed with a simultaneous decrease in absorbance at 590 nm. Continued increase in proton concentration causes a continued decrease in the 590 and the 630 nm features, while the absorption feature at 430 nm increases.

This protonation process of crystal violet is an equilibrium process. The equilibria and the equilibrium constants expressions are presented in equations (16) to (18).

$$H_2CV^{3+} \xleftrightarrow{K_1} HCV^{2+} + H^+ \xleftrightarrow{K_2} CV^+ + H^+ \qquad (16)$$

Where the equilibrium constants are expressed in the following manner:

$$K_1 = \frac{[HCV^{2+}][H^+]}{[H_2CV^{3+}]} \qquad (17)$$

$$K_2 = \frac{[CV][H^+]}{[HCV^{2+}]} \qquad (18)$$

From these expressions and these data, we determined the constants for protonation/deprotonation equilibria, by applying Beer's law to each of the solutions and solving a system of simultaneous equations, presented in equations (19) to (21),

$$A_{430} = \varepsilon_{430}^{VIOLET} bc_{430}^{VIOLET} + \varepsilon_{430}^{GREEN} bc_{430}^{GREEN} + \varepsilon_{430}^{YELLOW} bc_{430}^{YELLOW} \qquad (19)$$

$$A_{590} = \varepsilon_{590}^{VIOLET} bc_{590}^{VIOLET} + \varepsilon_{590}^{GREEN} bc_{590}^{GREEN} + \varepsilon_{590}^{YELLOW} bc_{590}^{YELLOW} \qquad (20)$$

$$A_{630} = \varepsilon_{630}^{VIOLET} bc_{630}^{VIOLET} + \varepsilon_{630}^{GREEN} bc_{630}^{GREEN} + \varepsilon_{630}^{YELLOW} bc_{630}^{YELLOW} \qquad (21)$$

where A_λ is the total absorbance at wavelength λ (nm), $\varepsilon_\lambda^{COLOR}$ is the molar absorptivity[11] of the indicated colored species at λ for each level of protonation, b is the path length (1.0

cm) and c_{λ}^{COLOR} is the concentration of each species of each protonation condition. As a check, the sum of these concentrations was compared to the total concentration of the crystal violet stock solution used in these experiments. The calculated total concentration was found to be within experimental uncertainty of the total concentration of the stock solution. We calculated the equilibrium constant values K_1 and K_2 as presented in equations (17) and (18). K_1 was determined to be (2.5 ± 1.5) x 10^{-2} M and K_2 was calculated to be (6.7 ± 2.5) x 10^{-3} M. These values correspond to $pK_1 = 1.67 \pm 0.29$ and $pK_2 = 2.20 \pm 0.19$, which is in reasonable agreement with the first pK_a value of a structurally related triphenylmethane dye, malachite green, reported to be ~1.3 in the literature.[2]

With these data, it is possible to determine the relative concentrations of each species in any solution of crystal violet as a function of solution pH based on absorbance measurements, through the use of α values. α-Values are unitless ratios of the concentration of individual species to the total analytical concentration of all the related species.[12] The sum of all the fractions in a system must equal unity. The α values are readily expressed in terms of $[H^+]$ and the equilibrium constants K_1 and K_2, previously determined here, by rearranging the equilibrium constant expressions:

$$\alpha_0 = \frac{[H_2CV^{3+}]}{C_T} = \frac{[H^+]^2}{[H^+]^2 + K_1[H^+]^2 + K_1K_2} \qquad (22)$$

$$\alpha_1 = \frac{[HCV^{2+}]}{C_T} = \frac{[H^+]K_1}{[H^+]^2 + K_1[H^+]^2 + K_1K_2} \qquad (23)$$

$$\alpha_2 = \frac{\left[CV^+\right]}{C_T} = \frac{K_1 K_2}{\left[H^+\right]^2 + K_1\left[H^+\right]^2 + K_1 K_2} \qquad (24)$$

where $[H_2CV^{3+}]$ is the concentration of the diprotonated yellow colored species, $[HCV^{2+}]$ is the concentration of the monoprotonated green colored species, and $[CV^+]$ is the concentration of the native form of crystal violet, which is purple in color. The total concentration, C_T, is the sum of these three concentrations of crystal violet in various forms of protonation. It is then possible to relate the measurable quantities of pH and the absorption characteristics to the concentration of each species and its level of protonation. We present our calibration curve for crystal violet in Figure 36. Using this set of curves, we can then apply measured absorbance quantities to proton concentration as the result of exposure, and determine the fraction of each species as a function of pH.

We have examined the changes in the steady state absorption response of crystal violet doped into the photoresist as a function of processing and present these data in Figure 37. Initially, the absorption spectrum is characterized with a single dominant feature at 590 nm, attributed to the native form of crystal violet $[CV^+]$. Immediately after exposure of the entire slide to DUV radiation and post exposure bake, the feature at 590 nm has diminished and a feature at 430 nm dominates the spectrum. Assuming that the data from our solution studies can be used to interpret the polymer data, this corresponds to the diprotonated form $[H_2CV^{3+}]$ and is indicative of a high proton concentration.

Subsequent absorption spectra collected showed a decrease in the 430 nm feature and an increase in the 630 nm feature followed by a recovery at 590 nm. We ascribe this trend to the evaporation or neutralization of the photoacid in the film. One possible mechanism for proton loss is long-term exposure of the film to airborne amines.[13,14]

This trend corresponds to a multistep process in the photoresist film. The first step is protonation of the crystal violet due to photacid production from the photoinitiator in the photoresist formulation. This process occurs within a second of exposure to the source. As the protons react with airborne bases, the crystal violet probe molecule level of protonation will decrease, with the corresponding changes in the absorption spectra. These changes will be similar to the changes observed in the liquid state. Kinetically, this process is slower, as it occurs over hours to days (*vide infra).* We present an example of these changes as a function of time in Figure 38. A major source of amines that contribute to airborne molecular contamination is the human factor, as many amines are generated and are released as a result of metabolism in the human body. Bases that have been found in semiconductor manufacturing facilities include airborne ammonia, *n*-methyl pyrrolidinone (NMP), 1,4-diaminobutane, and 1,5-diaminopentane. Each of these airborne bases can be absorbed into the polymer matrix, causing defects in the device.

In this set of experiments, the entire slide was exposed to DUV radiation. This is different from the methodology of semiconductor manufacturing, in which the illumination of the regions of the photoresist is carefully controlled through the use of quartz/chromium photomasks. These features that are transferred to the silicon dioxide layers have critical dimensions on the order of microns in size. It is possible through the use of proper near field optics (NFO's) to build an absorption spectrometer that would sample a microscopic area, on the same length scale as these critical dimensions, and interrogate the absorption behavior of a probe molecule doped into the region. From these changes, as we have demonstrated here, it is possible to determine the changes in the pH of the local environment, and calculate the amount of photoacid generated in a

specific region. With sufficient spatial resolution, the extent of a photoacid gradient could be determined, and the acid mobility as a function of time and processing conditions could also be examined. This information is important to the semiconductor fabrication community.

Conclusions

With appropriate near field optics (NFO's), it may be possible to determine the absorbance of crystal violet at a specific point and then relate that observation to acid concentration using the data presented here. This will help to accomplish our goal of quantifying the amount of the photoacid generated by the photoinitiator, and then provide information about the location and diffusion behavior of the photoacid. This information can be used to model more accurately the photoacid behavior in photoresists used in microlithographic applications.

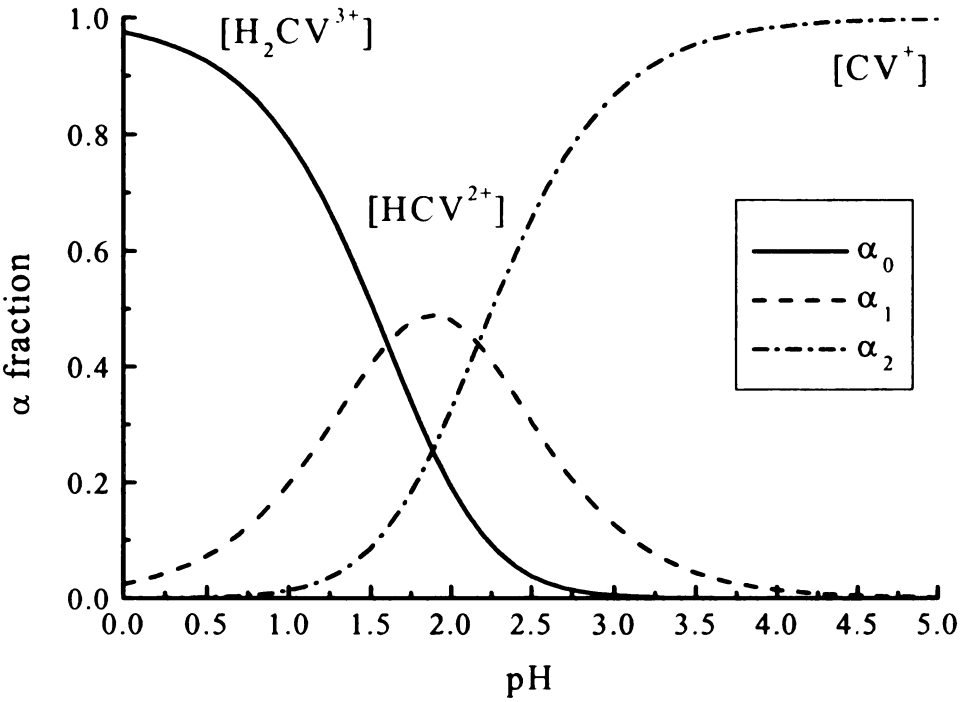

Figure 36 – α value calibration curve for crystal violet as a function of pH. The α values provide concentration data by relating absorbance.

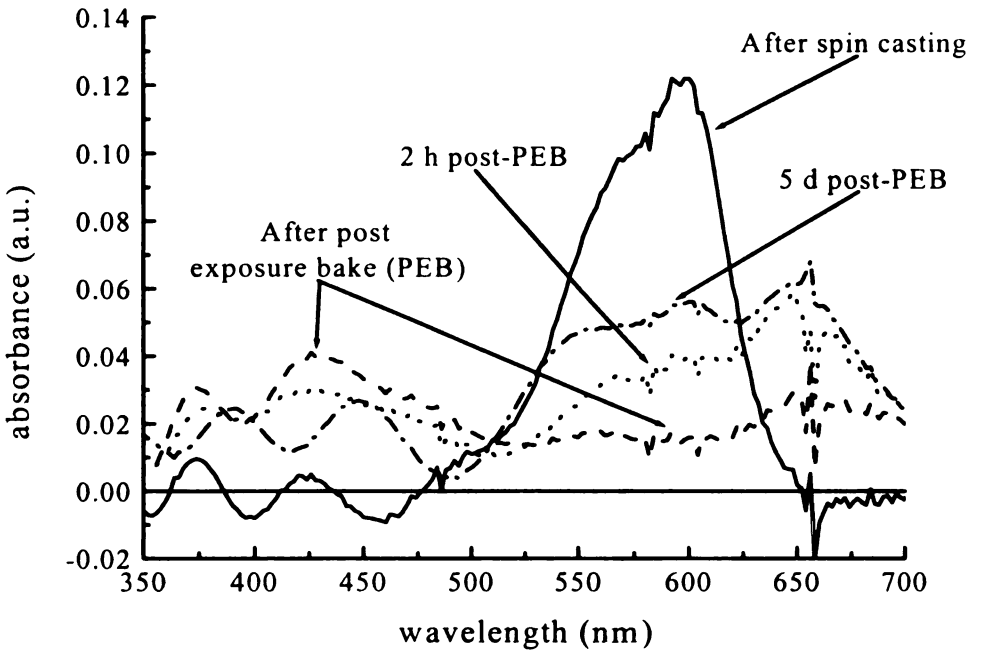

Figure 37 – Changes in the steady state absorption response of crystal violet doped into a polymer film as a function of processing. See text for a discussion.

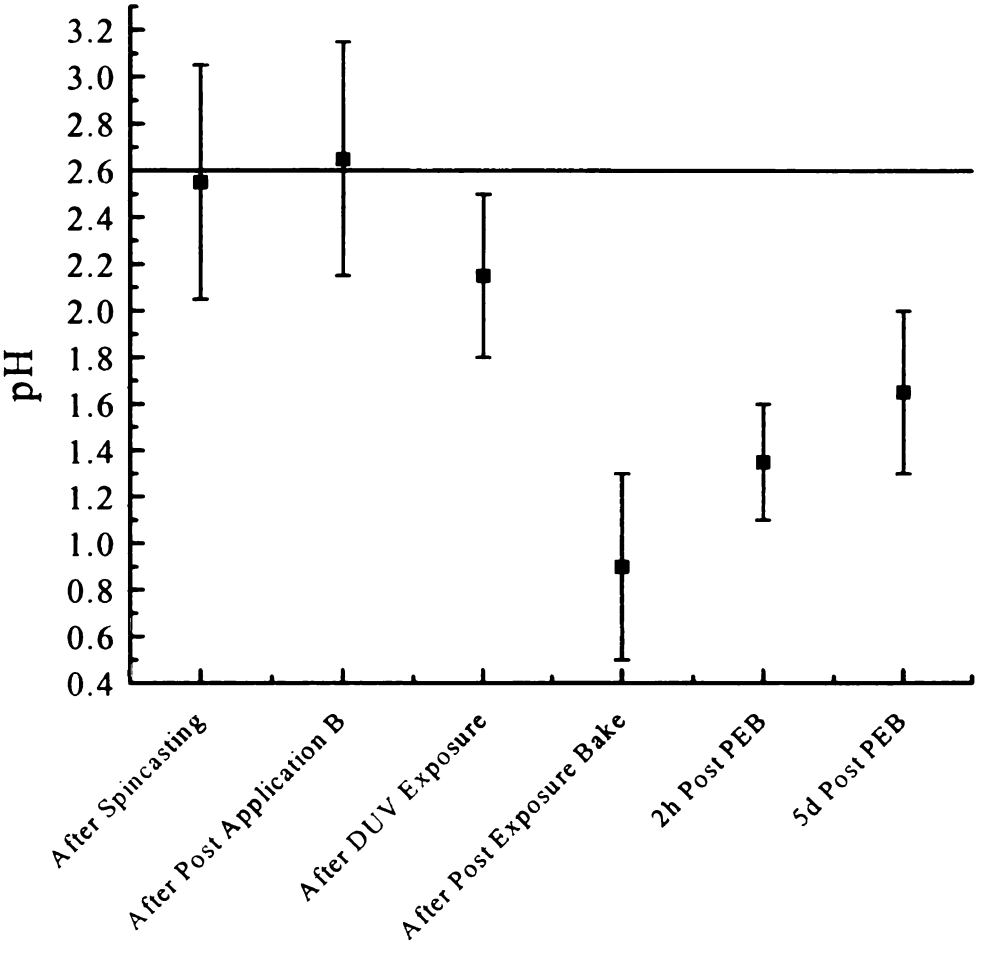

Figure 38 – Changes in pH *in-situ* as a function of processing time.

Literature Cited

1. This work, and the work of Chapter 5, will be submitted for publication to *J. Phys. Chem. B.*

2. "Indicators for Non-Aqueous Acid-Base Titrations"; Bishop, E. In *Indicators*; Bishop, E., Ed.; Pergamon: New York, 1972.

3. Duxbury, D. F. *Chem. Rev.* **1993**, *93*, 381.

4. Ben-Amotz, D.; Harris, C. B. *Chem. Phys. Lett.* **1985**, *119*, 305.

5. Ben-Amotz, D.; Harris, C. B. *J. Chem. Phys.* **1987**, *86*, 4856.

6. Ishikawa, M.; Ye, J. Y.; Maruyama, Y; Nakatsuka, H.; *J. Phys. Chem. A.* **1999**, *103*, 4319.

7. Maruyama, Y.; Ishikawa, M.; Satozono, H.; *J. Am. Chem. Soc.* **1996**, *118*, 6257.

8. Maruyama, Y.; Magnin, O. Satozono, H.; Ishiakawa, M. *J. Phys. Chem. A.* **1999**, *103*, 5629.

9. Tuthill, S. M.; Kolling, O. W.; Roberts, K. H. *Anal. Chem.* **1960**, *32*, 1678.

10. *Lange's Handbook of Chemistry*, 14th ed.; Dean, J. A., Ed.; McGraw-Hill: New York, **1992;** 8.106.

11. Conant, J. B.; Werner, T. H.; *J. Am. Chem. Soc.*, **1930**, *52*, 4436.

12. Skoog, D. A.; West, D. M.; Holler, F. J. *Fundamentals of Analytical Chemistry*, 5th ed. Saunders: Chicago, **1988,** 227.

13. Thompson, L. F.; "Resist Processing" In *Introduction to Microlithography*, 2nd ed.; Thompson, L. F.; Willson, C. G.; Bowden, M. J. Eds.; ACS Professional Reference Book: Washington, DC, **1994**, 269.

14. Mack, C. A.; "Lithographic Effects of Acid Diffusion in Chemically Amplified Resists" In *Microelectronics Technology: Polymers for Advanced Imaging and Packaging*; Reischmanis, E.; Ober, C. K.; MacDonald, S. A.; Iwayanagi, T.; Nishikubo, T. Eds.; American Chemical Society: Washington, DC, **1995**, 56.

Chapter 5

IN-SITU CHARACTERIZATION OF FREE VOLUME GENERATION DURING POST EXPOSURE BAKE (PEB) IN A COMMERICAL PHOTORESIST[1]

Introduction

As described in the previous chapter, photoresists are used to facilitate the transfer of circuit patterns of a microprocessor to silicon dioxide layers deposited on a silicon wafer using light and a quartz/chromium photomask. These photoresists have been formulated with additives that will amplify the number of photon absorption events in a polymeric matrix using chemical means thereby improving sensitivity and efficiency, so that the shorter DUV wavelengths can be used to produce smaller feature sizes. One of these means is through the use of photoinitiators. A photoinitiator is activated by a DUV photon, which then dissociates to generate a photoacid molecule. In the polymer, the degradation process involves cleavage of pendant groups from the polymeric backbone through the use of this photoacid. These photoacids serve as catalysts in the amplification of the photons, since a single photon can generate several photoacid molecules that are regenerated in the course of the deprotection reaction.

As a result of this reaction, carbon dioxide and isobutylene gases are generated and diffuse from the polymer. This process creates free volume in the polymer matrix, through which the regenerated photoacid can diffuse and cause many additional cleavage events to occur. This chain of events results from the absorption of a single photon. Though this process enables the use of shorter wavelengths for device manufacture, it can cause problems through the uncontrolled diffusion of the photoacid outside of the intended circuit pattern. For this reason, it is important to understand the diffusional

characteristics of the photoacid. The two processing steps that have the greatest impact on the concentration and diffusional mobility of the photoacid are photo-exposure and post exposure bake (PEB). We have described a novel method for determining the concentration of the photoacid generated in the previous chapter. In this chapter, we are interested in characterizing the diffusional characteristics of the photoacid in the polymer matrix.

The temperature and duration of the PEB both influence the diffusional mobility of the acid and the rate of the deprotection reaction. The PEB is the time in which the actual acid diffusion and deprotection reactions take place, and therefore the PEB conditions have the greatest impact on the resulting device feature dimensions. Higher PEB temperatures increase the sensitivity of the resist and also increase the diffusivity of the acid, giving rise to results that depend sensitively on process variations. Both reaction and photoacid diffusion are very sensitive to temperature and time, and even slight non-uniformity on hot plates or a delay in reaching a cool plate (and therefore a delay in quenching of the reaction) can cause significant changes in device structure critical dimensions (CDs). These nonlinear interactions between exposure light intensity, chemical reaction and a non-constant diffusion make optimizing and running a stable process a challenge. This situation gives rise to non-uniform line shapes, which can result in incorrect or imperfect circuit patterns on a chip. To understand and account for these processes, it is necessary to characterize the free volume generated as a function of processing. We present a new method here that will accomplish these tasks *in situ* and allow for better mathematical modeling of these processes.

Experimental

The picosecond pump-probe laser spectrometer used for the ground state recovery measurements has been described in detail previously,[2] and we present only a brief outline of its performance characteristics here. A mode-locked CW Nd:YAG laser (Coherent Antares 76-S) produces 30 W of average power (1064 nm, 100 ps pulses, 76 MHz repetition rate). The output of this laser is frequency-doubled to produce ~2.1 W of average power at 532 nm. The second harmonic light is used to excite two cavity-dumped dye lasers synchronously (Coherent 702-3). Both lasers operate with Rhodamine 6G laser dye (Kodak). The output of each laser is ~100 mW average power at 8 MHz repetition rate with a pulse that produces a 7 ps FWHM autocorrelation trace using a three plate birefringent filter. The time resolution of this system, ~10 ps, is determined by the cross-correlation between the pump and probe laser pulse trains. The pump laser wavelength was set to 589.5 nm, coincident with the absorption maximum of the first singlet transition of crystal violet. The probe wavelength was chosen to lie within the absorption band of crystal violet. The probe beam was polarized at 54.7° with respect to the pump beam to eliminate molecular reorientation contributions to the signal. Detection of the transient signals was accomplished using a radio and audio frequency triple-modulation scheme, with synchronous demodulation detection.[3-5] Each reported time constant is the average of at least five individual determinations that are themselves the average of seven to ten time-scans.

Samples for these experiments were prepared by spin coating APEX E-2408 DUV photoresist, (Shipley Co.) doped with 0.1 wt% crystal violet (Sigma-Aldrich) at 2000 rpm onto 1" x 2" quartz slides using a PWM 32 spinner (Headway Research Inc.).

A film layer of ~1 μm resulted. The slide was then heated at 90°C for 60 seconds (post application bake, PAB) to evaporate the solvent (propylene glycol, mono-methyl ether acetate, PGMEA). The samples were then divided into two sets. One set of samples experienced no further processing subsequent to spin-coating and post-application bake, while a second set of samples was exposed to 200 W Hg(Xe) lamp (Oriel) for 30 seconds and then baked for 90 seconds at 90°C. The samples were mounted in a manually driven translation stage and the two laser beams were co-focused on them. To minimize the effects of photobleaching and thermal degradation, the slide was translated as the sample was scanned, and neutral density filters were used to attenuate the incident light.

Liquid phase samples of ~1 x 10^{-4} M crystal violet in ethylene glycol, 1,3-propanediol, propylene glycol, 1,4-butanediol, 1,3-butanediol, and glycerol were made using chemicals of the highest purity available (Aldrich, Spectrum). All chemicals were used as received. The ground state recovery of each liquid phase sample was measured using a flow cell system to minimize thermal lensing considerations. The sample solutions were flowed through a 1 mm path length quartz flow cell, and the sample temperature was controlled at 300 ± 0.1 K using a thermostated bath.

Solution viscosities were determined using a Brookfield Model DV-I+ viscometer with spindle #18 for the diol solutions and #34 for glycerol. The viscosities of ethylene glycol and propylene glycol were acquired from the literature.[6]

Results and Discussion

In addition to being a well-characterized acid-base indicator, crystal violet is a widely used probe of microviscosity in solution. Crystal violet (Scheme 4, Chapter 4 – this work), a member of the triphenylmethane dye family, is predominantly a D_3

"propeller" shaped molecule in solution with three identical N,N-dimethylaniline rings bound to a central carbon atom tilted slightly out of the molecular plane. Ring rotation around the bonds between the phenyl rings to the central carbon atom in what is believed to be a barrierless process along the excited state potential energy surface. Studies have indicated a strong dependence of the excited state lifetime on solvent viscosity, which is indicative of essentially no intra-molecular rotational barrier to ring rotation.[7,8] The characteristically low fluorescence quantum yield of this family of molecules prevents us from using a fluorescence lifetime measurement to explore these changes. Instead, we examine the recovery of the ground state population by detecting the transient change in absorption of the probe pulse resulting from excitation by the pump laser pulse, to sense changes in the local environment in the photoresist thin films. We are able to characterize two film properties using this widely available chromophore because of its combined sensitivity to local acid concentration (Chapter 4, this work) and viscosity.

We observe an exponential decay of the ground-state recovery signal for the un-exposed, spin-coated, doped resist film, and we show these data in Figure 39. A fit of the decay to a sum of two exponentials results in a 25 ± 4 ps short time component (τ_1) and a longer 120 ± 18 ps time (τ_2) component. The double exponential decay behavior observed is similar to fluorescence decay experiments using malachite green, another triphenylmethane dye at similar temperatures in highly viscous systems, such as a solid SiO_2-ZrO_2 matrix[9] and in polymethyl methacrylate (PMMA) and polyvinyl alcohol (PVA) films.[10,11,12,13] However, the physical meaning of the observation of two exponential decay components for a triphenylmethane dye is the subject of an ongoing debate in the literature. None-the-less, there is a well-established relationship between

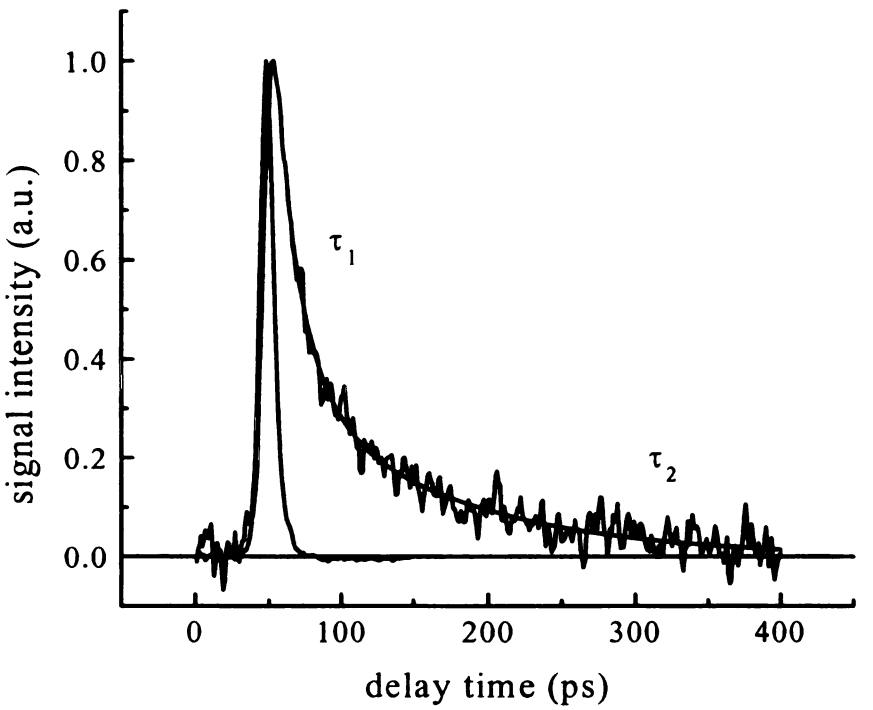

Figure 39 – Instrument response function and ground state recovery measurement of crystal violet in unprocessed spin cast film. The solid line through the data is the best-fit double exponential decay function.

the values of both decay time constants and the bulk viscosity of the medium, with the constants increasing with increasing viscosity. The values of the two time constants we observed are similar to the time constants obtained by Ben-Amotz and Harris,[7] Canva *et al.*[9] and Ippen, Shank and Bergman.[14] Ippen *et al.*[14] have developed a theory that relates the recovery time to the viscosity of the matrix.

Using these theories, we have determined the ground state recovery (GSR) behavior of crystal violet in a series of viscous matrices. We present representative data for the two extremes of our calibration curve in Figure 40 and Figure 41. We present the short-time component of the exponential decay for the series of viscous solutions in Figure 42. The short time component shows a linear relationship with solvent viscosity. Several of the solutions we used as matrices could only be fit to a single exponential decay. We believe that this is due to fitting parameters used by our computer program (Microcal Origin) and not indicative of a change in behavior of our probe molecule. By using these data as a calibration curve, we are able to extrapolate that the local viscosity experienced by crystal violet in the *unexposed* film is approximately 150 cP.

We have been able to apply these methods and data to the *exposed* photoresist film. We present the difference in the ground state recovery behavior of crystal violet in the exposed and unexposed film in Figure 43. The average double exponential decay best fit to a 30 ± 8 ps short time component (τ_1) and a long 190 ± 75 ps (τ_2) component. These values are beyond the limits of our calibration curve, but indicate that the viscosity of the exposed matrix increases to approximately 180-200 cP. This is also indicated by the comparison of the ground state recovery behavior of crystal violet in the two polymer films, presented in Figure 43. The change in the behavior of the crystal violet is related

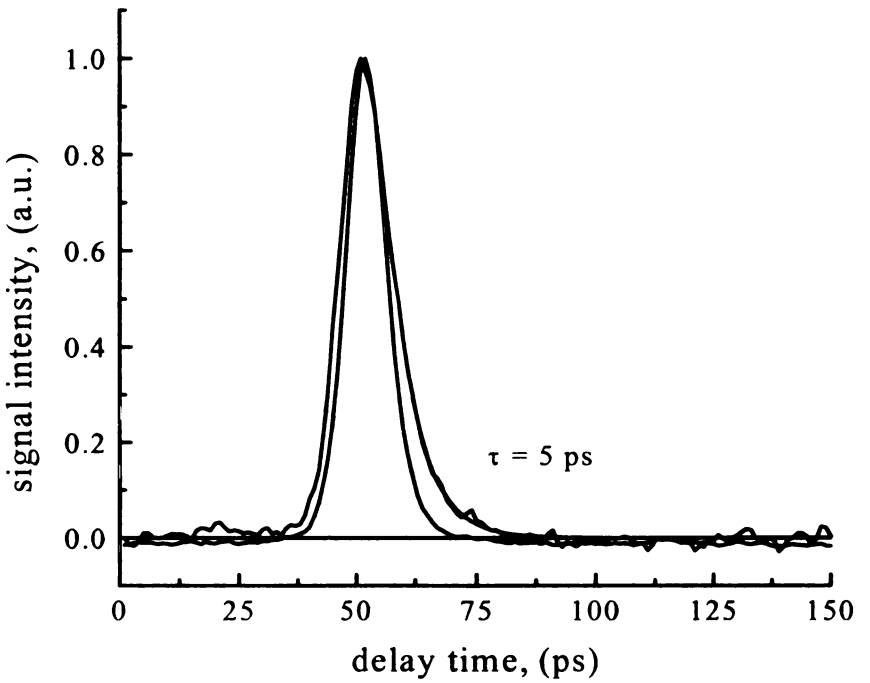

Figure 40 – Ground state recovery dynamics of crystal violet in ethylene glycol solvent. The instrument response function is also provided for reference.

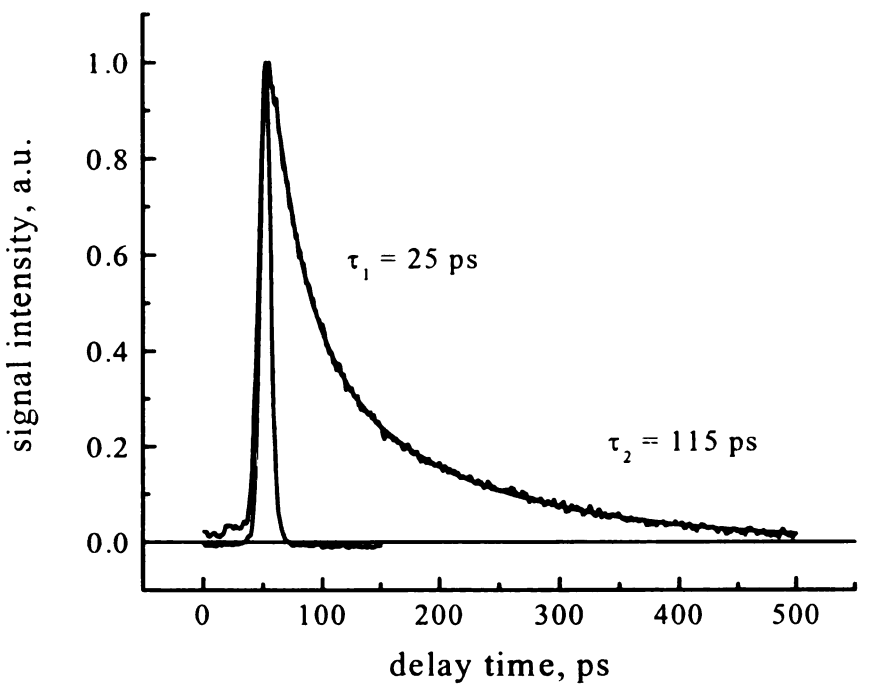

Figure 41 – Ground state recovery dynamics of crystal violet in glycol solvent. The instrument response function is also provided for reference.

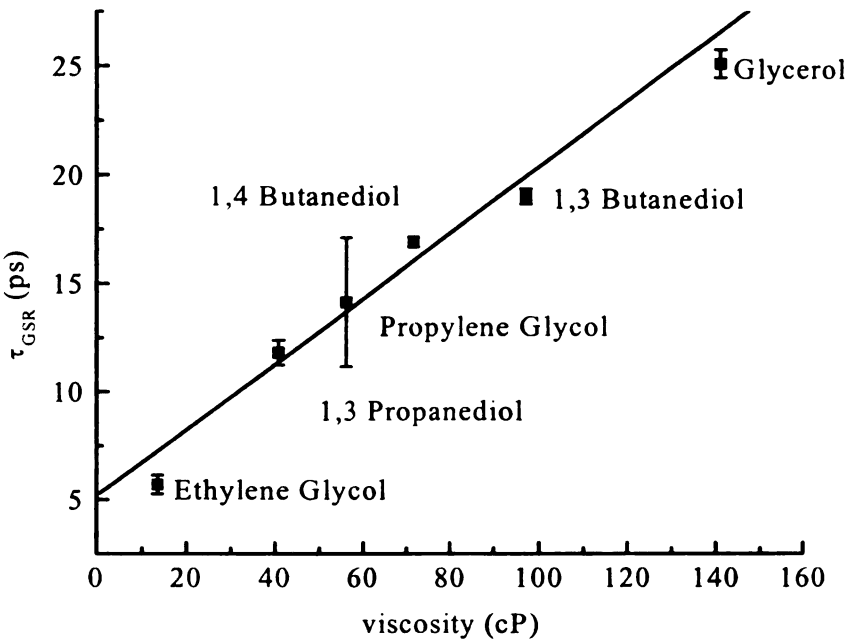

Figure 42 – Viscous matrix calibration curve relating viscosity of media to ground state recovery of crystal violet. The line presented is the linear best fit to the data.

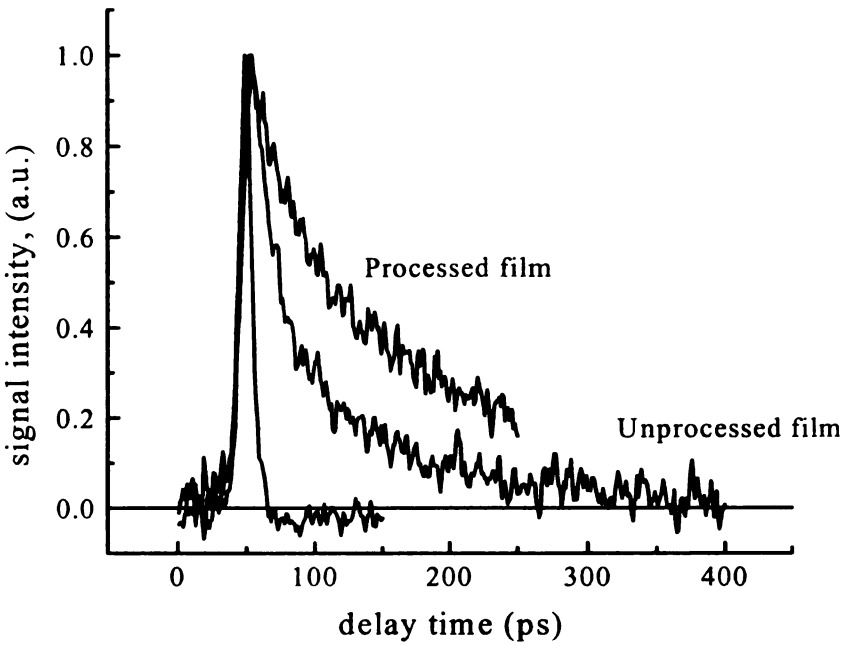

Figure 43 – Instrument response function and ground state recovery behavior of crystal violet in processed (post application bake, UV exposure, post exposure bake) and unprocessed (post application bake only) films.

to the changing viscosity of the photoresist matrix. The change in the viscosity is attributed to the relaxation of the polymer chains into free volume created by the diffusion of carbon dioxide and the isobutylene gases from the photoresist as the cleavage of the pendant chains along the polymer backbone continues during the post-exposure bake. The amount of free volume generated can be better determined through these data.

There are a number of probe molecules that exhibit an increase in the fluorescence signal and excited-state lifetime as the local viscosity is increased. As the molecular rotations become hindered, non-radiative pathways for energy transfer are less efficient; therefore, more of the excited-state energy must be dispelled through radiative (fluorescent) pathways. Crystal violet and malachite green are two such "propeller" probe molecules that have been used to investigate free volume in solid matrices. Other free volume sensitive probes are based upon photoisomerization and intramolecular excimer formation. With a small amount of a viscosity-sensitive molecule, the micro-viscosity or free volume of the system can be measured. For example, Francis Wang *et al.* have used 1,3-bis-(1-pyrene) (BPP) to monitor the polymerization of methyl methacrylate *in situ*.[15] Moorjani and coworkers further demonstrated the utility of fluorescence monitoring when dealing with diffusion-controlled reactions in media of different viscosity.[16] Victor and Torkelson have also used molecular probes to measure the free volume available in polymer structures.[17]

Crystal violet (Scheme 4), a member of the triphenylmethane dye family, is predominantly a D_3 propeller shape molecule in solution with three identical N,N-dimethylaniline rings bound to a central carbon atom tilted slightly out of the molecular plane. In addition to being a widely used acid-base indicator, crystal violet is a useful

probe of microviscosity or free volume. Ring rotation around the bonds between the phenyl rings to the central carbon atom in what is believed to be a barrierless process along the excited state potential energy surface. Studies have indicated a strong dependence of the excited state lifetime on solvent viscosity, which is indicative of essentially no intra-molecular rotational barrier to ring rotation.[7,8] The characteristically low fluorescence quantum yield of this family of molecules prevents us from using a fluorescence lifetime measurement to explore these changes. We instead examine the recovery of the ground state population by detecting the transient change in absorption of the probe pulse resulting from excitation by the pump laser pulse, to sense changes in the local environment in the photoresist thin films. We are able to characterize two film properties using this widely available chromophore because of its combined sensitivity to local acid concentration and viscosity.

Conclusions

We have developed a pump-probe spectroscopic method to determine changes in free volume in a photoresist matrix through the examination of changes in ground state recovery times of crystal violet. We have quantified the change in the local viscosity *in-situ* as a function of processing step. We attribute the changes in local viscosity as the result of diffusion of gases from the polymer matrix that result when pendant chains are removed through exposure to UV light in microlithographic applications. This experimentally determined information can then be applied to mathematical models currently used to describe this process in the microlithographic field, to better understand the manufacturing process.

Literature Cited

1. This work, and the work of Chapter 4, will be submitted for publication to *J. Phys. Chem. B.*

2. Jiang, Y.; Hambir, S. A.; Blanchard, G. J., *Opt. Commun.* **1993**, *99*, 216.

3. Bado, P.; Wilson, S. B.; Wilson, K. R., *Rev. Sci. Instrum.* **1982**, *53*, 606.

4. Andor, L.; Lorincz, A.; Siemion, J.; Smith, D. D.; Rice, S. A., *Rev. Sci. Instrum.* **1984**, *55*, 64.

5. Blanchard, G. J.; Wirth, M. J.; *Anal. Chem.* **1986**, *56*, 532.

6. *Lange's Handbook of Chemistry*, 14th ed.; Dean, J. A., Ed.; McGraw-Hill: New York, **1992;** 8.106.

7. Ben-Amotz, D.; Harris, C. B.; *J. Chem. Phys.* **1987**, *86*, 4856.

8. Ben-Amotz, D.; Harris, C. B.; *J. Chem. Phys.* **1987**, *86*, 5433.

9. Canva, M.; Le Saux, G.; Georges, P.; Brun, A.; Chaput, F.; Boilot, J. P.; *Chem Phys. Lett.* **1991**, *176*, 495.

10. Abedin, K. M.; Ye, J. Y.; Inouye, H.; Hattori, T.; Sumi, H.; Nakatsuka, H.; *J. Chem. Phys.* **1995,** *103*, 6414.

11. Abedin, K. M.; Ye, J. Y.; Inouye, H.; Hattori, T.; Nakatsuka, H.; *J. of Luminescence.* **1995,** *64*, 135.

12. Ye, J.Y.; Hattori, T.; Inouye, H.; Ueta, H.; Nakatsuka, H.; Maruyama, Y.; Ishikawa, M.; *Phys. Rev. B.* **1996,** *52*, 8349.

13. Ye, J.Y.; Hattori, T.; Nakatsuka, H.; Maruyama, Y.; Ishikawa, M.; *Phys. Rev. B.* **1997,** *56*, 5286.

14. Ippen, E. P.; Shank, C. V.; Bergman, A.; *Chem. Phys. Lett.* **1976**, *38*, 611.

15. Wang, F.W.; Lowry, R.E.; Grant, W.H.; *Polymer*, **1984**, *25*, 690.

16. Moorjani, S.K.; Rangarajan, B.; Scranton, A.B.; "Effect of viscosity on the rate of photosensitization of diaryliodonium salts by anthracene," In *Photopolymerization: Fundamentals and Applications*; Scranton, A.B.; Bowman, C.N.; Peiffer, R.W. Eds. American Chemical Society: Washington, D.C., 95.

17. Victor, J.G.; Torkelson, J.M.; *Macromolecules*, **1987,** *20*, 2241.

Chapter 6

CONCLUSIONS AND FUTURE WORK

In this dissertation, we have studied the rotational and vibrational population relaxation dynamics of perylene and 1-methylperylene in *n*-alkanols, aliphatic aldehydes and ketones. We have concluded that the presence of a labile proton is more important than solvent dipole moments to the solvation processes of an essentially nonpolar species. To better understand the effect of the presence of this labile proton on the rotational and vibrational population relaxation dynamics of the two probe molecules in solution, a more complete set of ketone solvents with a larger range of hydrodynamic volumes in solution could add to the understanding from the perspective of the changing solvent dipole moment. To continue to examine the effects of the labile hydrogen atom, these same rotational and vibrational population relaxation dynamic measurements of perylene and 1-methylperylene could be made in a series of carboxylic acid solvents, where the hydrodynamic volume is varied and the positioning of the carbonyl functional group relative to the probe molecule. The carboxylic acid solvent would be the next logical step in increasing complexity of the functional group, and would give additional insight into the mediation of solvent structure around the solute.

In Chapter 3 of this dissertation, the deviation from the R(0) value was partially attributed to the possible contributions from excited state absorption by perylene and 1-methylperylene in aldehydes and ketones, but due to the lack of data, further inferences could not be made. Excited state absorption measurements for the probe molecules in the

aldehydes and ketones would add to this body of work, and begin to address the possible reasons why the value of R(0) does not reach the expected value of 0.40.

The work performed in chapters 4 and 5 of this dissertation, regarding the characterization of photoresist materials used in microlithographic applications has the greatest potential for continued study. The characterization of acid mobility *in situ* of actual process samples would require the construction of a near field optical system that would be able to interrogate the regions immediately surrounding the lines transferred to the silicon wafer. The amount of acid and its location and the diffusion behavior of the acid molecule has been shown to be valuable information to the microlithographic community, and if a simple enough instrument could be constructed, it is suspected that the instrument and the information that could be obtained would be well received.

It may be possible to construct a system that will use the uptake of airborne bases as a monitor for exposure. The kinetics of airborne base uptake is dependent upon the specific matrix that the indicator is doped into. A systematic study of the matrix used and the effect on the kinetics of the uptake mechanism would be beneficial to better understand how the matrix affects the sensitivity to the airborne bases. Airborne contaminants, usually in the form of bases have been shown to have detrimental effects on the line shape of the semiconductor circuit patterns.

The methodology developed in Chapter 5 could be used to determine the intermediate changes in free-volume as a function of processing step. The effect of DUV dosage amount could be explored, as could the effect of changing the post exposure bake time and temperature. These results would better improve the understanding of the creation of free volume in the polymer during the manufacturing process.

Both of the techniques in Chapters 4 and 5 could be applied to other photoresists used in semiconductor fabrication. The field of microlithography is rapidly changing. New materials that allow for smaller and smaller features have replaced the materials used in this dissertation. These techniques and methods developed here could be used to characterize the new materials, with the information obtained of similar value to the community.

APPENDIX

APPENDIX A

NATIONAL INSTRUMENTS LABVIEW® BASED DATA ACQUISITION SOFTWARE FOR PUMP-PROBE LASER SPECTROMETER

This section presents the National Instruments LabView® virtual instrument (VI) written in our laboratory to control the pump-probe spectrophotometer (Figure 44) used in many of the experiments presented in this dissertation. This VI was written for operation in Microsoft Windows NT v4.0 operating system using, National Instruments LabView® v5.0.1, and National Instruments NI-DAQ software v6.0 software packages. The hardware used was a Pentium based personal computer with 64MB of memory, a National Instruments SC-2040 simultaneous sample and hold card, a National Instruments AT-MIO-16E-10 data acquisition card, and a National Instruments AT-GPIB-NT card for instrument control.

The VI is designed to obtain two analog voltage signals from the output of the lock-in amplifiers used in the pump-probe experiment, and to process the data to account for any gain applied by the electronics. The data are displayed for each individual channel on the front panel (user interface). The VI is also used to control the motion of the translation stage located on the laser table, either low-resolution or high-resolution. The translation stage controls the differential delay time between the pump and probe laser pulses in this experiment. The control signals are sent to the stepping motor controller using the GPIB interface. The VI has file management functionality built in, with the data acquisition parameters and file information included in the output file automatically.

The VI is based on a hardware timed, non-buffered technique of data acquisition, where the scan clock on the data acquisition board controls the acquisition timing. The front panel, which serves as the user interface, is presented in Figure 45. It is designed to accept data acquisition parameters, including file and sample information, the total delay time, the number of scans, the resolution of the stage expressed in ps/step, and the number of time constants to wait at each step before the data run begins, and write these parameters to the data file automatically. The front panel will also display the data from each of the four input channels individually in the smaller graphical displays, while displaying the signal averaged data from channel 0 (signal) and channel 1 (reference).

The overall circuit diagram for the VI is presented in Figure 46. The dominant feature of this first figure is a primary for-next loop that will cause its contents to occur for the number of cycles indicated by the number of scans control on the front panel. The VI will first obtain the number of scans, the total delay, the stepper motor resolution, and the system time constants to wait from the front panel (Figure 45). The VI will then create an array filled with zeros, the length of which is based on the total number of delay points from the front panel. The delay between each step of the translation stage is also obtained and set here, based on user input from the front panel. This delay between each step is designed to ensure that enough time elapses before data acquisition to allow for the mechanics of the system to settle properly. Before any new data are acquired, and before the VI progresses beyond the initial actions of the primary for-next loop, the graphical displays are cleared by sending a zero value to the history data attribute of each display. The creation of a data file, with the sample information and run date and time, then occurs, with all parameters separated with a carriage return and line feed to facilitate

data importation to other programs using ASCII format. At the conclusion of the for-next loop, the output data array is appended to this file and transposed from row major (horizontal) to column major (vertical) format.

Inside this primary for-next loop is a nested secondary sequence loop, consisting of four total frames. The first frame of this sequence loop, frame 0 (Figure 46), contains a secondary for-next loop and a three-framed secondary sequence loop nested in the secondary for-next loop. The secondary sequence loop is designed to acquire the individual data points that make up the total data set (Figure 46), move the stage forward one step between each data point, (Figure 47 and Figure 48), and facilitates a time delay for the mechanical settling after the stage has moved (Figure 49). This secondary sequence loop will occur as long as the secondary for-next loop is not satisfied, which is based on the total delay time of each individual data run set on the front panel. If this condition is satisfied, this secondary for-next loop will terminate, and the primary sequence loop will advance to frame 1 (Figure 47). Frame 0 in the secondary sequence loop (Figure 46) is designed to acquire the data point from each of four channels simultaneously, through the use of the SC-2040 simultaneous sample and hold card and the AT-MIO-16E-10 data acquisition card. The raw data are processed in this frame, where the gain applied by each of the lock-in amplifiers is accounted for in the conversion of the raw data to voltages. Each of these data points is collected and displayed on individual graphical displays, and the quotient of the sample and reference channel is averaged over the dataset. This average is also displayed on a separate graphical display.

In frame one of the secondary sequence loop, the movement of the translation stage such that the delay between the pump pulse and the probe pulse is changed by one picosecond using the GPIB interface. There is a switch on the front panel that is set to match the resolution of the stage in use, and determine the string sent via the GPIB interface to the stepper motor controller. The low state, or false state (Figure 47), is for the low-resolution stage where a picosecond is 15 steps in length. The high state, or true state (Figure 48), is for the high-resolution stepper motor controller, where a picosecond is 150 steps in length.

After the stage is moved forward one step in the first frame of the secondary sequence loop, the VI is designed to wait a number of time constants as a delay to allow for mechanical and electronic settling. The number of time constants is based on the input from the user on the front panel and the actual time constant settings for the electronics of the system. These settings are set on the front panel such that they are equal to the physical settings of the reference audio frequency lock-in amplifier. The clock used to time this delay is CPU process dependent, and may need to be changed if several processes are running simultaneously. The alternative settings for the time constant indicators are presented in Figure 50, and are controlled by the indicator on the front panel.

This completes the description of the secondary sequence loop functions. The secondary sequence loop will occur until the total number of steps is equal to the total delay time set on the front panel. This is determined through the use of the secondary sequence for-next loop in the VI. When the secondary for-next loop completes its cycle, the primary sequence loop will advance to frame 1 and rewind the stage to its original

position. The same switch on the front panel that determines the string sent to the stepper motor controller via GPIB for forward motion is also used to determine the string sent for the rewind function. The false or low state is to rewind the low-resolution stage (Figure 51), while the true or high state is to rewind the high-resolution stage (Figure 52.)

In frame two of the primary sequence loop (Figure 53), a delay to allow for mechanical settling after stage rewind is built in to the VI. It is necessary, since the program continues to progress after the command signals are sent via GPIB to the stepper motor controller, and the mechanical stage requires some time to rewind. It was found that 17500 cycles was sufficient for 1000 ps. Additional time can be added through a front panel control, and may be necessary for delay times longer than 1000 ps.

In the final frame of the primary sequence loop (Figure 54), the history data attribute of the sample, reference, and average signal graphical displays are cleared if the number of scans requested does not equal the current scan number (false state). Otherwise (true state, Figure 55), the loop will hold the values on the display until the VI is re-run.

The primary sequence loop will continue as long as the primary for-next loop is active. This is based on the condition that the scan number does not equal the number of scans requested on the front panel. When the two are equal, the primary for-next loop will terminate and the data array will be appended to the file, after it is transposed from row major (horizontal) to column major (vertical) format.

A complete list of sub-virtual instruments used is presented in Table 15 for reference. The disk locations are the default install locations on a typical installation of the LabView® 5.0.1 program.

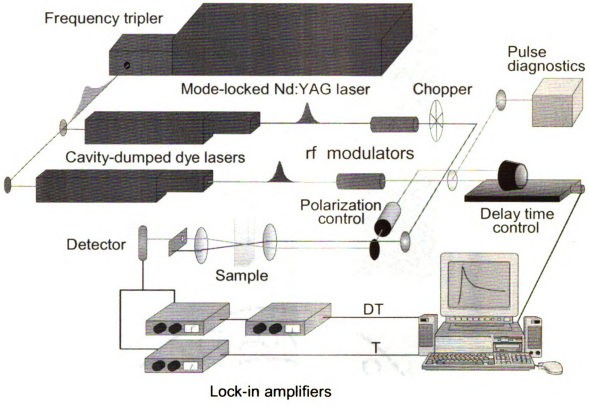

Figure 44 – Pump-probe laser spectrometer schematic.

Figure 45 – Front panel of LabView® pump-probe data acquisition virtual instrument.

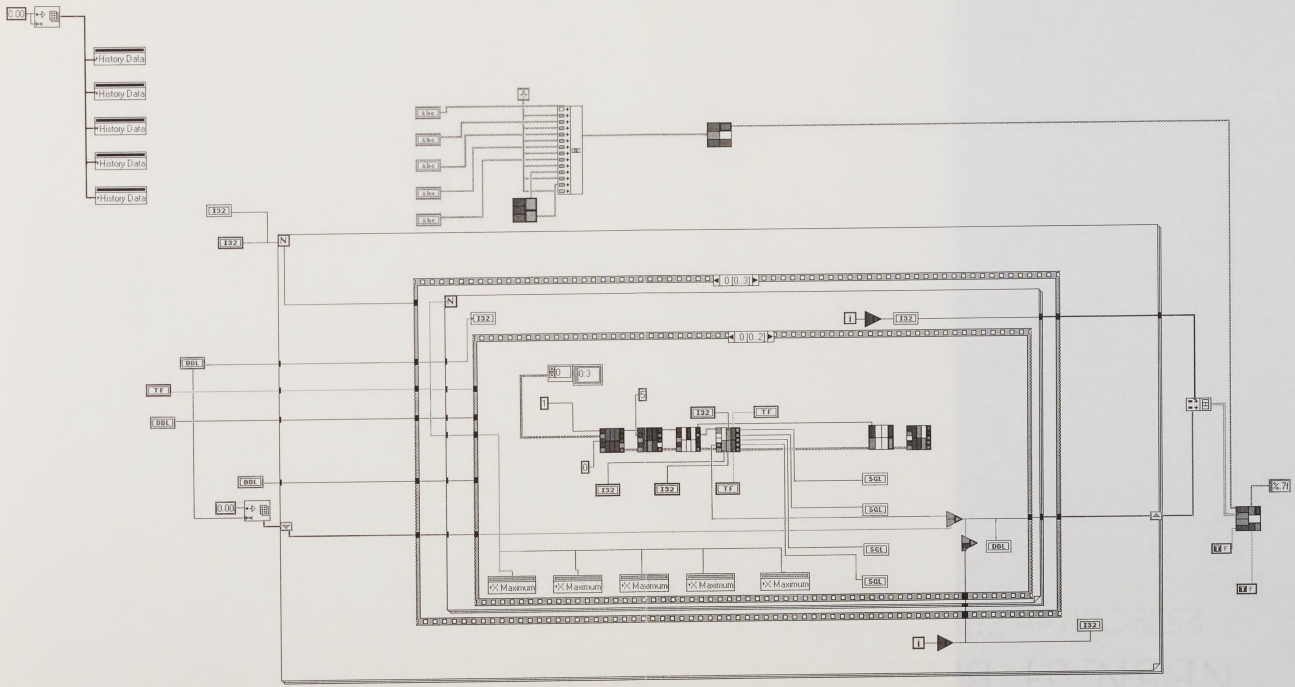

Figure 46 – Complete circuit diagram for LabView ® pump-probe data acquisition virtual instrument.

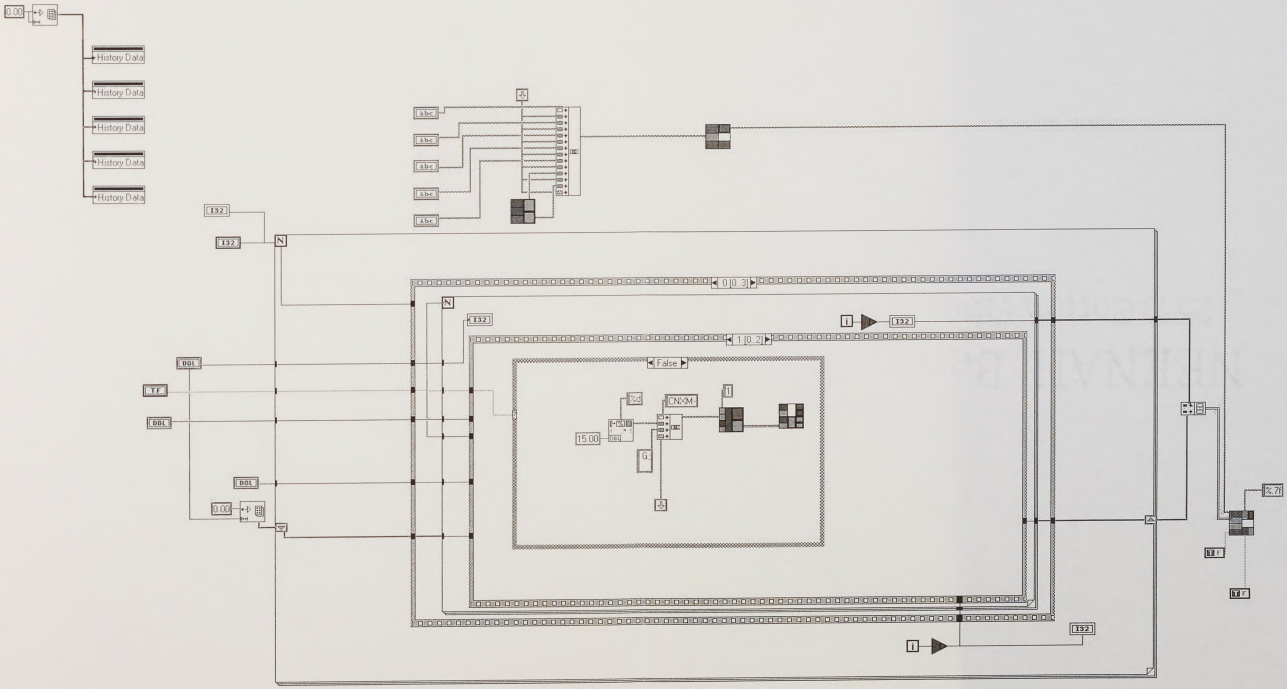

Figure 47 – Complete circuit diagram of pump-probe data acquisition virtual instrument, showing second frame of secondary sequence loop.

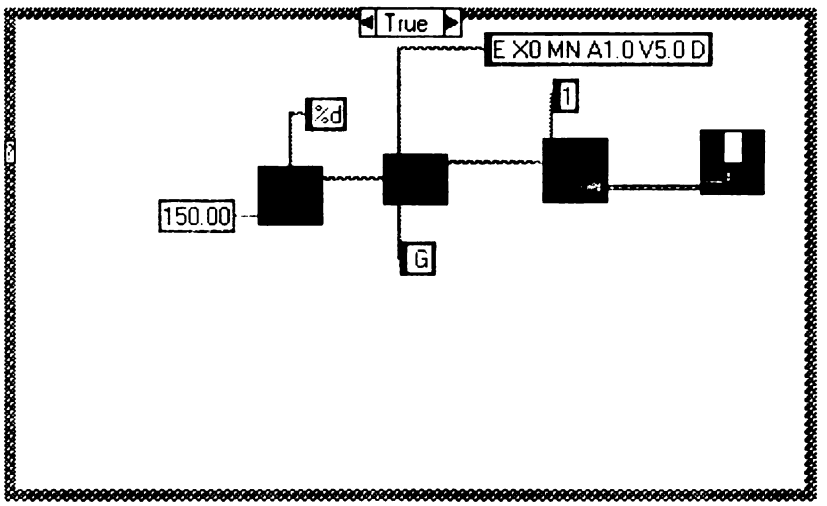

Figure 48 – High-resolution stage forward function.

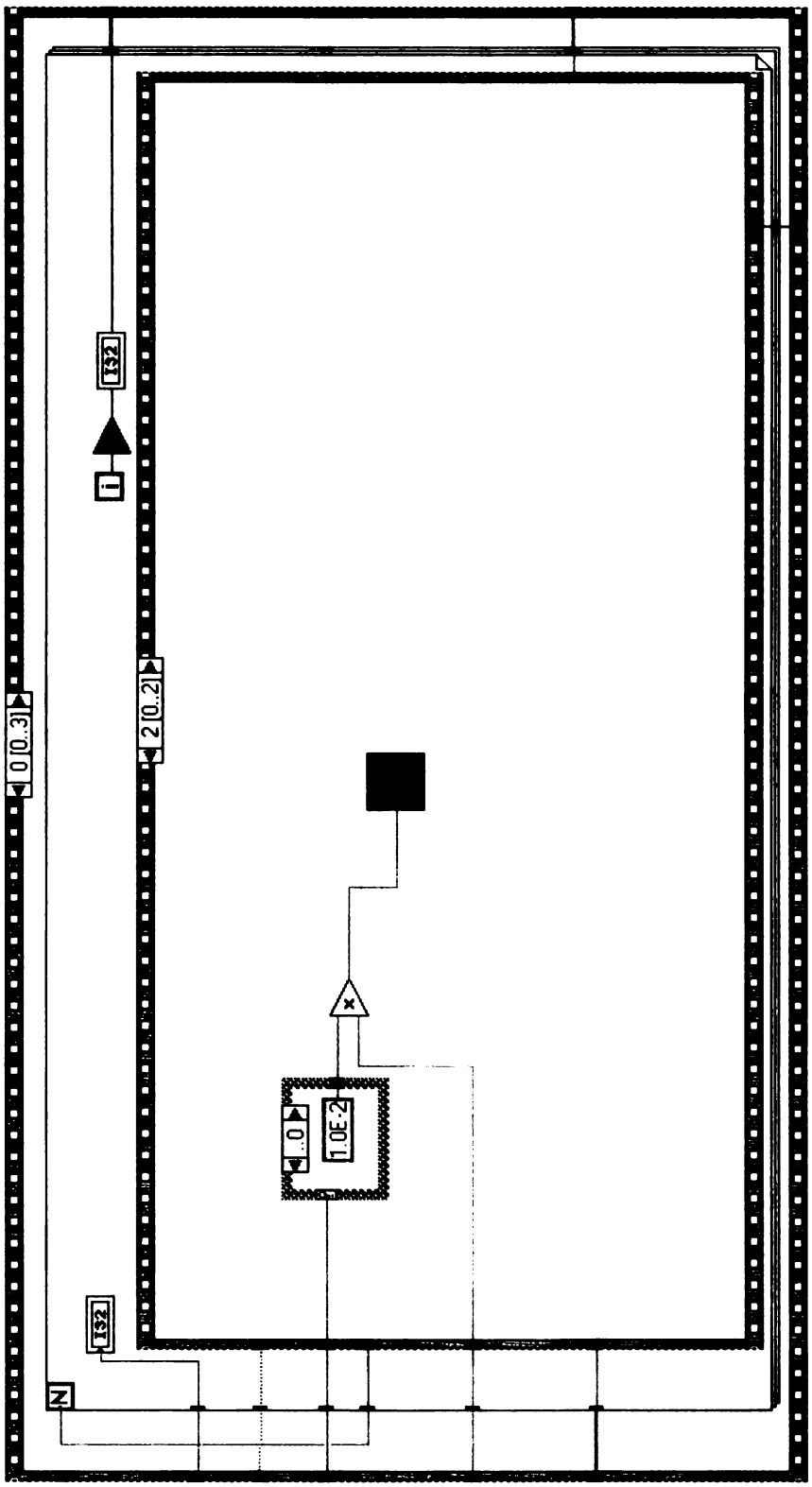

Figure 49 – Final frame of secondary sequence loop nested in first frame of primary sequence loop.

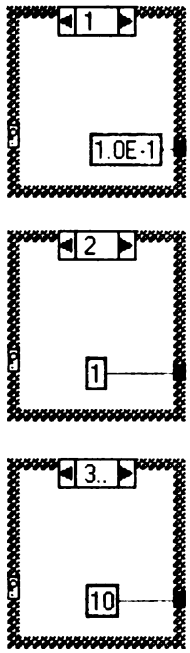

Figure 50 – Alternatives for electronic time constant settings in secondary sequence loop panel presented in Figure 49.

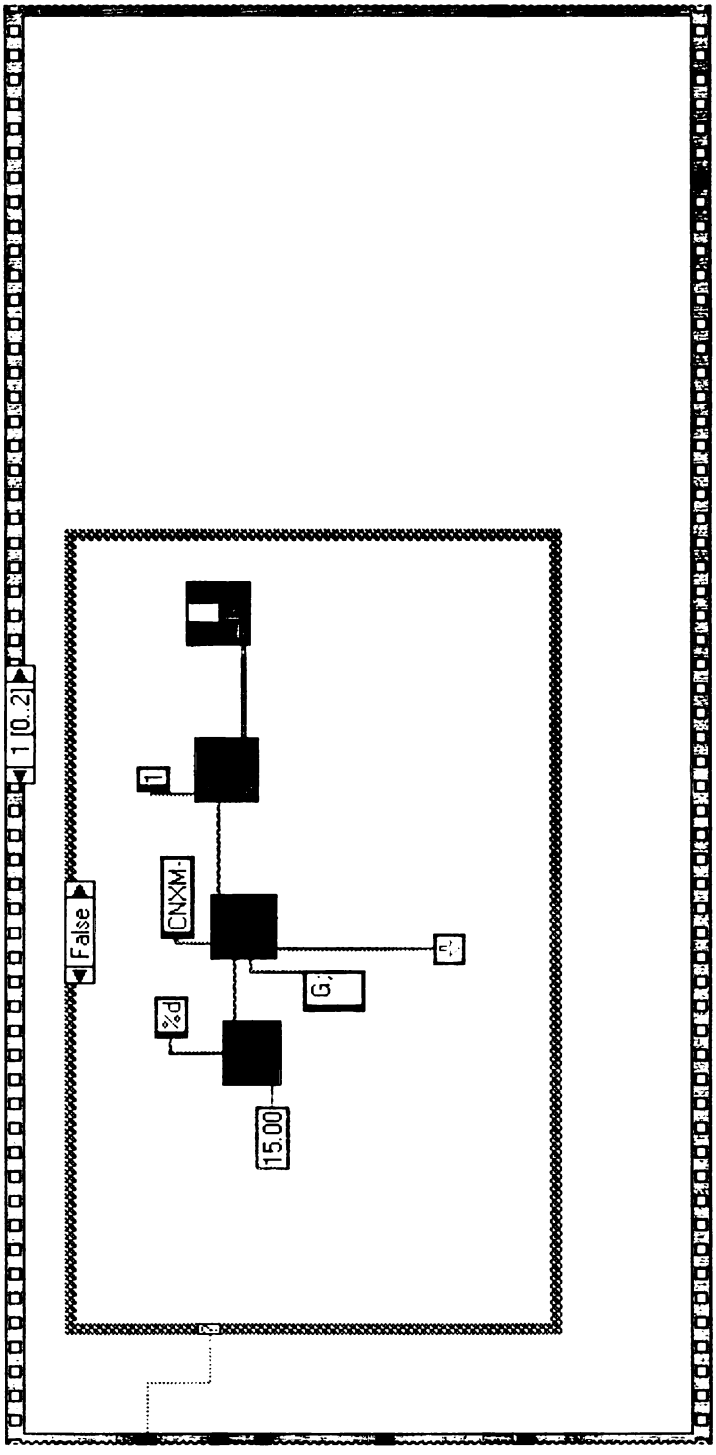

Figure 51 – Second frame of primary sequence loop, with low resolution move stage forward function.

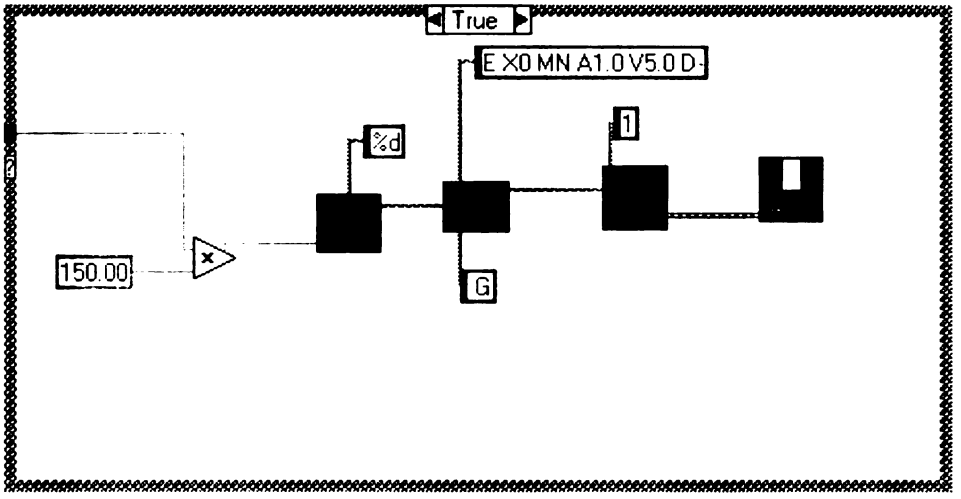

Figure 52 – High-resolution stage rewind function.

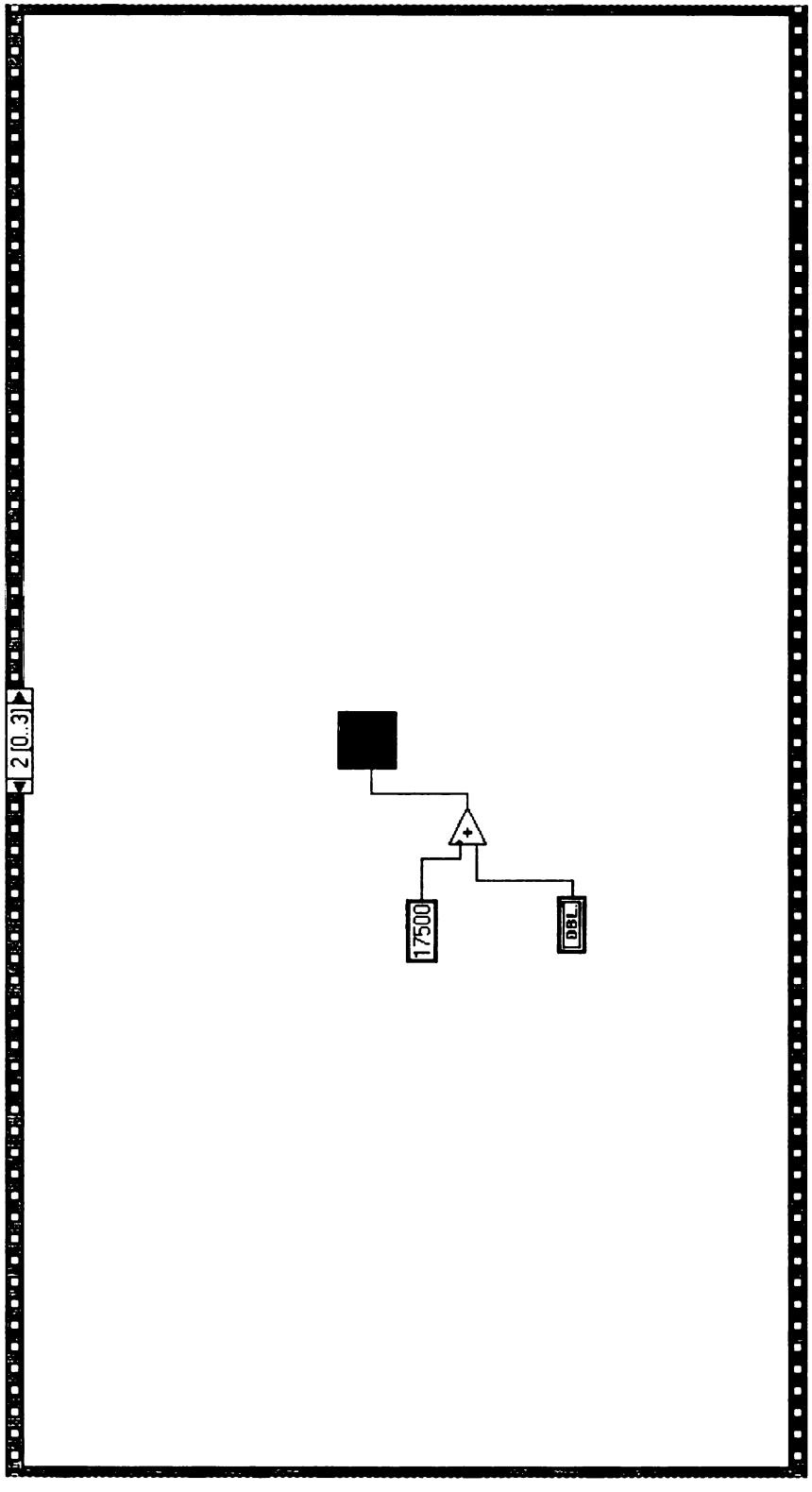

Figure 53 - Third frame of primary sequence loop.

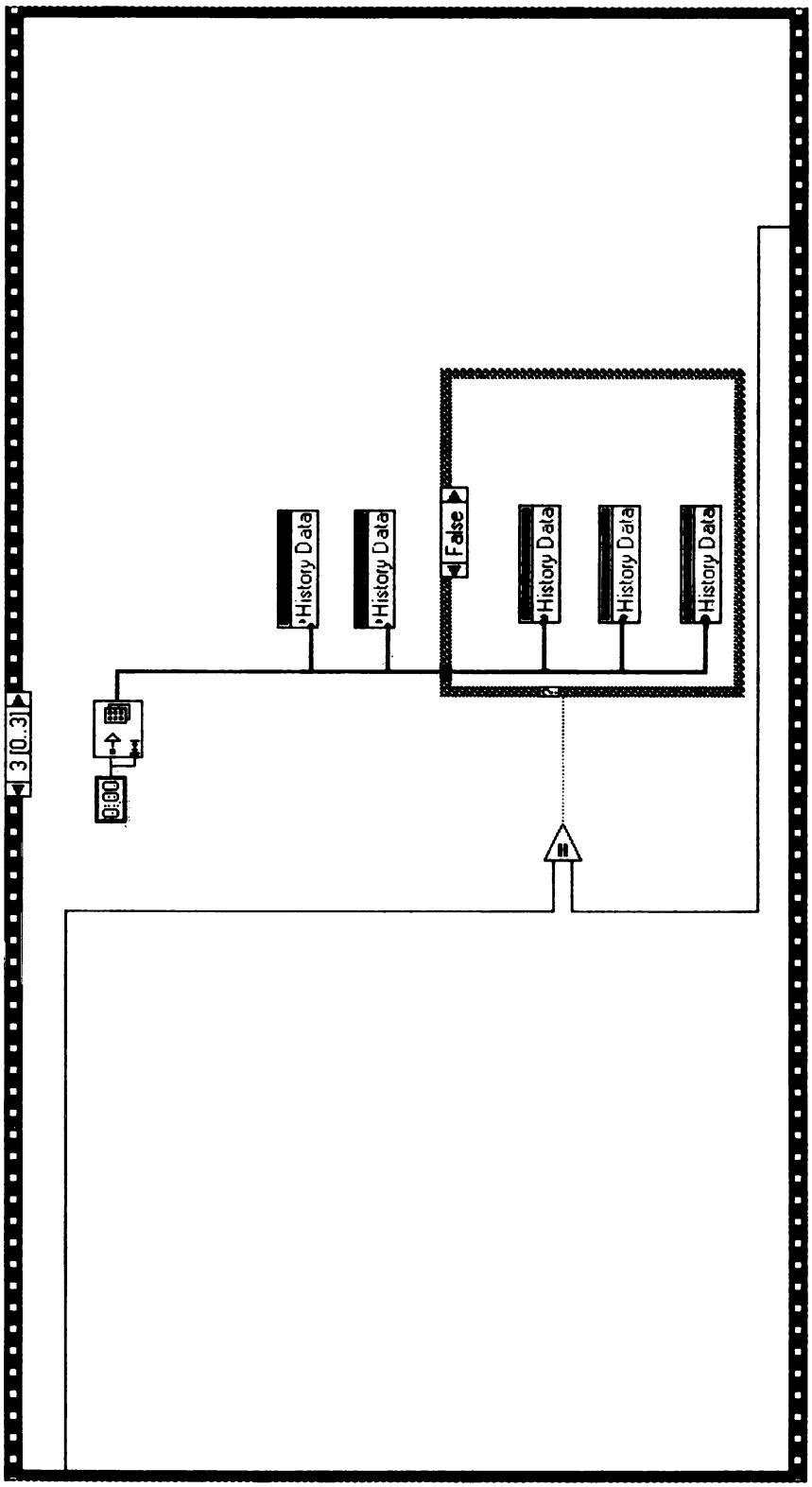

Figure 54 – Fourth (final) frame of primary sequence loop.

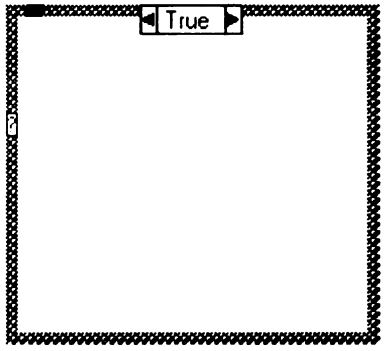

Figure 55 – Alternative to true/false state function in Figure 54. This frame is intentionally left empty, so that no processing occurs.

Table 15 – Table of sub-virtual instruments used in the pump-probe data acquisition virtual instrument.

General Error Handler.vi
C:\Program Files\National Instruments\LabVIEW\vi.lib\Utility\error.llb\General Error Handler.vi

AI Clear.vi
C:\Program Files\National Instruments\LabVIEW\vi.lib\DAQ\AI.LLB\AI Clear.vi

AI Config.vi
C:\Program Files\National Instruments\LabVIEW\vi.lib\DAQ\AI.LLB\AI Config.vi

AI Single Scan.vi
C:\Program Files\National Instruments\LabVIEW\vi.lib\DAQ\AI.LLB\AI Single Scan.vi

AI Start.vi
C:\Program Files\National Instruments\LabVIEW\vi.lib\DAQ\AI.LLB\AI Start.vi

Simple Error Handler.vi
C:\Program Files\National Instruments\LabVIEW\vi.lib\Utility\error.llb\Simple Error Handler.vi

Write To Spreadsheet File.vi
C:\Program Files\National Instruments\LabVIEW\vi.lib\Utility\file.llb\Write To Spreadsheet File.vi

Write Characters To File.vi
C:\Program Files\National Instruments\LabVIEW\vi.lib\Utility\file.llb\Write Characters To File.vi

DataProcessing
C:\Program Files\National Instruments\LabVIEW\user.lib\PumpProbeVI's.llb\DataProcessing